DISSERTATION

AFRICA'S FUELWOOD FOOTPRINT AND THE BIOME-LEVEL IMPACTS OF TREE

HARVEST

Submitted by

Andrew T. Tredennick

Graduate Degree Program in Ecology

In partial fulfillment of the requirements

For the Degree of Doctor of Philosophy

Colorado State University

Fort Collins, Colorado

Summer 2014

Doctoral Committee:

    Advisor: Kathleen Galvin
    Co-Advisor: Niall P. Hanan

    Michael Coughenour
    Stephen Leisz

ABSTRACT

AFRICA'S FUELWOOD FOOTPRINT AND THE BIOME-LEVEL IMPACTS OF TREE

HARVEST

Wood biomass is the dominant energy source in sub-Saharan Africa (SSA), supplying some 75-90% of African families with the necessary energy to meet their basic human needs. Yet, despite the importance of fuelwood (firewood and charcoal) to food and energy securities in SSA, no comprehensive assessment of fuelwood supply and demand exists. Likewise, we have little understanding of how harvesting of trees affects vegetation dynamics in savannas and forests. Empirical and theoretical work over the past twenty years has focused on disturbance from fire and herbivory in savannas and forests, but most other human impacts have been ignored. This dissertation aims to increase our understanding of fuelwood dynamics from applied and theoretical angles. Specifically, I focus on four objectives: (1) empirically testing the ability of theoretical allometric scaling models to predict the relationships between morphological traits (e.g., stem diameter and height) of savanna trees important for rapid biomass assessments and ecological theory; (2) using remote sensing to estimate available wood biomass for harvest in Mali, West Africa; (3) quantifying and mapping annual fuelwood supply and demand for all of SSA; and (4) integrating fuelwood harvest into our theoretical understanding of savanna and forest vegetation dynamics.

In Chapter 2 I present a rigorous test of plant scaling models in savanna systems. Empirical data is not always available for estimating plant biomass from easily measured variables (e.g., stem

diameter), so it is important to discover if theoretical models of plant scaling based on allometri-cally ideal plants can be used in systems where multiple selective pressures may drive allometries away from ideal predictions. I found that the predictions of Metabolic Scaling Theory were most consistent with data from harvested trees from three savanna sites in West Africa. Especially for biomass, Metabolic Scaling Theory out performed the other models tested. However, I found significant departures of the Metabolic Scaling Theory prediction for stem height or branch length based on stem or branch diameter: length scaling exponents at all sites were higher than expected by theory. I hypothesized that savanna trees have realized height/length scaling exponents that are larger than predicted by underlying theory because of selection for rapid vertical growth to escape fires that are so frequent in savanna systems. Among sites there is variation in length/height scaling exponents, indicating an interaction between resource availability and selective pressure for rapid growth. However, the analysis indicates that where data is unavailable the prediction of Metabolic Scaling Theory for estimating biomass from stem diameter is able to capture the mean tendency of allometric scaling in savanna trees.

Chapters 3 and 4 present new analyses of fuelwood supply and demand at different spatial extents. In Chapter 3 I use satellite remote sensing and an extensive database to estimate wood biomass available for tree harvest in Mali, West Africa. My estimates, while associated with high uncertainty, show that wood biomass in Mali is greater than estimated from previous global and continental scale biomass mapping efforts. Chapter 4 builds on that approach to assess the patterns of fuelwood supply and demand for all of SSA. Using best-available fuelwood demand statistics, a growth model based on remotely sensed data, and current biomass estimates I created a series of maps, with associated uncertainties, showing the amount of wood needed by humans for energy in SSA and the amount produced annually. I estimate total annual wood demand is

17-35% of annual wood production. But this varies greatly at local and regional scales. Regional fuelwood consumption varies from ~14-40% of annual wood production and localized areas in Central Africa, Ethiopia, and the west coast require greater than 100% of local production. In large urban centers, fuelwood appropriation of local production can exceed 1,000%. Though people are not limited to using local wood production, the areas in excess of 100% clearly require external inputs to meet local demand.

In Chapter 5 I present a theoretical analysis to explore if, on average and given our current knowledge of savanna systems, fuelwood harvest affects the stability of savanna and forest systems. To do so I incorporate tree harvest into a population dynamic model of forest, savanna, and grassland vegetation dynamics. I use assumptions about the differential demographic responses of savanna trees and forest trees to harvest to show how tree harvest influences tree cover, demography, and community composition. Tree harvest can erode the intrinsic basin of attraction for forest and make a state transition via fire to savanna more likely. The savanna state is generally resilient to all but high levels of tree harvest due to the resprouting abilities of savanna trees. In the absence of active fire suppression my analysis suggests we can expect to see large and potentially irreversible shifts from forest to savanna as demand increases for charcoal in sub-Saharan Africa. On the other hand, savanna tree species' traits seem likely to promote savanna stability in the face of low-to-moderate harvest pressure.

My dissertation work suggests that, overall, there is no large-scale fuelwood crisis in SSA and that in moderately populated savannas tree harvest is a sustainable livelihood practice. My applied work at the continental scale shows that local fuelwood shortages can be overcome if adequate mechanisms are in place to import wood from high production areas. This implies that fuelwood crises may proximately be an ecological issue, but ultimately fuelwood shortages are a social

and economic issue. My work allows for identification of localities in need of targeted socio-economic analyses and policy intervention at an unprecedented scale and extent. In savannas we find, based on well supported assumptions, that the savanna biome is generally resilient to tree harvest. However, our analysis suggests a demographic shift to low biomass tree sizes. Thus, even though savannas may be stable in the face of tree harvest, reductions in tree biomass on the landscape means there is less fuelwood available for human appropriation.

communicate my science. I only hope I can provide her with the same combination of support and

challenge as she undertakes her PhD.

TABLE OF CONTENTS

Chapter 1

Introduction

A major challenge of contemporary ecology is to integrate uniquely anthropogenic processes into our fundamental understanding of population, community, and ecosystem dynamics (Keller et al. 2008, Cardinale 2013, Chapin III and Fernandez 2013). Thus, ecologists living in the Anthropocene (Crutzen 2002) are charged with bringing basic science to bear on applied ecological problems related to sustainability and ecosystem stewardship (Chapin III et al. 2010). At the fore of such efforts linking basic and applied ecology is work centered on forecasting the, often negative, impacts of climate change (e.g., Adler et al. 2012), biodiversity loss (e.g., Cardinale et al. 2012), invasive species (e.g., Levine and D'Antonio 2003), and land-use change (e.g., Foley et al. 2005) on ecological systems across levels of organization. However, human impacts need not always be negative, and in many ecosystems humans have been integral parts for millennia. In such cases our focus should be on *i*) the roles humans play in regulating ecosystem structure and function, and *ii*) under what conditions ecosystems can sustain continued human appropriation of ecosystem services. This is especially important in regions of the world where people depend directly on natural products to meet their basic human needs.

African savannas are a particularly compelling example of a biome influenced by humans on long time scales, as well as a biome that provides critical ecosystem services. Most evidence points toward African savannas being the origin of *Homo sapiens* evolution (e.g., White et al. 2003 and reviewed in Reid 2012), and recent work suggests humans have played a key role in regulating fire regimes in Africa from anywhere between 4,000 to 40,000 years before present (Archibald et al. 2012). Likewise, the dominant livelihood throughout much of Africa's savannas, pastoralism, has persisted for centuries, mostly in concert with land and wildlife conservation (Galvin 2009, Galvin and Reid 2011, Reid 2012). Through the centuries of humans manipulating fire regimes as a range

management tactic and actively herding large mammals in Africa's savannas, they have also been using wood biomass for the most basic of needs: cooking and heating.

Humans have likely used wood for energy for over 500,000 years (Sharpe 1976, Gowlett et al. 1981, Goren-Inbar et al. 2004), and it remains the primary energy source in sub-Saharan Africa (SSA) (Kebede et al. 2010, Sander et al. 2011) and in most developing and transition economies of the world. But compared to other human activities like pastoralism and active fire manipulation, the use of trees for wood is understudied. Several efforts focus on local-scale sustainability of fuelwood harvest in terms of deforestation (Shackleton 1993, Madubansi and Shackleton 2007, Morton 2007, Wessels et al. 2013), but rarely is tree harvest explicitly considered as an important ecological process that may influence savanna stability, structure, and function. Likewise, after receiving a large amount of attention during the 'fuelwood crisis' years of the 1970s and 1980s, large scale efforts to quantify fuelwood supply and demand ceased, and no contemporary analysis exists.

Currently, the highest resolution estimates of fuelwood supply and demand are at the national scale, calculated from UN Food and Agricultural Organization databases (e.g., Bailis et al. 2005). National-level studies, while informative, lack the spatial detail necessary to identify areas in need of targeted policy intervention. Local-scale studies are important for understanding the detailed drivers of fuelwood supply and demand at scales relevant to human use, but these studies are difficult to scale up and apply to other areas. The limitations of these two approaches calls for a "middle-of-the-road" approach that allows us to identify fuelwood scarcity 'hotspots' at relevant scales and spatial extents.

Though limited, available fuelwood demand statistics (Arnold et al. 2006) and applied research (Shackleton 1993; 2001, Ahrends et al. 2010, Wessels et al. 2013) do indicate tree harvest is a considerable disturbance in African savannas and forests. Yet, most ecological research over the past three decades has focused exclusively on herbivory and fire as key disturbances in tropical savannas and forests (see Scholes and Archer 1997, Sankaran et al. 2004, Bond 2008, for reviews). This focus, particularly on fire, has led to key insights into the role of demographic bottlenecks

in creating and maintaining the savanna biome (Higgins et al. 2000, Sankaran et al. 2005), and constraining forest and savanna as alternate stable states (Staver et al. 2011*a;b*, Hirota et al. 2011). The fundamental mechanism in mesic savannas is fire limiting the recruitment of tree saplings to adult life stages. It makes intuitive sense that harvest may also play a role in regulating the stability of forests and savannas because when trees resprout after harvest they go from being outside the flame zone (or 'fire trap') as adults to being back in the flame zone as coppicing saplings. Across the spectrum – from applied to theoretical work – more research is needed to fully understand the impacts of fuelwood harvest in savannas and forests.

The objective of my dissertation is to improve our overall understanding of the sustainability of tree harvest for fuelwood (firewood and charcoal) in SSA by focusing on the supply and demand of fuelwood as well as the ecological consequences of tree harvest in forests and savannas. Specifically, I sought to answer four questions:

1. Can universal allometric scaling theories provide a basis for estimating tree biomass across diverse savannas?

2. What is the current standing stock of tree biomass available for fuelwood harvest in Mali, West Africa?

3. What is the spatial distribution of fuelwood supply and demand across sub-Saharan Africa and in what areas does annual supply exceed annual demand?

4. Does tree harvest effect the stable-state dynamics of forest and savanna?

In each of the chapters that follow I use different approaches (theoretical, modeling, and empirical) at different spatial scales (local, regional, and continental) to answer my questions.

At the local scale, Chapter 2 tests the ability of 'universal' scaling theories to predict morphological traits of savanna trees existing under diverse resource environments and disturbance regimes. At the regional scale, Chapter 3 uses satellite remote sensing to estimate aboveground woody biomass in Mali, West Africa. At the continental scale, Chapter 4 uses a combination of

empirical and modeling approaches to estimate the current pattern of fuelwood supply and demand in SSA. Lastly, Chapter 5 takes a theoretical modeling approach to investigate the biome-level impacts of tree harvest on the stability of forest and savanna. In Chapter 6 I synthesize my findings and discuss how in combination my results show that fuelwood harvesting is a mostly sustainable livelihood strategy in African savannas.

Chapter 2

Allometric convergence in savanna trees and implications for plant scaling models in variable ecosystems[1]

Summary

Theoretical models of allometric scaling provide frameworks for understanding and predicting how and why the morphology and function of organisms vary with scale. It remains unclear, however, if the predictions of 'universal' scaling models for vascular plants hold across diverse species in variable environments. Phenomena such as competition and disturbance may drive allometric scaling relationships away from theoretical predictions based on an optimized tree. Here, we use a hierarchical Bayesian approach to calculate tree-specific, species-specific, and 'global' (i.e. interspecific) scaling exponents for several allometric relationships using tree- and branch-level data harvested from three savanna sites across a rainfall gradient in Mali, West Africa. We use these exponents to provide a rigorous test of three plant scaling models (Metabolic Scaling Theory (MST), Geometric Similarity, and Stress Similarity) in savanna systems. For the allometric relationships we evaluated (stem diameter vs. length, aboveground mass, stem mass, and leaf mass) the empirically calculated exponents broadly overlapped among species from diverse environments, except for the scaling exponents for length, which increased with tree cover and density. When we compare empirical scaling exponents to the theoretical predictions from the three models we find MST predictions are most consistent with our observed allometries. In those situations where observations are inconsistent with MST we find that departure from theory corresponds with expected tradeoffs related to disturbance and competitive interactions. We hypothesize savanna trees have greater length-scaling exponents than predicted by MST due to an evolutionary tradeoff between

---

[1]This chapter is an edited version of Tredennick A.T., Bentley, L.P., and Hanan, N.P. 2013. *PLoS One* **8**, reproduced here under a Creative Commons ⓒ license.

fire escape and optimization of mechanical stability and internal resource transport. Future research on the drivers of systematic allometric variation could reconcile the differences between observed scaling relationships in variable ecosystems and those predicted by ideal models such as MST.

2.1 Introduction

One of the central goals of ecology is to identify and understand the underlying rules and mechanisms that govern the form and function of organisms. In particular, the existence of consistent allometric relationships across diverse taxa has led to theories that attempt to use physical first principles to predict biological scaling – that is, how organism traits vary with size. For plants, there are several 'universal' scaling theories that produce testable predictions including Metabolic Scaling Theory (MST; West et al. 1999), the Geometric Similarity model (GEOM; Niklas 1994), and the Stress Similarity model (STRESS; McMahon and Kronauer 1976) (Table 2.1). These models all assume physical constraints to arrive at predictions of allometric scaling. However, given the variability inherent in many ecological systems, the utility of these idealized (i.e. "optimal") models to predict real ecological phenomena (Kozĺowski and Konarzewski 2004, Muller-Landau et al. 2006) across multiple scales of inquiry (Tilman et al. 2004) has come into question (Coomes 2006, Muller-Landau et al. 2006, Coomes and Allen 2009, Price et al. 2009, Moncrieff et al. 2011, but see Brown et al. 2005, Stark et al. 2011).

Indeed, the extent to which variability and disturbances such as herbivory and fire may invalidate the allometric predictions of universal models based only on physical first principles remains uncertain. Since these models are based on optimizing assumptions about mechanical constraints that ignore the role of resources (GEOM and STRESS), or optimize resource distribution and plant uptake (MST) they may fail to predict scaling relationships in temporally and spatially heterogeneous environments where resource uptake is constrained by resource limitation (Muller-Landau et al. 2006). Further, demographic processes may not be entirely resource-based in variable envi-

ronments where populations may be maintained in a non-equilibrium or disequilibrium state (Ellis and Swift 1988, Sankaran et al. 2005) by disturbances and resource pulses (Chesson et al. 2004). In these cases, selection for traits adaptive under conditions of spatiotemporal variability and disturbance may be more important than selection for optimal mechanical or physiological architecture (Russo et al. 2007) – the only selective forces invoked by zero-order scaling models (see **Materials and Methods: Scaling models**).

Savannas therefore offer an interesting test case for universal scaling models because the dominant paradigms of savanna ecology invoke competition, environmental variability, and anthropogenic disturbances as mediators of tree cover and structure (Sankaran et al. 2004). Savannas are highly variable two-layer tree-grass systems broadly defined by a discontinuous and dynamic tree layer with a continuous herbaceous layer (Ratnam et al. 2011). Climate plays an integral role in constraining potential tree cover of savannas, but realized tree cover is highly variable in space and time (Sankaran et al. 2005). Moreover, tree biomass and architecture may vary in savannas based on the magnitude and extent of disturbances such as browsing (Moncrieff et al. 2011) and fire (Archibald and Bond 2003). Inter- and intra-annual variability in precipitation, competition for water, and multiple disturbances including fire, herbivory, and tree harvest establish broad environmental gradients and create conditions that may select for modified allometries and lead to greater allometric variation at the level of individuals and species.

To test the ability of universal scaling models (MST, GEOM, and STRESS) to predict whole-tree and within-tree allometric relationships in variable systems we examine allometric scaling relationships for three tree species from three savanna sites in West Africa. We use a hierarchical Bayesian (HB) approach to estimate scaling parameters (a, the normalizing constant, and b, the scaling exponent) from the general allometric equation,

$$Y \; = \; aX^b \tag{2.1}$$

a power-law. In this analysis we treat branch (or basal) diameter as the independent variable (X)

7

and calculate its relationship with four branch (or tree) traits: 1) length, 2) aboveground mass, 3) stem mass, and 4) leaf mass (Ys in Equation 2.1). We evaluate the competing scaling models by comparing our empirical estimates to theoretical predictions. All are power-law models that make specific predictions (Table 2.1) for the scaling exponent b (Equation 2.1) relating plant morphology (Y, e.g. length, mass) to plant size (X, e.g. diameter).

Specifically, the objectives of our study are to determine: 1) if tree species in savannas exhibit similar scaling relationships for length, aboveground mass, stem mass, and leaf mass; 2) if there is more variability in scaling relationships among or within species; and 3) if the scaling exponents derived from our combined branch and tree data support or reject MST and/or other scaling model predictions. Our main hypothesis is that since universal scaling models make idealizing assumptions regarding plant architecture and the environment within which plants live, we will observe deviations from model predictions for an idealized network structure since savanna trees must respond to variable environmental conditions. To assess this hypothesis we proceed in two stages: 1) identify the "best" model as the model (MST, GEOM, or STRESS) with the most predictions included within our calculated 95% credible intervals for each scaling relationship; and 2) interpret any deviations from the best model by considering how factors specific to savanna systems may interact with the idealizing assumptions of the theoretical model to cause allometric deviations.

2.2   Materials and Methods

2.2.1   Field data

We collected data from three savanna sites that span the tropical rainfall gradient in Mali, West Africa. The sites vary in mean annual precipitation, tree architecture, canopy cover and height, fire frequency, grazing intensity, and species composition (Table 2.2). Across the sites mean annual precipitation ranges from 570-1,400 mm yr^{-1} (north to south) and fire frequency ranges from 0.9 yr^{-1} at the northernmost site (Lakamané) to 0.35 yr^{-1} at the southernmost site (Tiendéga). Large, wild herbivores are effectively absent in West African savannas, but each site does receive some

8

level of grazing by cattle and browsing by goats (Table 2.2). At each site, we chose ten trees of the dominant species for harvest, except at one site (Tiorola) where we only harvested five individuals.

We felled each tree and for every branch with a diameter greater than or equal to 2 cm measured: 1) branch (or basal) diameter within 5 cm of the branch points (or within 10 cm of the soil for basal measurements), 2) length, 3) wood wet weight, and 4) leaf wet weight. We took subsamples of main stem (i.e. trunk) wood (one sample per tree) and leaves (approximately 30g wet weight per tree) to obtain species-specific dry:wet weight ratios used to account for the contribution of water content to wet weights of wood and leaf. We aggregated biomass data by branch. That is, the biomass (leaf, wood) of each daughter branch was summed for each parent branch to ensure all biomass downstream of any particular branching node is attributed to that branch's diameter. Since not all trees had branches with diameters greater than 2 cm we only used dry:wet weight ratios from the trunk, but for trees where we took sub-samples of trunk and branch wood there is a near 1:1 relationship between trunk and branch dry:wet weight ratios (data not shown) indicating there is no systematic variation in dry:wet weight ratios with regards to branch order. The dataset contains observations for 25 individual trees composed of 286 branches (including main stems) representing three savanna tree species: *Deterium microcarpum* Guill. and Perr. ($n_{tree} = 10$; n_{branch} = 103), *Combretum geitynophylum* Loefl. ($n_{tree} = 5$; $n_{branch} = 30$), and *Combretum glutinosum* Perr. ($n_{tree} = 10$; $n_{branch} = 128$). We conducted the subsequent analysis using a combined dataset comprised of tree and branch data. Each branch, including the main stem or whole-tree, is treated as an observation and is indexed by tree and species (see **Data analysis: hierarchical Bayesian model**).

All necessary permits were obtained for the described field studies. All field sites are in public lands administered by the Malian Nature Ministry (Departement des Eaux et Forets). Data collection at field sites was made possible through a memorandum of understanding covering the creation and long-term operation of the sites. Field data collection did not involve or cause harm to any endangered or protected species.

2.2.2 Scaling models

The MST botanical model by West, Brown, and Enquist (WBE; West et al. 1999) postulates rules that govern plant branching architecture and can serve as a baseline for variation in plant form. In so doing, this model invokes the existence of, and selection for, optimally branching resource distribution networks (e.g. plant vascular systems). In particular, the original WBE model of plant architecture proposes that vascular networks have evolved to minimize hydrodynamic resistance and to maximize the scaling of exchange surfaces such as leaves (West et al. 1999, Enquist 2002). Quarter-power scaling then emerges as a consequence of these physiological goals and physical constraints related to buckling (West et al. 1999). Based on these assumptions, MST makes specific predictions for the scaling of branch/tree length/height (l) and total aboveground biomass (M) with branch (or basal) diameter (D) (Table 2.1). Further developments by Enquist and Niklas (2002) predict the allocation of total biomass to leaf mass (L) and stem mass (S) within the plant based on size (Table 2.1). If 'space-filling' and 'area-preserving' are the primary evolutionary drivers of network architecture across taxa and resources are homogeneously distributed, then WBE scaling exponents should be identical across divergent taxa that may differ functionally due to other traits (Enquist and Bentley 2012).

In addition to MST, we also evaluate two other scaling models that invoke biophysical limitations to derive scaling exponents from first principles. As in Price et al. (2009), we consider the Stress Similarity model (STRESS; McMahon and Kronauer 1976) and the Geometric Similarity model (GEOM; Niklas 1994). The STRESS model assumes that for a trunk or branch there is a constant maximum biomechanical stress level maintained throughout (McMahon and Kronauer 1976). This assumption is based on engineering principles of stress levels in beams necessary to resist buckling. GEOM has been considered a null model of plant scaling (Price et al. 2009) and it assumes length and radius (or diameter) scale isometrically (i.e., $l \propto D$, leading to $b_l = 1$). These models (MST, GEOM, and STRESS) all make predictions assuming an allometrically ideal plant, that is, a plant that follows the assumptions laid out by any given general theory of allometric

scaling. An ideal plant is then model-specific. Thus, we refer to any given model prediction as an "ideal" prediction.

We do not explicitly consider the elastic similarity model (ELAS) (McMahon 1973, McMahon and Kronauer 1976) because the original fractal-branching model of WBE includes the assumption of elastic similarity (West et al. 1999) and thus MST and ELAS make similar predictions for the scaling of mass and length with tree diameter (Enquist and Niklas 2002, Price et al. 2010). Also, we do not consider models of increased complexity, such as the PES model described by Price et al. (2009) or models that include competitive interactions such as proposed by Muller-Landau et al. (2006) or Rüger and Condit (2012) because our goal is to focus on simple, universal scaling models that do not need specific environmental data. Specific allometric predictions for all models are in Table 2.1.

2.2.3 Data analysis: hierarchical Bayesian model

We used a hierarchical Bayesian (HB) approach to simultaneously estimate multiple scaling relationships using the general allometric power-law in Equation 2.1 where Y is the dependent variable or plant trait/characteristic, X is branch (or basal) diameter (hereafter D in equations), a is a normalizing constant, and b is the scaling exponent. Parameters were fit using the log-form of Equation 2.1:

$$\log(Y) \quad = \quad \log(a) + b \times \log(D), \tag{2.2}$$

because recent work suggests biological power-laws are best characterized assuming multiplicative error distributions (Kerkhoff and Enquist 2009, Xiao et al. 2011).

The hierarchical Bayesian approach allows us to explicitly model measurement error on independent variable D and allows for under-represented species to borrow statistical strength by assuming the allometric parameters come from some global population. Moreover, our approach allows us to simultaneously estimate tree, species, and interspecific level scaling parameters using

partial pooling (Gelman and Hill 2009).

To account for measurement error in diameter (D) for each observation i we used a Berkson "error-in-variables" model assuming 5% error on at least 5% of trees (Dellaportas and Stephens 1995) and used conditioning parameters from Price et al. (2009) to inform the prior error distribution, σ_ρ. We assumed measurement error to be log-normally distributed as:

$$\log(\rho_i) \quad \sim \quad N\left(\log(D_i), \sigma_\rho^2\right), \tag{2.3}$$

where ρ_i is the latent ("true") diameter for observation i and σ_ρ^2 is the measurement error variance. We used a multivariate normal likelihood to estimate the parameters of several scaling relationships simultaneously (Price et al. 2009):

$$\begin{bmatrix} \log(l_i) \\ \log(M_i) \\ \log(L_i) \\ \log(S_i) \end{bmatrix} \quad \sim \quad N\left(\begin{bmatrix} \log\left(a_{l,s(t(i))}\right) & b_{l,s(t(i))} \\ \log\left(a_{M,s(t(i))}\right) & b_{M,s(t(i))} \\ \log\left(a_{L,s(t(i))}\right) & b_{L,s(t(i))} \\ \log\left(a_{S,s(t(i))}\right) & b_{S,s(t(i))} \end{bmatrix} \begin{bmatrix} 1 \\ \log\left(\rho_i\right) \end{bmatrix}, \Sigma \right), \tag{2.4}$$

where a's are normalizing constants and b's are scaling exponents for the relationships between l (branch length), M (total aboveground biomass), L (leaf biomass), or S (stem biomass) and ρ, and Σ is a 4×4 covariance matrix. Subscripts i, t, and s refer to observation, tree, and species respectively and $s(t(i))$ indicates "species s associated with tree t associated with observation i".

As suggested by the subscripts, our analysis includes a hierarchical structure to explicitly account for the nested structure of our dataset (i.e. branches nested within individual trees; trees nested within species). Specifically, we account for data dependencies within species and within trees. We account for the fact that all branches within a given tree are related by including a "tree level" in the HB model (denoted by subscript t), but we do not account for specific parent-daughter branch relationships. Adding the amount of layers necessary to account for such dependencies in our hierarchical model is unreasonable due to our relatively small sample size. We acknowledge

this limitation but we believe the three-level structure described below is sufficiently conservative. Note that "tree level" does not refer to scaling exponents calculated using whole-tree data, but rather the tree level of the HB model.

Scaling exponents for the relationships between l, M, L, and S and D were calculated using the full dataset combining branch and whole-tree data at both a tree, species, and population level. Thus, for variable Y ($Y = l$, M, L, or S) and species s associated with tree t, the tree-level parameters, $a_{s(t)}$ and $b_{s(t)}$, are hierarchically drawn from species-level parameter distributions with prior:

$$
\begin{aligned}
a_{Y,s(t)} &\sim N\left(\bar{a}_{Y,s}, \sigma^2_{\bar{a}_Y}\right), \\
b_{Y,s(t)} &\sim N\left(\bar{b}_{Y,s}, \sigma^2_{\bar{b}_Y}\right),
\end{aligned}
\tag{2.5}
$$

where $a_{Y,s}$ and $b_{Y,s}$ are the intraspecific (species-specific) normalizing constants and scaling coefficients, and $\sigma^2_{\bar{a}_Y}$ and $\sigma^2_{\bar{b}_Y}$ are the within species variances describing tree-to-tree variability in the parameter. To assess the overall tendency of the model coefficients regardless of species but while still explicitly accounting for multiple sources of error (partial pooling) we define $\bar{a}_{Y,s}$ and $\bar{b}_{Y,s}$ as coming from an overall 'global' population (Price et al. 2009):

$$
\begin{aligned}
\bar{a}_{Y,s} &\sim N\left(A_Y, \sigma^2_{A_Y}\right), \\
\bar{b}_{Y,s} &\sim N\left(B_Y, \sigma^2_{B_Y}\right),
\end{aligned}
\tag{2.6}
$$

where A and B are the interspecific, population-level normalizing constant and scaling exponent, respectively. The variance terms ($\sigma^2_{A_Y}$ and $\sigma^2_{B_Y}$) describe the variability among species for both parameters. All priors (for error terms and the hyper-parameters A and B) were chosen to follow non-informative, uniform distributions (Gelman 2006). We used a non-informative Wishart distribution for the precision matrix (Σ^{-1}) in Equation 2.4 (Dietze et al. 2008, Gelman and Hill 2009, Price et al. 2009).

We used Markov chain Monte Carlo (MCMC) methods to estimate the joint posterior distributions of each parameter as implemented using JAGS (Plummer 2003) within the statistical package

13

'R' (R Development Core Team 2012). Three parallel MCMC chains were run with only the co-variance matrix Σ initially estimated to define the structure of the matrix. We obtained 1,000,000 iterations of each chain, thinned by 10, after discarding an initial 200,000 iterations as burn-in. We achieved convergence of MCMC chains as assessed using the Heidelberger (Heidelberger and Welch 1983) diagnostic within the 'coda' package of 'R' (Plummer et al. 2010).

Since our hypothesis is that environmental factors will influence plant allometries we also conducted the analysis above with additional explanatory variables from Table 2.2. We took two approaches: 1) we included mean annual precipitation, fire frequency, and percent tree cover as potential explanatory variables in Equation 2.4 (similar to the approach taken by Rüger and Condit (2012)), and 2) we included mean annual precipitation, fire frequency, and percent tree cover as hyperparameters in a regression equation that served as a prior for the species-specific normalizing constant ($a_{Y,s}$) in Equation 2.5. However, for both cases the posterior distributions for the coefficients of each variable (except diameter) broadly overlapped zero and r^2 values did not increase. Likewise, some parameters in our HB model did not achieve convergence with the extra variables included. This is most likely because the environmental variables (specifically mean annual precipitation and fire frequency) in Table 2.2 are taken from continental-scale, coarse-resolution remote sensing datasets. Even though those factors may be important for tree allometries in savannas, the data are not highly resolved enough to be statistically important.

2.2.4   Data analysis: posterior predictive checks

To check HB model fit we take a simple approach comparing replicated datasets as simulated from the model to the data that were used to estimate parameters (Gelman and Hill 2009). If the distribution of the simulated data is not congruent with the distribution of the real data then there may be problems with the model itself or with the prior probability distributions (Hobbs et al. 2012). Here we use posterior predictive checks (Gelman and Hill 2009) that use a test statistic from the replicated data (T^{rep}) and an identical test statistic from the real data (T^{obs}; following the notation of Hobbs et al. (2012)). Using these test statistics we test for lack of fit by calculating P_B,

the probability that the replicated data is more extreme than the real data:

$$P_B = \Pr\left(T^{rep}\left(y^{rep}, \theta\right) \geq T^{obs}\left(y, \theta\right) | y\right), \tag{2.7}$$

where θ is the vector of power-law parameters (a and b). The model shows lack of fit if P_B is near 0 or 1, since it is a two-tailed probability (Gelman et al. 2004). Values nearer 0.5 indicate no lack-of-fit. To assess goodness-of-fit we calculate correlation coefficients (r^2) between observed and replicated datasets. For our log-log regressions we used two test statistics, one to assess the ability of the model to capture the mean tendency of the data (Equation 2.8), and a second to assess the model's ability to portray the variation in the data (Equation 2.9). For each trait (length, mass, leaf mass, and stem mass) we used:

$$T^{obs} = \frac{\sum_{i=1}^{N} Y_i}{N} \quad , \quad T^{rep} = \frac{\sum_{i=1}^{N} Y_i^{rep}}{N}, \tag{2.8}$$

and

$$T^{obs} = \sum_{i=1}^{N} \frac{(Y_i - \mu_i)^2}{\mu_i} \quad , \quad T^{rep} = \sum_{i=1}^{N} \frac{\left(Y_i^{rep} - \mu_i\right)^2}{\mu_i}, \tag{2.9}$$

where Y_i is the real data, Y_i^{rep} is the replicated data, and μ_i is the model prediction for length, mass, leaf mass, or stem mass. Essentially, Equation 2.9 uses a sums-of-squares approach to evaluate model fit (Hobbs et al. 2012). We refer to the corresponding P_B values as P_B^{mean} and P_B^{fit} for Equations 2.8 and 2.9, respectively.

2.2.5 Data analysis: scaling model and exponent comparison

To compare the scaling models (MST, STRESS, and GEOM) we examined the mean, median, and 95% credible intervals (CIs) of the posterior distributions of the global exponents for scaling parameters estimated by our HB model. If a theoretical prediction is included in the 95% CI, then we consider that model supported by the data. More specifically, when the predicted parameters

of one of the scaling models fall within the CI of the empirical observations, that model cannot be excluded. We calculate the percentage of all CIs (at all hierarchical levels) that include the theoretical prediction of each model. We consider the scaling model with the highest percentage of inclusion to be the best model.

To compare scaling exponents for a particular relationship among species we examined the overlap of the 95% CIs. Further, we used the HB model to estimate the posterior distribution of the difference between exponents. We then used this distribution to calculate the probability that a difference between two exponents is greater than zero.

2.3 Results

2.3.1 HB model evaluation

All models explain $\geq 84\%$ of the variation for a given trait (Table 2.3). Posterior predictive checks show the HB model is capable of replicating data consistent with the mean of the observations, with all P_B^{mean} values near 0.5 (Table 2.3). However, the HB model is less able to accurately replicate the variability inherent in the observed data since all P_B^{fit} values are nearer to 1 or 0 than P_B^{mean} values (Table 2.3). In particular, when predicting diameter—length scaling there is much unaccounted variability ($P_B^{fit} = 0.048$). This greater variation in model fit for length and leaf mass scaling compared to aboveground mass and stem mass scaling is also reflected by lower r^2 values (Table 2.3). Raw data and fitted 'global' level allometries are shown in Figure 2.1.

2.3.2 Scaling exponents: tree, species, and 'global' levels

Within-trees there is considerable branch-level variability as indicated by the 95% CIs associated with tree-level means (Figure 2.2). Tree-to-tree variability of scaling exponents within species is extremely low for each trait scaling relationship (Table 2.4 and Figure 2.2 'Tree and branch level'). Only the scaling exponents for leaf mass scaling show substantial tree-to-tree variability (Figure 2.2D).

At the species level, only length scaling exponents show any interspecific variability. Fitted length scaling exponents are greater than predicted by MST and increase with mean annual precipitation (Figure 2.2A, 'Species level' and Table 2.2). Importantly, for the species on the extreme ends of the savanna gradient we sampled (*D. microcarpum* and *C. glutinosum*), there is a 99% probability that the difference between length scaling exponents is greater than zero (Figure 2.3). There is 76% probability the scaling exponents for *D. microcarpum* and *C. geitynophylum* are different, and a 92% probability the scaling exponents for *C. geitynophylum* and *C. glutinosum* are different (Figure 2.3). Similarly, the length-scaling normalization constants also show a directional trend, but with *D. microcarpum* having the lowest value and *C. glutinosum* having the highest value (Figure 2.4).

Given the low variance at the tree-level, species-specific exponents have 95% CIs that are primarily driven by branch-level variance, not tree-level variance. For example, for all trait scaling relationships and all species the average difference in CI width between the tree level and the species level is 0.037. However, species-level variance is greater than tree-level variance (Table 2.4). Except for the leaf mass scaling relationship, the normalization constants of *D. microcarpum* are lower than that of *C. geitynophylum* and *C. glutinosum* (Figure 2.4) and the 95% CIs do not overlap the means.

The combination of branch-level variability (95% CIs on tree means) and variability among species results in wide 95% CIs at the 'global', interspecific level (Figures 2.1 and 2.2). Tree-level variability does not contribute greatly to interspecific variation since that variance is low (Table 2.4). The 'global' means and associated 95% CIs indicate the overall distribution from which subsequent levels (tree and species) are derived. These distributions serve as indicators of 'naturally possible' scaling exponents regardless of species.

The scaling exponents arising from our dataset are generally consistent with those calculated in other studies using a diversity of species and tree functional types. For example, diameter-length scaling exponents tend to fall between values of approximately 0.3 – 0.8 (Muller-Landau et al. 2006, Dietze et al. 2008, Price et al. 2009, Moncrieff et al. 2011) and diameter-aboveground

biomass scaling exponents tend to fall between approximately 2.0 – 3.0 (Enquist 2002, Muller-Landau et al. 2006, Price et al. 2009). Few studies have examined the scaling of diameter to stem or leaf biomass specifically. But, our results for stem and leaf biomass scaling are consistent with those presented by Enquist and Niklas (2002) in their initial derivation of the proposed MST exponents. Likewise, our results for leaf mass scaling are broadly consistent with those presented by Price et al. (2009), using 2,362 individuals from over 100 species, that show leaf area scaling exponents (which are equivalent to leaf biomass exponents under the assumption that leaf biomass and area scales isometrically) to be in the range of approximately 1.3 – 2.8.

2.3.3 Scaling exponents: empirical support for theoretical scaling models

The wide 95% CIs at the 'global', interspecific level precludes the exclusion of any of the theoretical scaling models. However, the universal models we evaluated make predictions assuming species-specific normalizing constants that influence the scaling exponents (Enquist and Bentley 2012). Therefore, it is important to evaluate the models with reference to all the levels in our HB model (the tree and species levels). At the tree and species levels, GEOM is most supported for length scaling and MST under predicts the length scaling exponents (Figure 2.2A). MST is generally supported for aboveground mass scaling with STRESS receiving nominal support (Figure 2.2B). MST and GEOM make predictions for biomass partitioning and they perform reasonably well but with MST tending to under-predict and GEOM tending to over-predict wood-mass scaling (Figure 2.2C). For leaf-mass scaling MST and GEOM are equally well supported (since the predictions are identical) given their abilities to capture the means (Figure 2.2D). For all scaling relationships, and including all hierarchical levels (29 calculated exponents per scaling relationship), MST predictions are included in 75% of the credible intervals and GEOM predictions in 57%. For the two scaling relationships that all three models predict (length and aboveground mass) MST predictions are included in 70% of CIs, GEOM in 33%, and STRESS in 52%.

2.4 Discussion

Departures from the ideal predictions of scaling models that do not include environmental factors and variability are to be expected in natural settings where local conditions may select for modified allometries. As such, our goal was to evaluate the extent to which variable environments result in departures of tree allometries from ideal predictions. The ability to determine appropriate allometric relationships in trees is critical to scaling carbon and water fluxes from the leaf to the ecosystem level. Since there is an urgent need to better understand terrestrial dynamics of West African savanna ecosystems in light of current land use change (Anyamba and Tucker 2005) and future climate change (Held et al. 2005), here we calculated scaling exponents and tested the utility of popular allometric scaling models in these systems. Since savannas have variable rainfall, fire, and herbivory regimes, we aimed to determine if theoretical models of plant form based in metabolic and mechanical scaling models could successfully be used in these ecosystems to scale allometries.

2.4.1 Allometric convergence among and within savanna trees

Despite differences in bottom-up (mean annual precipitation, light availability) and top-down (fire, herbivory) forces important to savanna trees (Sankaran et al. 2004, Hanan et al. 2008, Hoffmann et al. 2012, Staver et al. 2012), tree and branch scaling from three species from three sites appear to converge on similar mean allometries describing stem length, total above ground biomass and the stem and leaf mass components of total aboveground biomass (Figures 2.2 and 2.4). Thus, it appears that scaling characteristics in savanna trees converge on mean relationships among and within trees, indicating that some set of universal scaling rules applies. While the mean scaling exponents overlap among trees, there are different amounts of variation associated with exponents at each hierarchical level as discussed below.

Across all species, the most variability in exponent estimations exists around the tree and branch level scaling exponents (Figure 2.2, 'Tree and branch levels' 95% CIs). This indicates

that branches may have a greater "scaling space" (Sperry et al. 2012) than trees due to different limitations on mechanical strength and resource transport related to network size. For example, saplings tend to violate the MST assumption of a space-filling branching, and thus elastic similarity (McMahon and Kronauer 1976, Niklas and Spatz 2004), and there is evidence branches violate this assumption as well (von Allmen et al. 2012). Likewise, it is important to note that had we included branches smaller than 2 cm in diameter our exponent estimates may have been more variable. von Allmen et al. (2012) show that branches where diameter (D) is less than 2 cm tend to violate the elastic similarity assumption. As such, our results are biased toward branches and stems that meet the elastic similarity assumption.

With regard to exponents, the greatest variation among and within individual trees occurs in the leaf mass scaling exponents (Figure 2.2D, 'Tree and branch levels'). It is well known that leaf area and biomass are variable in space and time at a variety of scales (Sultan 2000, Osada et al. 2001, Myneni et al. 2007). Thus, leaf biomass may be more plastic in response to micro-environmental conditions than other wood-based traits (aboveground and stem mass and length) that are more tightly linked to diameter through mechanical constraints (McMahon and Kronauer 1976) and metabolic efficiency (West et al. 1999). Discovering how micro-environmental conditions and tree size interact to produce tree- and branch-specific allometric relationships, and the width of allowable allometries, is an important avenue for future research.

2.4.2 Empirical support for theoretical scaling models

Previous tests of 'universal' scaling models of plant form and function have found only limited empirical support for the theoretical models considered here (Muller-Landau et al. 2006, Dietze et al. 2008, Price et al. 2009, Moncrieff et al. 2011, Rüger and Condit 2012). Our analysis shows that none of the models tested (MST, GEOM, and STRESS) can be definitively excluded at the 'global', interspecific level (Figure 2.2), though the models do differ in overall performance at the species and tree levels as also found in a comprehensive analysis by Price et al. (2009). This is particularly interesting given the broad climate and disturbance gradient from which the data

were gathered, the diversity of species considered (Table 2.2), and the fact that we tested these models using branch-level data. In aggregate, however, MST outperforms STRESS and GEOM in predicting the scaling relationships we observed across all levels (Figure 2.2). Many other studies also report support for the predictions and assumptions related to external branching architecture as defined by WBE and MST. For example, area-preserving branching has been widely reported (Shinozaki et al. 1964, Leopold 1971, Barker et al. 1973, McMahon and Kronauer 1976, Bertram 1989, Day and Gould 1997, Horn 2000, Sone et al. 2005, Renton et al. 2006, Dahle and Grabosky 2010, Costes and Guédon 2012), and recent studies find empirical support for elastic similarity (von Allmen et al. 2012) and self-similarity (Bentley et al. 2013). However, since the length-scaling exponents are most consistent with the predictions of GEOM (Figure 2.2), it will be important for future research to focus on the underlying assumptions of the competing models (Price et al. 2012). Only then can we truly identify departures from model predictions, as opposed to comparing data to an incorrect or incomplete model.

It is important to note that we did not consider models of differing complexity. Several authors have begun to relax MST assumptions (Price et al. 2007) or include competitive interactions (Muller-Landau et al. 2006, Rüger and Condit 2012) to better account for diversity in botanical form and function (Price and Weitz 2012). These more complex models have been shown to provide better fits to empirical data (Price et al. 2009). Though we did not evaluate such models here, since our focus was on strictly universal models and we did not have adequate data, it is likely they would outperform the models we did evaluate. Nonetheless, our analysis does indicate MST may best capture the underlying constraints on allometric relationships, so extensions of it may prove most useful (Price and Enquist 2007, Price et al. 2007).

2.4.3 Implications for MST in 'non-ideal' systems

Given the data in hand and the competing scaling theories we tested, we consider MST the 'best' model since its predictions were included in the greatest percentage of credible intervals

(see **Results**). If MST is considered the 'best' model, what can we conclude regarding deviations from MST predictions?

The most striking deviation from MST predictions occurs in the scaling of diameter to length (Figure 2.2A) where MST shows a strong trend for under predicting the scaling exponent. In concert with this deviation from the MST prediction, the length-scaling parameters display a clear directional trend among species: the exponents increase with mean annual precipitation and tree cover (Table 2.2, Figures 2.2A and 2.3) while the normalization constants decrease (Figure 2.4). The normalization constants absorb some of the environmental variation among sites, as predicted by MST (Enquist 2002) and reflected in our analysis (Figure 2.4), but not enough to produce convergent exponents. We consider this variation among species' scaling exponents to represent an ecologically important deviation from MST and hypothesize that the following biological processes may differentially influence the scaling of tree height and branch length in savannas at multiple levels: 1) long-term adaptation to fire in savanna trees, and 2) differences in the intensity of resource competition among sites. Environmental factors such as fire frequency, woody cover (proxy for light competition), and mean annual precipitation were not statistically important in our model, but, as discussed previously, this was likely due to the spatial resolution of the environmental data as opposed to their lack of importance.

Fire plays a critical role in regulating savanna structure by constraining recruitment of juvenile trees into adult classes (Hanan et al. 2008). As such, fire is a strong selective force in savannas (Bond and Keeley 2005, Bond et al. 2005, Bond 2008, Staver et al. 2011*a;b*), and trees in fire-prone ecosystems may benefit from rapid vertical growth to escape the fire zone (Gignoux et al. 1997, Archibald and Bond 2003, Hoffmann et al. 2003). Therefore, we would expect, and our data shows, length-scaling exponents to trend toward values greater than expected from MST. As has been suggested before (Archibald and Bond 2003, Hoffmann et al. 2003; 2009), we hypothesize that savanna trees have evolved, via natural selection, to allocate growth toward height or branch length at the expense of mechanical stability and optimization of resource transport. Fire is a selective force in savannas that overrides the first-order optimization of plant vascular networks in response

to physical (water and nutrient transport) and mechanical (buckling) constraints. All species in our dataset reflect the allometric influence of fire toward a greater exponent, even while showing some interspecific variability (Figure 2.2A). Trees in South African and Brazilian savannas have shown qualitatively and quantitatively similar allometric trends (Archibald and Bond 2003, Dodonov et al. 2011, Moncrieff et al. 2011), suggesting a universal trade-off in savannas between fire escape and mechanical stability and optimization of resource transport.

While fire can explain overall deviation from the MST prediction, multiple selective pressures related to resource competition may be operating simultaneously at the intraspecific level (Figures 2.4A and 2.4). For example, light has been shown to influence forest tree allometries (Muller-Landau et al. 2006) and predictions based on optimal partitioning theory indicate that plants in reduced sunlight shift allocation toward height to gain a competitive advantage for light capture (McConnaughay and Coleman 1999). Since our calculated intraspecific exponents for length scaling increased with precipitation and woody cover (Table 2.2, Figures 2.2A and 2.3), our results are consistent with this theory. In dense savannas, as in forests, the competition for light may select for modified allometries with scaling exponents for diameter vs. height/length greater than 0.67 as observed here (Figure 2.2A). However, light competition in savannas has received very little attention, and water may still be the limiting factor. In that case we would not expect a light response in allometries. The directional trend observed among species could also be explained by an interaction between a bark thickness—height growth tradeoff and access to resources. Work in African, Australian, and Brazilian savannas suggests top-kill/mortality of savanna trees due to fire is most correlated (negatively) with bark thickness (Gignoux et al. 1997, Hoffmann et al. 2009, Lawes et al. 2011). Thus, Lawes et al. (2011) argue that fire escape height is better conceived as the height required to attain bark thick enough to resist fire damage; as opposed to simply being tall enough to avoid branch inflammation. Trees in fire-prone savannas must invest biomass in bark growth at the expense of height growth (Lawes et al. 2011). It follows, then, that this trade-off may be more pronounced in arid savannas where moisture is more limiting to overall growth. Then, as observed in this study, the fire response in arid savannas would lead to lower length-scaling

exponents than in more mesic savannas (Figure 2.2A). This proposed interaction among height (or length), bark thickness, and resource availability has yet to be thoroughly investigated (but see Gignoux et al. 1997).

In addition to light availability and fire frequency, browsing can also lead to intra and interspecific variation of length scaling and has been shown to influence savanna tree architecture (Archibald and Bond 2003, Moncrieff et al. 2011, Staver et al. 2012). Our dataset did not come from sites with large browsers, but interestingly, length-scaling exponents calculated for South African savanna trees protected from and exposed to large browsers (e.g., giraffe) are remarkably similar to our estimates (in the range of 0.57-0.74; Moncrieff et al. 2011). Moncrieff et al. (2011) do show that browsing can decrease length-scaling exponents below both our calculated value and the MST predicted value. However, the deviations from MST observed by Moncrieff et al. (2011) on trees subject to browsing may reflect near-term physiological responses to mechanical damage rather than long-term adaptations in growth strategy as proposed here.

2.5 Conclusions

Ultimately, observed plant allometries in any system will reflect some combination of multiple trade-offs that may be difficult to capture in general theories of plant form and function, such as MST. Deviations from the predictions of MST make intuitive sense when we consider the multiple costs, benefits and selective forces active in savannas. While plant architecture may reflect, in part, the morphological adaptations that optimize the efficiency of resource transport, when subject to selective forces unrelated to transport (e.g. mortality of shorter individuals in fire, or competition with neighbors for light) we can anticipate selection of traits (e.g. longer branch node-lengths) that balance the benefits of 'escape' from fire and competition with the potential mechanical and transport 'costs' associated with longer and thinner branches. However, unlike Moncrieff et al. (2011) who conclude that general theories including MST may be "neither general nor predictive in systems with frequent disturbance", we find that, even in disturbance-prone savannas, MST is

generally consistent with observations (i.e. allometries for leaf, stem, and total mass). Further, in those situations where observations are inconsistent with MST (i.e. stem length) we find that departure from theory corresponds with expected tradeoffs related to disturbance and competitive interactions. Thus, we suggest two future research priorities: 1) detailed studies that empirically test the validity of model assumptions related to length scaling and 2) theoretical work aimed toward quantitatively predicting the magnitude and direction of allometric modifications in response to selective drivers other than core physical principles. In combination, such work could lead to an improved plant scaling model that best represents observed scaling relationships in variable ecosystems.

2.6 Tables

Table 2.1: Model predictions for scaling exponents (*b*).

Scaling Model	Length	Aboveground Mass	Stem Mass	Leaf Mass
Metabolic Scaling Theory (MST)	2/3	8/3	8/3	2
Stress Similarity (STRESS)	1/2	5/2	NA	NA
Geometric Similarity (GEOM)	1	3	3	2

Note: The scaling exponents all refer to *b* in Equation 2.1 where the dependent variable (*X*) is diameter. For example, the 2/3 in the upper-left cell shows that under Metabolic Scaling Theory length is proportional to diameter to the 2/3 power ($l \propto D^{2/3}$).

Table 2.2: Site characteristics.

Site	Species	MAP (mm y^{-1})	Woody cover (%)	Domestic animal density	Fire frequency (y^{-1})
Tiendéga	*Detarium microcarpum*	1400	60.3	Low	0.35
Tiorola	*Combretum geitynophylum*	1200	61.3	Medium	0.5
Lakamané	*Combretum glutinosum*	570	12.4	High	0.9

Notes: Woody cover was estimated Sep.-Oct. 2008. Provisional estimates of the relative density (high/medium/low) of domestic animals were also made at that time. Fire frequency estimates were extracted from mapped continental-scale data. MAP = mean annual precipitation.

Table 2.3: Posterior predictive checks of the HB model.

Trait	r^2	P_B^{mean}	P_B^{fit}
Length	0.85	0.500	0.049
Aboveground mass	0.94	0.502	0.258
Stem mass	0.95	0.501	0.255
Leaf mass	0.85	0.502	0.369

Note: We calculated three test statistics: 1) Pearson's r^2 assessing the correlation between the observed data and the replicated data, 2) P_B^{mean} to assess the ability of the model to capture the mean tendency of the data, and 3) P_B^{fit} based on a sums-of-squares approach to assess overall model fit including its ability to capture data variability. A value of P_B (for both *mean* and *fit*) near 0 or 1 indicates lack of fit; values near 0.5 are acceptable.

Table 2.4: Variance components of the hierarchical Bayesian model for each scaling relationship (diameter vs. trait).

Trait	Tree-level variance ($\sigma^2_{b_Y}$)	Species-level variance ($\sigma^2_{B_Y}$)
Length	0.0016 (1.71×10^{-6}, 0.007)	0.2700 (0.002, 2.281)
Aboveground mass	0.0003 (2.77×10^{-7}, 0.002)	0.1323 (1.83×10^{-5}, 1.385)
Stem mass	0.0003 (2.77×10^{-7}, 0.002)	0.1698 (3.99×10^{-5}, 1.676)
Leaf mass	0.0160 (3.18×10^{-5}, 0.067)	0.2160 (3.56×10^{-5}, 2.026)

Note: Means are shown with 95% credible intervals displayed in parentheses.

2.7 Figures
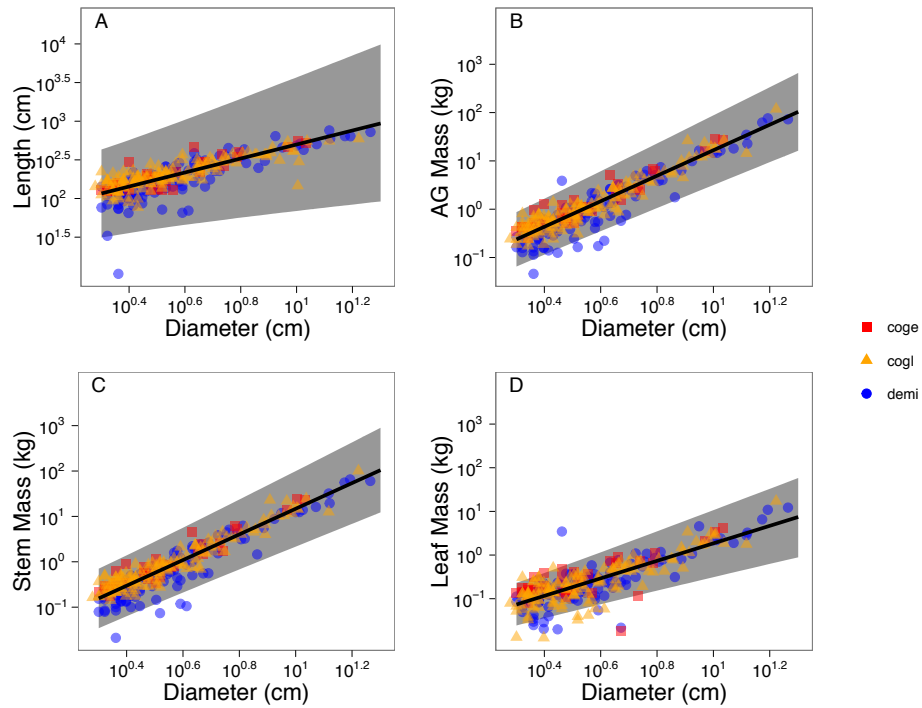
Figure 2.1: Fitted allometries for each allometric relationship using global level parameters. The symbols correspond to species as shown in the legend and are semi-transparent to show overlapping points. Lines show global level (interspecific) mean fit and the shaded regions are the 95% credible intervals. Note that all plots are in log-log space. Species codes: demi, *Detarium microcarpum* (MAP = 1400 mm y^{-1}); coge, *Combretum geitynophylum* (MAP = 1200 mm y^{-1}); cogl, *Combretum glutinosum* (MAP = 570 mm y^{-1}).
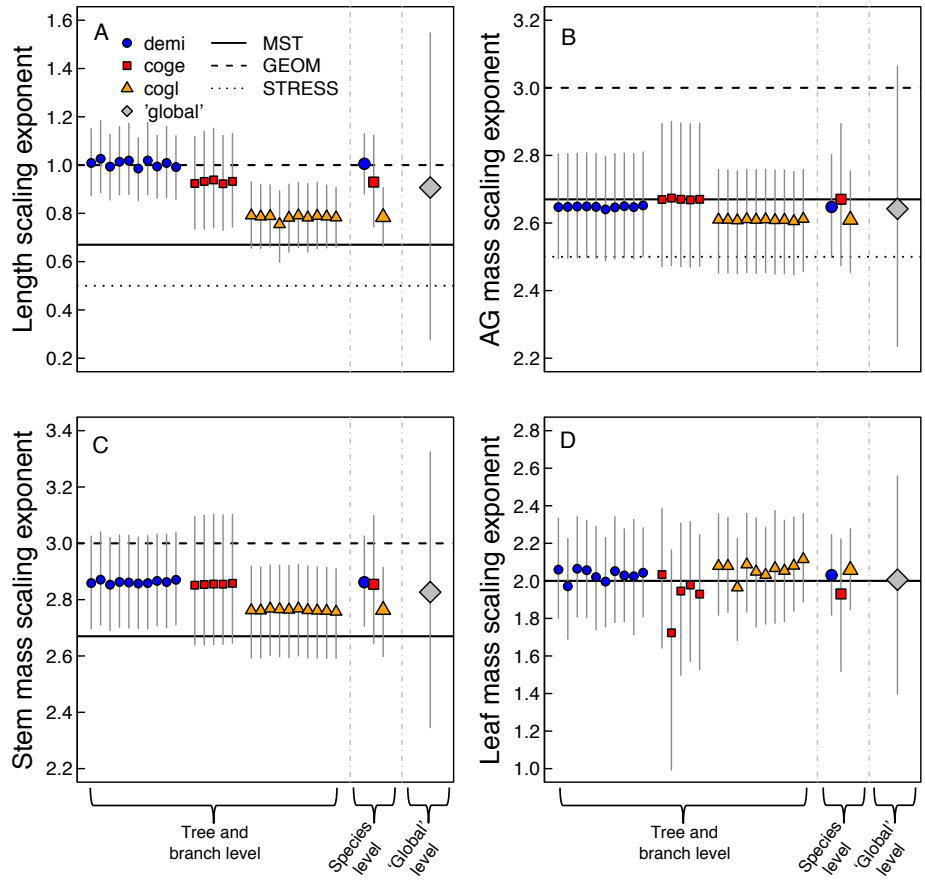
Figure 2.2: Posterior means and 95% credible intervals of scaling exponents (*b*) at different hierarchical levels. Symbols correspond to the species and the large diamond represents the interspecific, global-level scaling exponent. 95% credible intervals are shown as vertical lines on means. The levels along the *x*-axis refer to levels in the hierarchical Bayesian model. The horizontal lines represent the theoretical predictions of the three scaling models (note that in *D* MST and GEOM make the same prediction, see Table 2.1). Species codes are as in Figure 2.1. AG mass = aboveground mass.
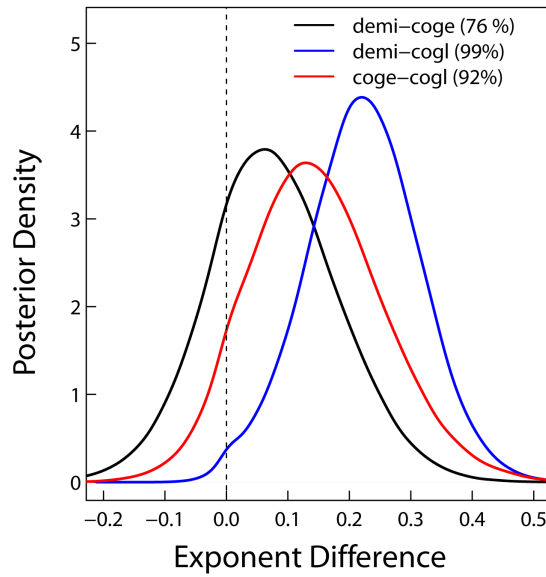
Figure 2.3: Posterior densities of the difference between species-specific diameter-length scaling exponents (b_l). The dashed line shows a difference of zero. Species contrasts are indicated by color as in the legend where "demi—coge" means the scaling exponent of *D. microcarpum* minus the scaling exponent of *C. geitynophylum*. The probability that a specific difference is greater than zero (which can be considered a significant difference between exponents) is displayed in parentheses in the legend. Species codes are as in Figure 2.1.
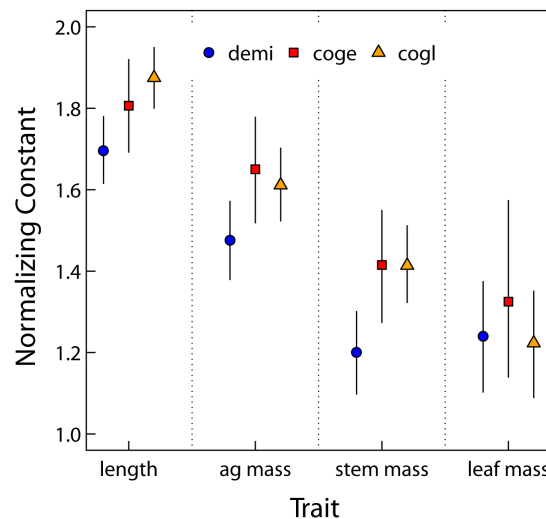
Figure 2.4: Species level posterior means and 95% credible intervals of normalization constants (*a*). Species codes are as in Figure 2.1 and "Traits" along *x*-axis refer to the scaling of diameter with that trait (e.g., "length" refers to the normalizing constants for the scaling relationship $l = aD^b$). Symbols correspond to the species and 95% credible intervals are shown as vertical lines on means.

Chapter 3

Estimates of aboveground woody biomass in the savannas of Mali (West Africa) using moderate resolution satellite data[2]

Summary

The woody component of savannas in Mali, West Africa provides essential provisioning and regulating ecosystem services. Over 90% of Malian people depend on wood biomass as fuelwood for cooking and there is potential for Mali to engage in international programs such as UN REDD by quantifying the distribution and amount of carbon and biomass stored in the nation's trees. However, the availability of reliable, cost effective, and easy-to-implement methods to estimate aboveground woody biomass in developing nations can impede inclusion in UN REDD or similar programs. Likewise, without spatially-explicit estimates of biomass density throughout the country, those charged with managing Mali's vast savannas face challenges in decision-making. We make use a large database of field-measured vegetation structure, together with freely available moderate resolution (30 m) satellite data (Landsat TM 5 optical data) and straightforward statistical techniques to estimate the spatial distribution of aboveground woody biomass in non-desert Mali. Using observations of wood volume from 157 sites distributed throughout Mali, we used cross-validated multiple linear regression to predict woody biomass from Landsat TM reflectances and spectral indices and a soil albedo dataset. Final predictor variables were chosen by backwards and forwards model selection based on Bayesian Information Criterion (BIC). The best model had a cross-validated $R^2 = 0.37$ and root mean square error (RMSE) of 13.76 Mg ha^{-1}. We extrapolated the model to the entirety of non-desert Mali and estimate total aboveground woody biomass to be 997.37 Gt. Assuming biomass is 50% carbon, total aboveground carbon storage in

---

Mali's trees is 498.68 Gt C. Even though our estimates are associated with high uncertainty, our nationally-derived estimate for total aboveground woody biomass is much higher than reported by continental and global scale efforts that tend to focus on forested regions and either underestimate or ignore woody biomass in savannas. We anticipate the future availability of pre-processed radar data will substantially improve our estimates and reduce model uncertainty. Nonetheless, this work represents the best-available woody biomass map for Mali, and future efforts can build on this work.

3.1 Introduction

Savannas account for ~20% of the global land surface and are increasingly being recognized for their large stores of carbon (Hill and Hanan 2011). Moreover, in developing regions the woody component of savannas provides key ecosystem services, including fuel and building materials (Arnold et al. 2006). Yet, great uncertainty surrounds estimates of woody biomass in savanna systems. The complex three-dimensional structure of savannas (i.e., the mixture of trees and grass) induces serious challenges to our ability to separate tree and grass biomass components. This has led to uncertainty in carbon density estimates in savannas and a bias toward remote assessment of biomass in tropical rain forests where the canopy structure is more uniform and amenable to remote sensing capabilities (Baccini et al. 2008, Saatchi et al. 2011, Hansen et al. 2013). However, given the economic importance of savannas in providing critical ecosystem services and the need for developing regions in Africa to account for carbon storage under the UN REDD program (Grassi et al. 2008), there is an urgent need to better quantify aboveground woody biomass in African savannas using remote sensing technology (Mitchard et al. 2009).

Savannas are mixed tree-grass systems that are highly variable in space and time (Sankaran et al. 2005; 2004, Scholes and Archer 1997). Tree cover is primarily a function of mean annual precipitation and edaphic constraints at large spatial extents (Good and Caylor 2011, Sankaran et al. 2005) but at smaller extents is further influenced by fire (Staver et al. 2011*a*;*b*), herbivory

(Bucini and Hanan 2007, Bucini et al. 2010), and other disturbances, such as fuelwood harvest. The result is an uneven distribution of trees with varying architectures on the landscape, which makes remote estimation of wood biomass at stand level (i.e. 1 ha) difficult. For example, often the field measures of biomass (stand volume, e.g.) do not relate readily to what is retrieved by remote sensors (Lucas et al. 2011). This creates a special challenge to passive, optical sensors such as Landsat TM and MODIS because reflectances may confound tree and grass components.

Using radar data, which can relate to woody biomass via backscatter intensification by branches and trunks, in combination with optical data can improve biomass estimates (Mitchard et al. 2009, Carreiras et al. 2012). However, over large areas (e.g., countries and continents) it is computationally-intensive to process and fit models to relatively high-resolution radar products like ALOS PALSAR (spatial resolution = 15 m). Thus, while advances in radar technology undoubtedly hold promise for remote estimation of biomass in mixed tree-grass systems, the sheer technological demands of using the data can preclude wide-spread use in developing nations where repeat analyses of country-wide biomass stocks are necessary for UN REDD programs.

Given the technical challenges of using radar data (until pre-processed, mosaicked data is readily available), our aim in this paper is to test whether optical data alone can adequately estimate aboveground woody biomass in Mali, West Africa. This represents an excellent test of remote sensing abilities in savannas because a strong environmental gradient exists in Mali driven by a precipitation gradient from 0 mm mean annual precipitation (MAP) in the Sahara desert to >1,500 mm MAP in the south of the country. Tree cover broadly follows this gradient leading to sparse tree densities in the Sahelian savannas to high-density woodlands in the south. This paper provides the best-available wood biomass density map for Mali, but there is high uncertainty in our estimates due to the limitations of optical data. This map can be used to quantify carbon stores and the availability of other key ecosystem provisioning services in terms of wood available for cooking and construction. This is especially important since previous studies conducted at continental (Baccini et al. 2008) and global (Saatchi et al. 2011, Hansen et al. 2013) extents report relatively low biomass quantities for Mali. In contrast, we report much higher estimates even when con-

sidering large uncertainty. Once available, including ALOS-PALSAR data in our analysis should greatly improve the accuracy of our biomass estimates.

3.2 Study area

Mali is a vast country in West Africa composed of diverse biomes ranging from the Sahara desert in the north to dense woodlands in the far south. There is a strong rainfall gradient in southern Mali ranging from less than 200 mm mean annual precipitation (MAP) to over 1,500 mm MAP (Fig. 3.1(a)). Thus, the savannas of Mali vary greatly in tree canopy cover and density; leading to an excellent test of, and a serious challenge to, remote sensing estimation of aboveground woody biomass. For this analysis we consider only non-desert Mali (approximately where MAP > 200 mm; see Fig. 3.1(a)).

3.3 Methods

3.3.1 Field based AGB estimates

We compiled a database of 157 field sites where volume of wood was measured and extrapolated to 1-ha plots. Field measurements of wood volume were collected in undisturbed and secondary savanna vegetation over multiple field seasons, mostly between between 2007 and 2008. At each field site, a 50×20m or 50×50m plot was delineated and within the plot circumference at breast height (1.3m) was measured for all trees with circumference $\geq$ 10cm. These circumference measurements are used to estimate total basal area (G; m^2) in the plot using the formula:

$$G = \frac{C^2}{4\pi} \tag{3.10}$$

where C is circumference at breast height. Volume of wood in the plot is calculated using the formula:

$$V = 10 \times P \times G \qquad (3.11)$$

where V is wood volume (m^3) in the plot, P is average site rainfall (in meters), G is the basal area, and 10 is constant value based on empirical fits (Clément 1982). Volume (V) in the plot is then extrapolated to the hectare scale so that all measurements are in units of m^3 ha^{-1}. Most sites are located in remote areas with low probability of major disturbance (e.g. clearance for agriculture) and low growth rates. We therefore consider the field measurements representative of conditions in the 2006-2007 periods for when satellite were collected.

We converted volume (m^3 ha^{-1}) to biomass (kg ha^{-1}) using the average wood density of trees in Africa from the Global Wood Density Database (Zanne et al. 2009). The 1 ha plots range from moist, densely wooded savannas in the south of Mali, to drier, Sahelian savannas in the north and east (Figure 3.1(a)). The data covered a woody biomass range from 0.075-87.9 Mg ha^{-1} with a mean = 14.11 Mg ha^{-1} and std. dev. = 17.34 (Figure 3.1(b)).

3.3.2   Remote sensing data

3.3.2.1   Landsat TM 5 data

We downloaded 47 Landsat TM 5 (LT5) scenes covering non-desert Mali processed at the L1T level (precision and terrain corrected) from the USGS Global Visualization Viewer[3]. All images are from 2007 (except for one scene from late 2006 due lack of availability in 2007) because that year had the most available scenes. Our selection criteria were as follows: 1) cloud cover < 90% and 2) from late dry season (January – April) to reduce potential confounding effects of herbaceous biomass on detection of tree canopies. All scenes were pre-processed using the LEDAPS tool provided by NASA (Masek et al. 2006). The LEDAPS processing procedure calibrates images us-

---

[3]Can be accessed at http://glovis.usgs.gov/.

ing scene-specific on-board lamp brightness values, corrects digital numbers to top-of-atmosphere (TOA) reflectances, and finally performs an atmospheric correction using MODIS/6S methods.

The LEDAPS atmospheric correction reduces scene-to-scene differences, but residual variation among scenes may exist due to differences in scene geometry and atmospheric conditions. Thus, we chose to further process the LT5 scenes using a relative normalization technique based on comparison of pixels in image overlap regions (Olthof et al. 2005). We first normalized within paths, since the acquisition dates were more similar, then normalized among paths using path mosaics of the within-path normalized scenes. In overlapping regions we removed outliers (reflectance values exceeding +/- five standard deviations from the mean of the sample), sampled 500,000 random points from each of the overlapping scenes, and performed a reduced-major axis regression. Within paths, we chose the northern-most scene as the 'master' because these scenes were all cloud and haze free. Thus, the scene to south was normalized relative to the 'master' and then that scene became the 'master' scene for the subsequent scene to its south. For the among-path normalizations we chose the path in the center of the resulting mosaic (path 197) as the master path for relative normalization.

We aggregated all normalized path mosaics (LT5 bands 1, 2, 3, 4, 7) to a pixel resolution of 100 m. This approach has the benefit of smoothing out image errors and allows us to work at a pixel resolution that matches our field-measured data (100×100 m = 1 ha). Working at 100 m resolution and on the normalized paths, we calculated several vegetation indices: normalized difference vegetation index (NDVI; Tucker 1979), enhanced vegetation index (EVI; Huete et al. 2002), and soil adjusted vegetation index (SAVI; Huete 1988). NDVI was calculated in the normal fashion as

$$NDVI = \frac{NIR - RED}{NIR + RED},$$
(3.12)

where *NIR* is near infrared reflectance (LT5 band 4) and *RED* is the visible red reflectance (LT5 band 3). We calculated EVI as

$$EVI = 2.5 \left(\frac{NIR - RED}{NIR + aRED - bBLUE - L} \right),$$
(3.13)

36

where *NIR* and *RED* are as in equation 3.12, *BLUE* is the visible blue reflectance (LT5 band 1), and the constant parameters a, b, and L are set to 6, 7.5, and 1 following Huete et al. (2002). Lastly, we calculated SAVI as

$$SAVI = \left(\frac{NIR - RED}{NIR + RED + L} \right) (1 + L), \qquad (3.14)$$

where, in contrast to equation 3.13, $L = 0.5$ (Huete 1988). Pixel values from path mosaics served as predictor data in our statistical analysis.

3.3.2.2 Soil albedo data

We used bare soil albedo data to account for variable soil backgrounds that may influence surface reflectances. We used a spatial database from Western Africa at 1 km resolution that includes soil albedo reflectance in the visible (0.3-0.7 μm; ρ_{vis}), near infrared (0.7-1.4 μm; ρ_{nir}), and shortwave infrared (1.4-3 μm; ρ_{swir}) produced by Kaptué et al. (2010). The original albedo scene (all of Western Africa) was subset and warped to Landsat path mosaics at 100m resolution with root mean square error less than 20 m (<0.67 Landsat pixel at native 30m resolution; <0.2 Landsat pixel at 100m resolution) for each scene.

3.3.3 Statistical analysis

We used multiple linear regression to develop a predictive model of above ground woody biomass (AGWB) from remote sensing data. We used backwards and forwards step-wise regression with variable selection based on BIC, where the penalty is $k = \log(n)$ at a significance level of $\alpha = 0.05$. Prior to running the analysis we excluded predictor variables that were highly correlated (Pearson's $\rho > 0.9$), leaving six variables (Tables 3.1 and 3.2). All variables that we dropped from the analysis were highly correlated with at least two other variables except for TM band 2, which was highly correlated with TM band 3 (Table 3.1). In this case, regardless of which band (2 or 3) we left out of the full model, our results did not change. To account for non-linear responses between AGWB and remote sensing variables we *a priori* included squared terms for each predictor variable and the following interaction terms: NDVI$\times\rho_{nir}$ and EVI$\times\rho_{nir}$. Thus, the full model

37

for which stepwise selection was carried out included 15 predictor variables (6 original terms, 6 squared terms, and 2 interaction terms). If an interaction or squared term was selected by the BIC, the non-transformed variable(s) were included in the final model.

Instead of separating our data into training and validation sets we performed cross-validation on the final model as selected by BIC. We used the 'CVlm' procedure within the 'R' package 'DAAG' to perform 10-fold cross-validation. From this procedure we retrieved cross-validated predictions used to assess model performance.

We assessed model performance by calculating three statistics: (1) root mean square error (RMSE), (2) the coefficient of determination (R^2), and (3) biomass classification accuracy. We calculated RMSE and R^2 as:

$$\text{RMSE} = \sqrt{\frac{1}{n}\sum_{i=1}^{n}(f_i - y_i)^2} \tag{3.15}$$

$$R^2 = 1 - \frac{SS_{\text{reg}}}{SS_{\text{tot}}} = 1 - \frac{\sum_{i=1}^{n}(f_i - \bar{y})^2}{\sum_{i=1}^{n}(y_i - \bar{y})^2} \tag{3.16}$$

where f_i is the model prediction for observation y_i, $\bar{y}$ is the average of the observations, and n is the number of observations. To calculate biomass classification accuracy we classified biomass observations and predictions into discrete bins (10 Mg ha^{-1} bin widths) and calculated the percentage of predictions assigned accurately.

Recent statistical and computing advances have led to improved techniques for building models that can account for complex responses between predictor variables and response variables. In the remote sensing literature, machine learning approaches such as MaxEnt (Saatchi et al. 2011), stochastic gradient boosting (Carreiras et al. 2012), and classification and regression trees (Hansen et al. 2003, Baccini et al. 2008) have been used with success. Also, in situations where model selection is highly dependent on the input data, bootstrapping of models can produce better estimates of model parameters (Carreiras et al. 2012). For our purposes, any method that bins data into discrete categories (e.g., MaxEnt and regression trees) is inappropriate and provided poor prediction because our data spanned a relatively small biomass range with many small values (Fig. 3.1(b)).

We tried the approach of Carreiras et al. (2012) by bagging the results of several stochastic gradient boosting models, but the model did not offer enough improvement to warrant the computational expense of predicting from that model for our entire study area. In the end, our multiple linear regression approach proved no worse than the advanced methods discussed above.

To account for uncertainty in our biomass estimates we use upper and lower 95% prediction intervals for each pixel. Prediction intervals for biomass estimated at each pixel (B_p) were calculated as:

$$B_{\pm 95} \quad = \quad B_p \pm t_{0.025, df=156} \times s, \tag{3.17}$$

where $B_{\pm 95}$ is the upper or lower prediction interval, t is the two-tailed critical value at $\alpha = 0.05$, and s is the residual standard error from the multiple linear regression model used to estimate B_p (s = 13.33). We report uncertainty in aggregated biomass estimates as $\pm\%$ based on the comparison between the sum of B_p and the sum of the upper 95% prediction intervals for each pixel. Since our statistical model does not include spatially-varying parameters, the residual error (s) is equal across all pixels. Thus, the $t_{0.025, d.f=156} \times s$ term in Equation 3.17 is equal across all pixels. All pixels are therefore scaled by ± 26.66 Mg ha^{-1} with a lower limit of 0 Mg ha^{-1}.

3.4   Results and Discussion

The final model included NDVI, ρ_{NIR}, and $(\rho_{\text{NIR}})^2$ as significant predictors of AGWB (Table 3.3). Model residuals are approximately normally distributed. As expected, AGWB is positively correlated with NDVI and negatively correlated with near-infrared albedo. The albedo terms likely represent the influence of bare ground. The model has a cross-validated RMSE = 13.76 Mg/ha and R^2 = 0.37 leaving over 60% of the variation in AGWB unexplained, and a classification accuracy of 52.2%. The relatively high RMSE and low classification accuracy is particularly problematic for estimation in low biomass areas. We anticipate that the inclusion of radar data that can accurately

detect canopy structure would lead to better estimation of low biomass areas and a lower RMSE. We plan to incorporate ALOS-PALSAR data as it becomes available.

In the validation plot (Fig. 3.2), a high density of points are scattered near the 1:1 line at low biomass (0-25 Mg/ha) but there is a tendency for the model to over-predict some low biomass sites and under-predict high biomass sites. This is likely due to our observation data being skewed toward low biomass sites (i.e., very few high biomass points to train the model) and our lack of radar data (radar data will likely improve our estimation of low biomass sites). Even though there are notable deviations from the 1:1 line, the densest cloud of points remains centered near perfect agreement. This indicates our model is suitable for estimating broad trends in biomass density, but may be inadequate to estimate local deviations.

When applied to the entirety of non-desert Mali our model appears to capture the expected spatial trend of biomass density from the south to the north (Fig. 3.3(a)). However, the use of albedo reflectance data does result in artificially-high biomass estimation in northeastern Mali (see green stripping in upper-right portion of Fig. 3.3(a)). In this region of Mali, albedo may be distorted by geomorphic features such as sand dunes and rock outcroppings. This indicates the potential need to stratify our model into different categories, but we lacked sufficient data to do so. Future efforts should focus on gathering evenly-distributed biomass data across wet and dry regions in Mali. Likewise, our model over-predicts biomass in densely populated cities such as the capitol of Mali, Bamako (see dark green patch in south-central Mali in Fig. 3.3(a)). This may arise for two reasons: 1) high albedo values that greatly influence the model through the $(\rho_{NIR})^2$ term, and/or 2) relatively high NDVI values due planting of trees in the city. Whether our estimates are correct in Mali's cities requires further investigation and potentially a statistical approach that stratifies biomass predictions by city/non-city areas.

Based on our model as extrapolated spatially for all of non-desert Mali, we estimate total aboveground woody biomass in Mali is 997.37 Gt ($\pm$39.7%). The distribution of our estimates reflects the spatial dominance of low-biomass savannas and near-deserts in Mali (Fig. 3.3(b)) and adequately captures the mean of our training data but with lower standard deviation about the mean

(mean$_{estimate}$ = 17.55, mean$_{observations}$ = 14.11; std. dev.$_{estimate}$ = 11.61, std. dev.$_{observations}$ = 17.34). Thus, the bulk of Mali's biomass is in low-biomass regions. This implies that significant effort should be put toward managing savannas in countries with large expanses of low-biomass areas such as Mali, rather than a sole focus on tropical forests and dense woodlands. Indeed, about 50% of Africa's land surface can be classified as savanna. Carbon-accounting efforts through programs such as UN-REDD and UN-REDD+ must take into account that large countries, even without large areas of tropical forest, can contain significant amounts of aboveground carbon. If we assume carbon represents about 50% woody biomass (as in Saatchi et al. 2011), our estimate of aboveground carbon storage in Mali is 498.68 Gt C ($\pm$39.7%).

Our estimates show broad agreement with the most recent effort to globally map biomass density by Saatchi et al. (2011) (Fig. 3.4). Saatchi et al. estimated total aboveground biomass rather than just the woody component, but their effort was centered on estimating biomass in tropical forests. Thus, the methods they employed and the training data they used resulted in a model that primarily related remote sensing reflectances and returns to woody biomass and tree cover. Their main approach was to relate height information from ground plots or Lidar returns to optical and microwave imagery to extrapolate carbon density across the landscape. Therefore, we consider the Saatchi et al. estimates to primarily represent woody biomass, even in savannas.

Our estimate of AGWB in Mali (997.37 Gt) is 1.4$\times$ larger that that estimated by Saatchi et al. for total aboveground biomass (715.91 Gt). Our level of uncertainty ($\pm$40%) is similar to pixel-level ($\pm$38%) and continental-level ($\pm$32%) uncertainties reported by Saatchi et al. (2011). At the pixel level there are very few areas where our estimates and those of Saatchi et al. disagree by more than 20 Mg/ha (Fig. 3.4(a)). However, there is a general trend where, compared to Saatchi et al., our estimates are lower in the southwest and higher in all other areas. Notably, our model predicts very few areas where woody biomass is absent, whereas Saatchi et al. estimates include many pixels that fall within 0-5 Mg/ha (Fig. 3.4(b-c)). Overall, our approach results in more evenly distributed biomass across Mali, especially in low-biomass classes (Fig. 3.4(b-c)). This could be due to our model responding to grass reflectance, but all TM 5 images were from the dry season

where grass biomass (and greenness) would be at a minimum. Alternatively, our nationally-based model may be more equipped to respond to low-biomass pixels because we are working across a more restricted range of biomass densities than global efforts like Saatchi et al. (2011).

3.5 Conclusions

We have presented the best-available woody biomass density map for Mali, West Africa. Although uncertainty in the estimates is high at the pixel level, our estimates compare favorably to recent biomass mapping efforts. Inclusion of radar data, once available, will likely reduce our uncertainty. Our woody biomass map shows that much of Mali's biomass is in low-biomass regions. Thus, efforts aimed at conserving woody biomass and carbon-accounting may need to consider that large countries store large amounts carbon even when tropical forests are absent from their landscapes. We hope this map can be used to begin biomass tracking in Mali and to inform ecosystem stewardship efforts to most equitably distribute wood biomass for human appropriation. In Mali about 90% of the population depends on wood biomass for cooking, and this map can serve as a useful tool for those managing Mali's woodlands and savannas for conservation and appropriation.

3.6 Tables

Table 3.1: Correlations between potential predictor variables. Correlations greater than ± 0.9 are shown in bold.

	NDVI	b_1	b_2	b_3	b_4	SAVI	EVI	ρ_{VIS}	ρ_{NIR}	ρ_{SWV}
NDVI	...	-0.15	-0.69	-0.76	-0.41	**0.95**	0.88	-0.69	-0.58	-0.62
b_1		...	0.57	0.31	0.30	-0.22	-0.03	-0.08	-0.18	-0.15
b_2			...	**0.93**	0.83	-0.75	-0.71	0.63	0.54	0.58
b_3				...	0.89	-0.81	-0.84	0.75	0.70	0.72
b_4					...	-0.46	-0.56	0.59	0.60	0.60
SAVI						...	**0.93**	-0.74	-0.62	-0.67
EVI							...	-0.86	-0.79	-0.83
ρ_{VIS}								...	**0.95**	**0.98**
ρ_{NIR}									...	**0.99**
ρ_{SWV}										...

Table 3.2: List of variables included in the full model after discarding highly correlated variables.

Data Source	Variable Description	Spatial Resolution	Model Notation
Landsat TM 5	Band 1 – blue reflectance	100 m	b_1
Landsat TM 5	Band 3 – red reflectance	100 m	b_3
Landsat TM 5	Band 4 – near -infrared reflectance	100 m	b_4
Landsat TM 5	Normalized Difference Vegetation Index	100 m	NDVI
Landsat TM 5	Enhanced Vegetation Index	100 m	EVI
MODIS	Bare Soil Albedo – near-infrared spectrum	1 km	ρ_{NIR}

Table 3.3: Coefficients included in final multiple linear regression model as selected by BIC. For this model, cross-validated R^2 = 0.37 and cross-validated RMSE = 13.76 Mg/ha. Coefficient estimates are reported based on the results from the 'lm' procedure in 'R' prior to cross-validation.

Coefficient	Estimate	Std. Error	*P*-value
intercept	159.6	40.02	0.000103
NDVI	0.004913	0.001059	7.42×10^{-6}
ρ_{NIR}	-0.7876	0.2269	0.000674
$(\rho_{NIR})^2$	0.0009673	0.0003167	0.002664

3.7 Figures
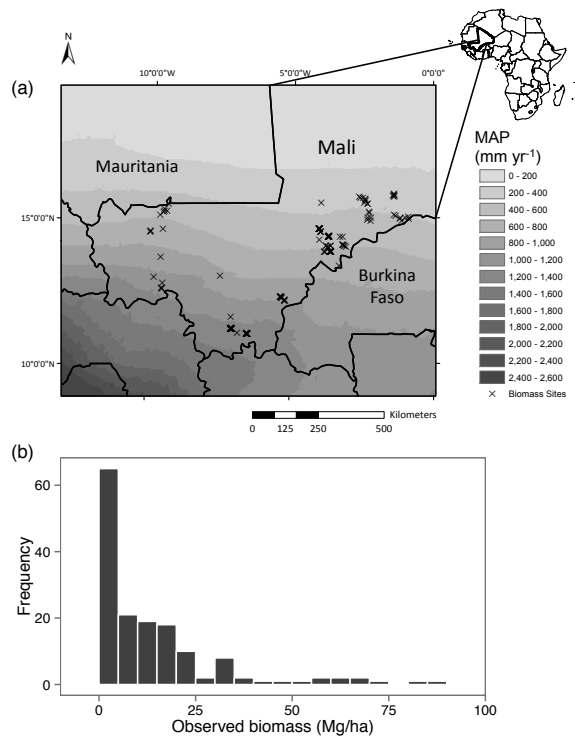
Figure 3.1: (a) Map of Mali, West Africa showing mean annual precipitation and distribution of training and validation data. The ×s designate biomass plots and darker ×s indicate multiple, close plots (n = 157). All plots are 1 ha. (b) Frequency distribution of plot-level observation data.
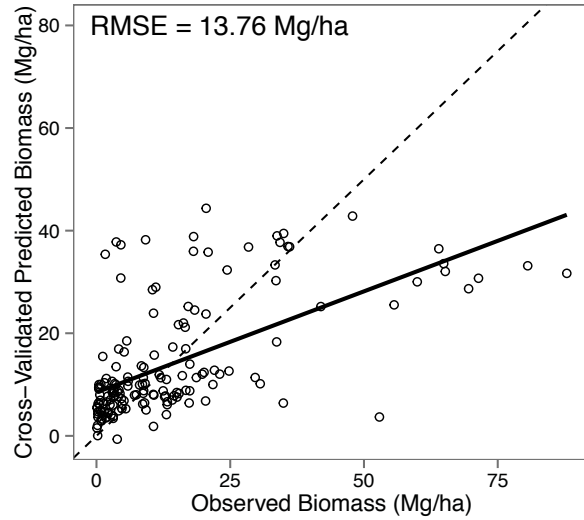
Figure 3.2: Observed vs. predicted biomass values. The dashed line shows the 1:1 line of perfect agreement between observed and predicted values. The solid line is the regression of predicted biomass on observed biomass ($y = 8.498 + 0.395x$, $R^2 = 0.37$)
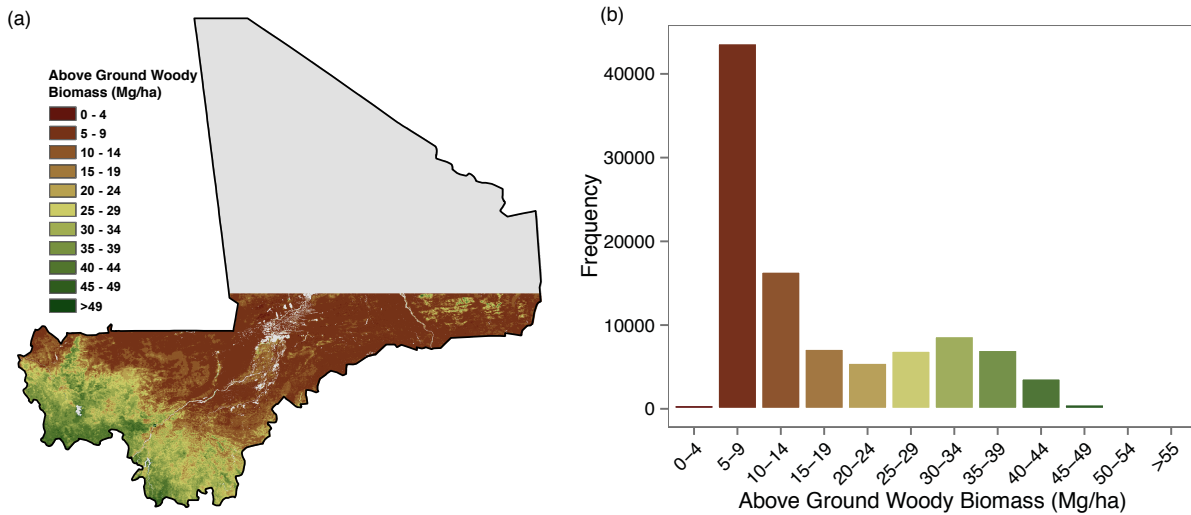
Figure 3.3: (a) Estimated above ground woody biomass in Mali, West Africa at 100m resolution. Grey area is the desert region of Mali where MAP < 200 mm. White areas are permanent and ephemeral water bodies from Kaptué et al. (2013). (b) Histogram of AGWB estimates from a random sample of 100,000 points from (a).

45
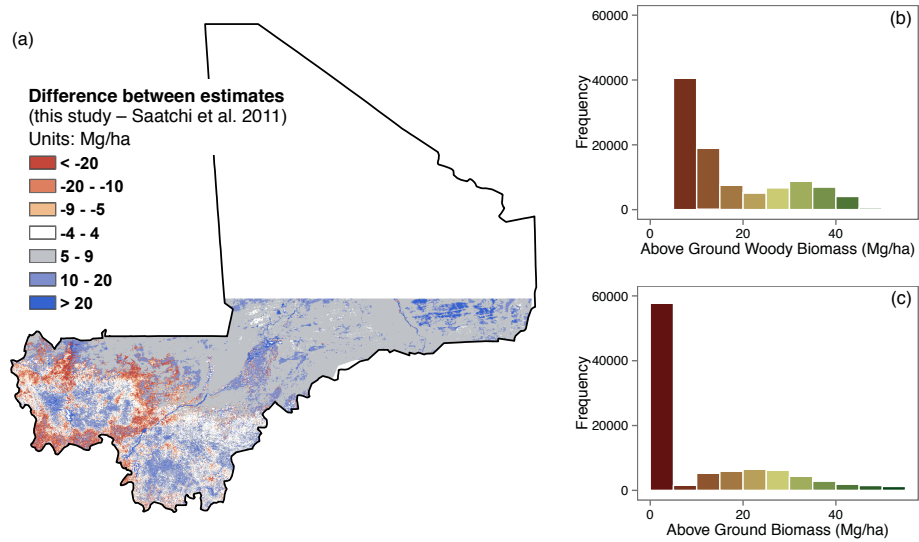
Figure 3.4: Comparison of our woody biomass estimates with aboveground biomass estimates from Saatchi et al., 2011. (a) Difference map where difference (in Mg/ha) was calculated as this study subtracted by Saatchi et al.'s estimates. Positive regions are those where our estimates are higher than Saatchi et al. and negative regions are where out estimates are lower than Saatchi et al. (b) Histogram of biomass densities from a 100,000 point random sample from our map aggregated to 1km resolution. (c) Histogram of biomass density for same points from (b) from Saatchi et al.'s biomass map, also at 1km resolution.

Chapter 4

Sub-Saharan Africa's fuelwood footprint: Current patterns of fuelwood supply and demand[4]

Summary

Food security is a major contemporary issue, but less attention is given to the inherent link among food and energy securities. In many developing regions of the world wood is the primary energy source used to cook food, and a majority of Africans (about 80%) depend upon wood to provide the energy necessary to meet basic human needs. While time devoted to fuelwood collection may impact effort devoted to food production, no comprehensive assessment of the current status of wood harvesting for energy in Sub-Saharan Africa (SSA) exists. The extraction and combustion of wood for energy, apart from its potentially negative environmental and health effects, may be a substantial social, economic, and political issue where demand outpaces production, even if at country and continental scales production outweighs demand. Here we present a continental scale analysis of fuelwood availability (standing stock), annual supply, and annual human demand in SSA. Using best-available fuelwood demand statistics, a growth model based on remotely sensed data, and current biomass estimates we create a series of maps, with associated uncertainties, showing the amount of wood needed by humans for energy in SSA and the amount produced annually. Summing across SSA, we estimate total annual wood demand is 279 Tg yr^{-1} – 438 Tg yr^{-1}, which is $17 - 35\%$ of the estimated 1,419 Tg yr^{-1} (1,240 – 1,597 Tg yr^{-1}) annual wood production. Using conservative estimates at the national level, 12 out of 42 countries appropriate over 50% of annual wood production to fuelwood, and four appropriate over 100%. At the pixel level, local fuelwood appropriation can exceed 1,000% of annual supply in densely populated cities. Our analysis shows no evidence of a continent-wide fuelwood crisis, but we do find

---

[4]This chapter is in preparation for submission to *Nature* with co-authors Niall P. Hanan, Gabriela Bucini, and William Parton.

hotspots of fuelwood shortage at national and local scales. This baseline assessment can be used to track fuelwood supply and demand through time, as well as identify areas in need of targeted policy intervention.

4.1 Introduction

Humans have used wood for energy for over 500,000 years (Sharpe 1976, Gowlett et al. 1981, Goren-Inbar et al. 2004), and it remains the primary energy source in SSA (Kebede et al. 2010, Sander et al. 2011) and in most developing and transition economies of the world. On average 75-85% of people in SSA have limited or no access to electricity and depend upon wood to provide the energy necessary to meet basic human needs (International Energy Agency 2000, Kebede et al. 2010, Sander et al. 2011, Smeets et al. 2012). Though access to alternate forms of energy is increasing, through wider availability and human migration to urban centers, the shift from wood energy to other sources has been slow primarily due to the increased cost over inexpensive, or free, fuelwood (Babanyara and Saleh 2010). Thus, the continued availability of woody biomass for harvest is essential to human well being in SSA, and the ecological and socio-economic implications thereof require further study.

The sustainability of fuelwood harvesting in Africa and other regions received a large amount of attention during the 'fuelwood crisis' years of the late 1970s and 1980s (Arnold et al. 2006). However, there is still no consensus in the scientific community on the sustainability of fuelwood harvesting in Africa (Arnold et al. 2003). Accounts of fuelwood shortages and surpluses are both empirically supported in the literature (e.g., Shackleton 1993, Mwampamba 2007, Wessels et al. 2013). But these are based on small-scale, site-specific observational studies in areas that occur under diverse social and bioclimatic conditions where the processes driving local wood demand and production vary by region. It is difficult to effectively scale up from these local analyses, and impossible to implement local studies at a continental extent. To overcome some of these limitations, we present a continental analysis at 1-km resolution that allows us to assess the situation for

SSA as a whole at multiple scales, using empirically-based estimates of annual wood production rates compared to annual fuelwood demand of local populations. The continental scale analysis of fuelwood supply and demand presented here will provide the context and impetus for necessary more detailed, and local scale, ecological and socio-economic studies.

4.2   Methods

4.2.1   Quantifying fuelwood demand

To quantify fuelwood demand we use data from The United Nations Food and Agricultural Organization (FAO) Forestry database (Food and Agriculture Organization of the United Nations 2010), which holds the most complete information on fuelwood consumption in Africa. FAO estimates are reported at the national-level in cubic meters per year including estimates of wood combusted as charcoal. Here we use 2008 estimates and convert from m^3 yr^{-1} to kg cap^{-1} yr^{-1} using population numbers from a gridded database (Center for International Earth Science Information Network 2005) and an average wood density of 605 kg m^{-3} for Africa from the Global Wood Density Database (Zanne et al. 2009). This method results in homogenous per capita fuelwood demand rates for each country (Table A1) which, while a simplifying assumption (Cline-Cole et al. 1990), allows for reasonable estimates of fuelwood demand at the scale of SSA. We applied calculated per capita wood consumption to the gridded database of human population with a 1 km spatial resolution (Center for International Earth Science Information Network 2005) to estimate spatially-continuous fuelwood demand for SSA.

We consider the FAO-based estimates conservative due to limitations in FAO data (e.g., under-reporting of rural areas; see Appendix). When compared to the few, more-detailed studies available in the literature and other databases, the fuelwood demand estimates reported by FAO appear to consistently under-report rural harvest (Table A2; see Tables A3 and A4 for complete database and data sources). We therefore calculated less conservative estimates of fuelwood demand ("high estimates") using linear regression relating economic variables from the African Economic Outlook

(2010) to alternative estimates of fuelwood use from the literature (Table S2). The best single-parameter model uses percent of the country in poverty as the explanatory variable ($R^2 = 0.48$, $n = 33$, $F_{1,31} = 30.11$, $P = 0.000004815$; see Appendix A section A.8.1.2, Tables A2 and A5, and Figure A1). This relationship between income and energy use is well supported (Arnold et al. 2003; 2006, Ouedraogo 2006).

4.2.2 Quantifying annual fuelwood supply

New and increasingly accurate methods for estimating biomass using satellite remote sensing offer an excellent opportunity to re-evaluate the status of Africa's woody biomass and investigate the sustainability of wood harvesting. We estimated annual wood supply (dB/dt) as the biomass growth increment using estimates of above-ground woody biomass (B_0) and climatic potential biomass (B_p) derived from remotely-sensed estimates of woody cover (Bucini 2010; see Appendix A) as parameters in a Hyper-Gompertz logistic growth model

$$\frac{dB_i}{dt} = r_i B_{0,i} \left[\ln \left(\frac{B_{p,i}}{B_{0,i}} \right) \right]^{\gamma_i},$$
(4.18)

where r is the intrinsic growth rate (yr^{-1}), $B_{0,i}$ is actual biomass ($kg\ km^{-2}$) at location i, $B_{p,i}$ is biomass at its climatic potential ($kg\ km^{-2}$) at location i, and γ is a fitted model parameter that influences the inflection point (Tsoularis 2001). Biomass estimates are at 1 km resolution and further information can be found in Appendix A.

Due to lack of available data to estimate r, we used the biogeochemical model Century (Parton et al. 1994), as parameterized for African systems (Parton et al. 2010), to develop yield tables of wood production at fifteen locations, and under four different soil texture-tree parameterization settings, along a climate transect from the moist tropical forests of Central Africa to the dry Sahara desert (see Appendix A). We used a Bayesian hierarchical model to fit Hyper-Gompertz logistic growth curves to Century-derived yield tables to estimate r and its variability with mean annual precipitation (variation due to soil-tree parameterizations was not statistically important; see Ap-

pendix A, Fig. A7). We found no support for varying γ with precipitation, so we use the mean value ($\gamma = 2.45$) for each pixel. With continent-wide actual and potential wood biomass and r from Century we used the logistic growth model to create a map of annual wood growth (annual supply; dB_i/dt) at a spatial resolution of 1 km for SSA. Further, we used the 95% CIs of r to estimate lower and upper bounds on annual fuelwood supply. We only consider annual wood growth in this analysis, assuming that even if local populations are primarily harvesting dead wood (Shackleton 1998), annual growth must keep pace with annual mortality at the landscape-scale to meet fuelwood demands.

4.3 Results and Discussion

Our analysis resulted in the creation of maps of fuelwood supply (Figure 4.1a,b) and demand (Figure 4.1c,d,e) across the entirety of SSA. Using these maps we summed for SSA and estimate total annual fuelwood demand is 279 – 438 Tg year^{-1} (1 Tg = 10^{12} g); a value congruent with previous estimates for all of Africa (Hao and Liu 1994). We estimate total annual wood production in SSA is 1,419 Tg year^{-1} (lower estimate = 1,240, upper estimate = 1,597; Figure 4.1c,d,e, Table 4.1). If we exclude biomass production in protected areas with IUCN designations prohibiting natural resource extraction, the mean estimated annual wood supply rate reduces to 1,315 Tg year^{-1}.

Total annual wood production in SSA exceeds human need by 802 – 1,319 Tg year^{-1} indicating that as a whole there is no immediate fuelwood crisis in SSA. Of greater interest, however, is the spatial heterogeneity in the balance between wood production and demand (Figure 4.2a,b). To compare the patterns of demand and supply we calculated the annual fuelwood balance as the difference between supply and demand at several spatial resolutions (Figure 4.2c). The distribution of annual fuelwood balance does not shift toward more positive values as spatial resolution increases, but small hotspots of very negative balance (as indicated by outliers in Figure 4.2c) do disappear as a greater area of wood supply can meet demand. This indicates the importance of

51

horizontal flows of wood from rural, wood-rich areas to urban centers where demand outpaces the local supply. About 60% of people in SSA are dependent on fuelwood markets as estimated by the fraction of people living in 10 km pixel locations where local supply does not meet demand (Figure 4.2d). We consider 10 km resolution a relevant spatial scale for walking to collect fuelwood, thus since only 40% of the SSA population lives within 10 km pixels where demand is less than 100% of annual supply, a further 60% are dependent on wood imports from adjacent pixels. Even when wood supply is aggregated at 1,000 km length scales about 20% of Africans' energy supply cannot be met, indicating the need for fuelwood markets and alternative energy sources.

We estimate people appropriate ~17-35% of annual wood production (total fuelwood supply) to fuelwood in SSA (Table 1), but this varies greatly at local (Figure 4.2b) and regional scales (Table 4.1). Regional fuelwood consumption varies from ~10-40% of annual wood production (Table 4.1) and areas in Central Africa, Ethiopia, and the west coast require greater than 100% of local (pixel level) production (Figure 4.2b). In large urban centers, fuelwood appropriation of local production can exceed 1,000%. Though people are not limited to using local wood production, the areas in excess of 100% clearly require external inputs to meet local demand, as represented in Figure 4.2c,d.

Standing stock of biomass can buffer short-term negativity in the supply-demand equation. Countries with low standing biomass where supply and demand are nearly equal or where supply does not meet demand may be particularly vulnerable to annual fluctuations in fuelwood demand. Using conservative estimates, four countries are in negative balance (Figure 4.3), and Somalia in particular is especially vulnerable to a negative annual balance, given relatively low standing stock to buffer fuelwood demand (Figure A9). Countries in positive balance but with relatively low standing stock (e.g., Eritrea, Uganda) are also vulnerable to annual fluctuations in supply and demand (Figure A9).

4.4 Conclusions

Patterns of fuelwood consumption will undoubtedly change with economic development in Africa and as access to alternative fuels increases, but currently over 80% of people in SSA depend upon wood for energy (Kebede et al. 2010) and scenarios of energy futures for SSA suggest wood biomass will continue to comprise a large portion of household energy budgets (Bailis et al. 2005). Changes in fuelwood demand will be difficult to predict, as will the adaptation and diversification strategies employed by people when faced with changing patterns of fuelwood availability (Arnold et al. 2006). However, this paper provides a baseline from which we can begin to monitor changes in the balance of fuelwood demand and production, allowing for targeted policy intervention and the identification of wood scarcity 'hotspots' at multiple scales. Likewise, the spatial databases presented here can be used in more detailed analyses aimed at mapping fuelwood flows on the landscape using road maps.

Our multi-scale analysis highlights the importance of fuelwood imports to meet demand in populous regions. Indeed, at scales relevant to fuelwood collection by households, we estimate over 60% of the SSA population lives in areas where local supply does not meet local demand. Even at coarse spatial resolution (1,000 km) about 20% of the SSA population lives in negative fuelwood balance. However, our analysis indicates that at continental and regional scales annual supply far outpaces demand (by about 10-40% at regional scales). Increasing access to alternative energy sources and high-efficiency cookstoves will of course alleviate demand, but special attention should also be paid to fuelwood 'corridors' to transport wood from high yield-low population areas to low yield-high population areas. As demand for fuelwood (wood and charcoal) increases in the future, the growth of fuelwood markets will need to be managed wisely to avoid local fuelwood shortages and promote the sustainable exploitation of available wood resources.

4.5 Tables

Table 4.1: Annual fuelwood demand, supply, and balance for sub-regions of SSA.

Region	Population ($\times 10^6$)	Fuelwood Demand (Tg yr^{-1})	Annual Supply (Tg yr^{-1})	Fuelwood Appropriation (%)
West Africa	194	88 – 169	387 (339 – 438)	23 (20 – 39)
Central Africa	81	45 – 68	402 (352 – 451)	11 (10 – 19)
East Africa	226	132 – 178	547 (478 – 615)	24 (21 – 37)
South Africa	39	13 – 23	82 (71 – 94)	16 (14 – 33)
SSA	540	279 – 438	1,419 (1,240 – 1,597)	20 (17 – 35)

Notes: Annual fuelwood demand shown as a range where low end is the FAO estimate and high end is our modeled estimate. Wood production is shown as mean with upper and lower estimates (calculated using 95% credible limits of *r*) in parentheses. Regional fuelwood balance is shown as a mean estimate with low and high extremes in parentheses. UN geographical sub-regions of Africa are as in United Nations and Social Affairs (2011) but we excluded Madagascar and placed Sudan in Eastern Africa. Since this analysis is for SSA we do not include a row for Northern Africa, but small parts of Algeria, Egypt, Libya, and Western Sahara are included in the totals (demand contribution = 0.010 – 0.016 Tg yr^{-1}; supply contribution = 0 Tg yr^{-1}). Population estimates are as in Center for International Earth Science Information Network (2005) to correspond with the data used to calculate fuelwood demand. Fuelwood appropriation statistics reflect the percent of annual wood supply needed to meet fuelwood demand and are calculated as: mean = (mean demand / low supply)$\times$100; low estimate = (low demand / high supply)$\times$100; high estimate = (high demand / low supply)$\times$100.

4.6 Figures
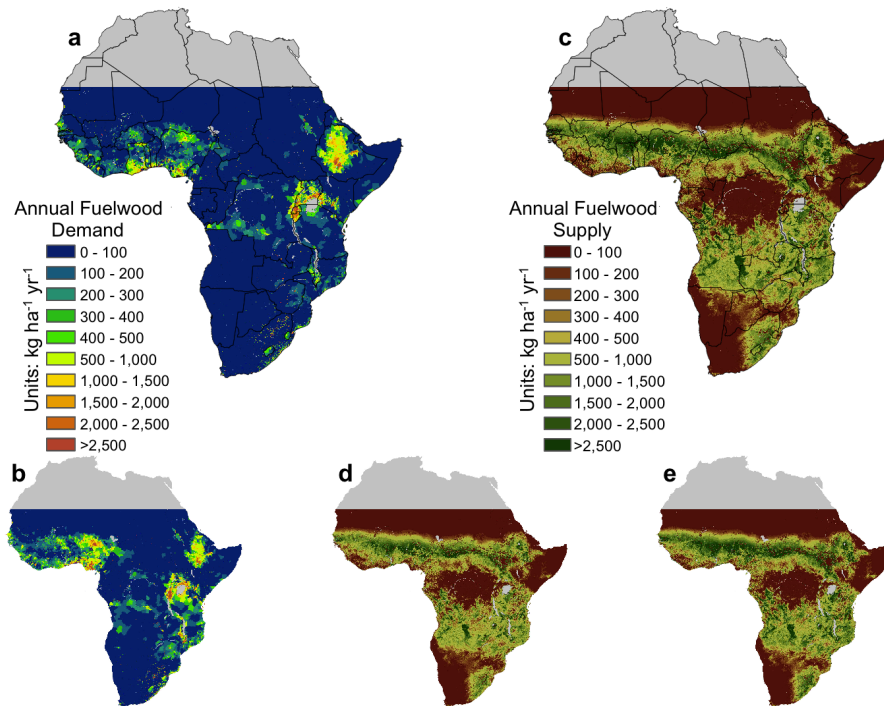
Figure 4.1: Rates of change in fuelwood availability for SSA. **a-b**, Low (**a**) and high (**b**) estimates of annual fuelwood demand (kg ha^{-1} yr^{-1}). **c-e**, Mean (**c**) and lower (**d**) and upper (**e**) estimates of annual fuelwood supply (*dB/dt*, kg ha^{-1} yr^{-1}) calculated using *r* from Bayesian model and actual and potential biomass. Upper and lower estimates in **d** and **e** were calculated using the 95% credible limits of *r* at each pixel location. All methods are described in main text and in Appendix **??**.
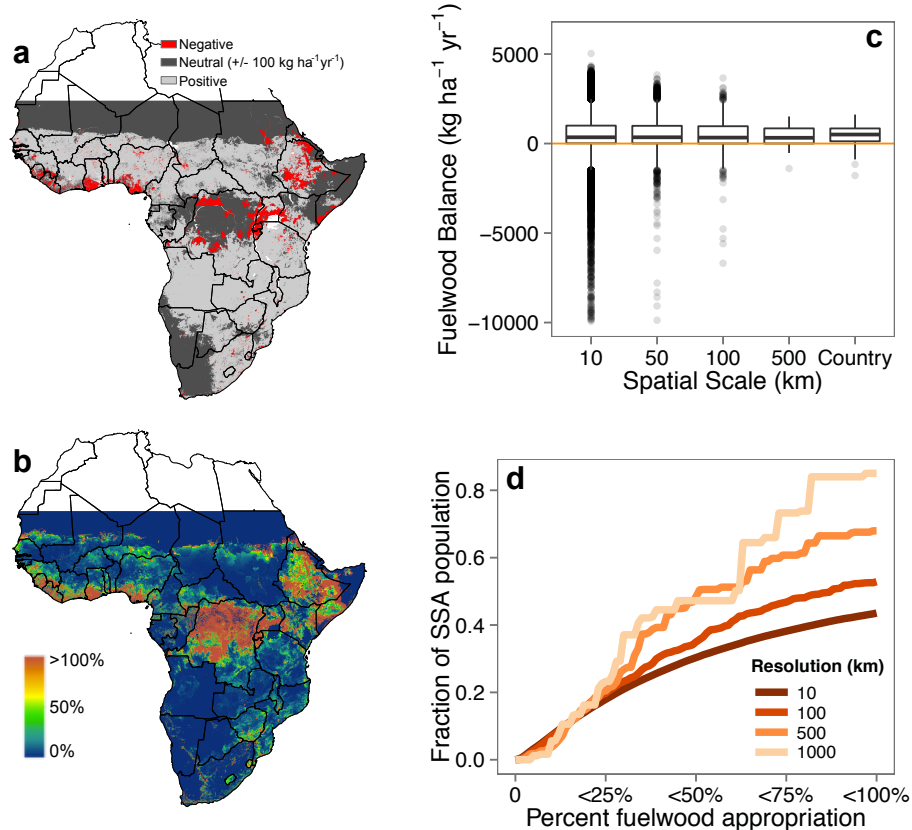
Figure 4.2: Annual fuelwood balance and appropriation in SSA. **a**, The annual fuelwood balance (supply – demand) at 1km resolution, expressed as negative (when supply–demand < -100 kg ha^{-1} yr^{-1}), neutral (when -100 < supply–demand < 100 kg ha^{-1} yr^{-1}), and positive (when supply–demand > 100 kg ha^{-1} yr^{-1}) **b**, annual appropriation of wood supply to fuelwood, expressed as percent of wood supply $\left(100 \times \frac{\text{demand}}{\text{supply}}\right)$. **c**, Boxplots of the numerical distributions of annual fuelwood balance at different spatial resolutions, and at the country scale, to show the effect of diffusing supply and demand across the landscape. Thick lines within boxes are the medians; box represents the 25th and 75th percentiles; whiskers are the 5th and 95th percentiles. Open circles are outliers. In **c**, desert regions (mean annual precipitation < 100 mm y^{-1}) were excluded from the analysis to avoid over-inflation of neutral regions with near zero supply and demand; the figure is cut-off at a fuelwood balance of -10,000 kg ha^{-1} y^{-1} for visualization purposes (lowest fuelwood balance at 10 km resolution often < -50,000 kg ha^{-1} yr^{-1} in the most densely populated cities). **d**, The effect of spatial resolution on the fraction of SSA population living in areas of different fuelwood appropriation. Curves are cumulative and show the total fraction of SSA population living within pixels (whose size change with spatial resolution as shown in the legend) that match the fuelwood appropriation on the *x*-axis. For example, at 10 km resolution about 40% of the SSA population lives in pixels where fuelwood demand is less than 100% of annual supply. As the spatial resolution decreases (becomes more coarse) greater areas of fuelwood supply can meet demand. In all panels fuelwood balance was calculated using low estimate of fuelwood demand (Figure 4.1a) and mean estimate of fuelwood supply (Figure 4.1c).
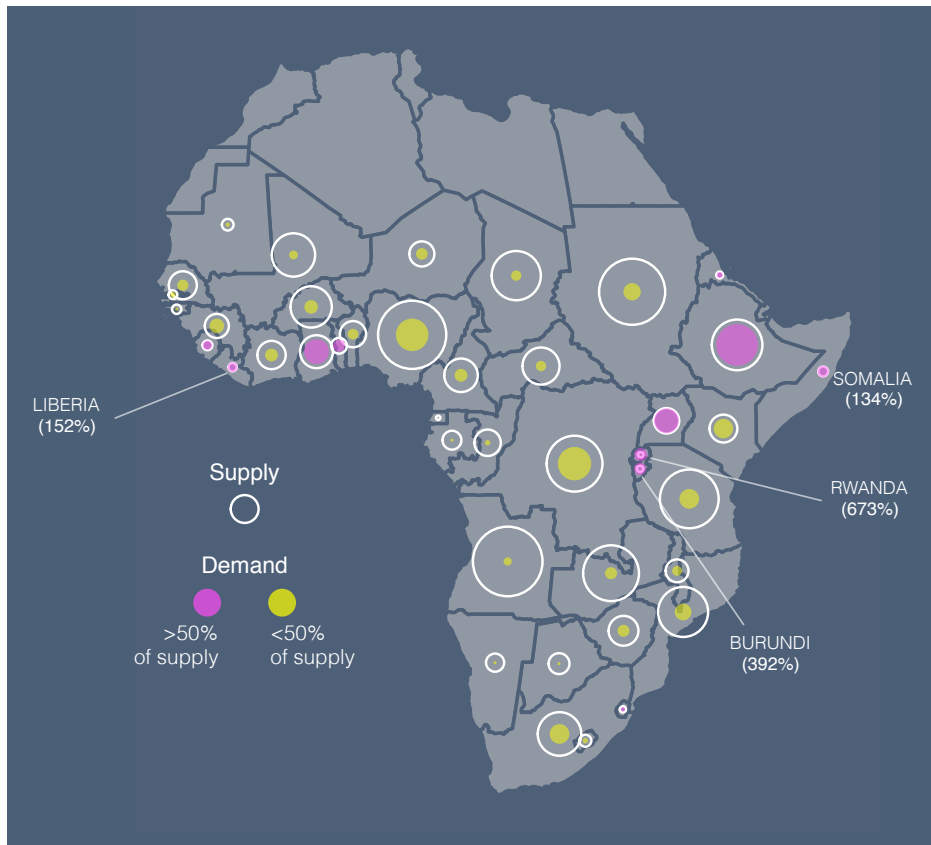
Figure 4.3: National-level fuelwood supply and demand for Sub-Saharan Africa. Circles represent supply (open, white circles; from median estimates) and demand (closed, colored circles; from low estimates) summed for each country. The area of the circles is scaled by supply and demand so that larger circles represent larger supply or demand. Color of demand circles corresponds to the percentage of annual supply (wood production) appropriated to annual demand as indicated in the figure. Labeled countries are those where annual demand is greater than 100% of annual supply, with percentage shown in parentheses. A similar figure using high demand estimates can be found in Appendix **??** (Figure A8). Four countries appropriate over 100% of annual supply, and twelve countries appropriate over 50% of annual supply.

Chapter 5

Effects of tree harvest on the stable-state dynamics of savanna and forest[5]

Summary

Contemporary theory on the maintenance and stability of the savanna biome has focused extensively on how climate and disturbances interact to affect tree growth and demography. In particular, the role of fire in reducing tree cover from a climatic maximum is now well appreciated, and in certain cases herbivory also strongly affects tree cover. However, in African savannas and forests, harvest of trees by humans for cooking and heating is an oft overlooked disturbance. Thus, we incorporate tree harvest into a population dynamic model of grasses, savanna saplings, savanna trees, and forest trees. We use assumptions about the differential demographic responses of savanna trees (they usually resprout following fire- or harvest-induced top-kill) and forest trees (they usually do not resprout) to show how tree harvest influences not only tree cover but tree demography and community composition. Where savanna and forest are alternatively stable, we find that tree harvest can erode the intrinsic basin of attraction for forest and make a state transition via fire to savanna more likely. Where savanna is uniquely stable, the savanna state is generally resilient to all but high levels of tree harvest due to the resprouting abilities of savanna trees. Only with high tree harvest rates that likely occur near villages and towns does harvest promote savanna transition to a grassland (treeless) state. In terms of ecosystem stewardship, our theory of how tree harvest impacts forest-savanna transitions suggests that, in the absence of active fire suppression, as demand increases for charcoal in sub-Saharan Africa we can expect to see large and potentially irreversible shifts from forest to savanna. On the other hand, savanna tree species traits, including the ability to resprout following topkill (by fire or, in this case, harvest), seem likely to promote savanna stability in the face of low-to-moderate harvest pressure.

---

[5]This chapter, co-authored with Niall P. Hanan, is currently in review at *The American Naturalist.*

5.1 Introduction

Intuitively, it is clear that tree harvest will impact savannas and forests by directly removing biomass. But, does tree harvest affect the stability and demographic dynamics of savannas and forests? This is important to consider because contemporary theory suggests the savanna biome is maintained by 'demographic bottlenecks' that are 1) removed at low rainfall to promote seedling establishment and 2) imposed at intermediate and high rainfall to prevent canopy closure (Sankaran et al. 2004). In fact, where rainfall is high enough to support a closed-canopy forest, savanna often persists (Sankaran et al. 2005, Lehmann et al. 2011). Such observations imply a large role for disturbance. Thus far, tree harvest by humans has been overlooked as a disturbance in savannas, with most researchers focusing on fire and herbivory.

Disturbance by fire can maintain the savanna state by excluding forest trees and limiting savanna sapling recruitment to adult size classes. As a functional type, forest trees suffer increased mortality following fires relative to savanna trees and tend to resprout less vigorously (Hoffmann et al. 2003; 2012). Thus, under frequent fire, even if the climate favors forest trees, savanna trees will dominate. A shift to the savanna state results in a positive feedback wherein fire reduces tree densities and increases grass cover, which leads to more frequent fires (Higgins et al. 2000, Sankaran et al. 2004, Bond 2008, Hanan et al. 2008, Higgins et al. 2010). At low and high rainfall savanna and forest are climax biomes respectively, but at intermediate rainfall they represent alternative stable states (Beckage et al. 2009, Hirota et al. 2011, Staver et al. 2011*b*, Hoffmann et al. 2012).

Recent observational evidence also points toward savanna and grassland as alternative stable states at the arid end of the distribution (Hirota et al. 2011). However, compelling evidence for a mechanism that delineates savanna and grassland as alternative stable states is lacking, and the observational evidence provided by Hirota et al. (2011) may be subject to non-random errors that artificially impose discontinuities in continuous data (Hanan et al. 2013). In arid and semi-arid savannas, occasional or frequent fire and/or persistent drought can completely eliminate trees if the death rate of savanna trees exceeds recruitment (Higgins et al. 2010), but whether the treeless

state is continuous with savanna or represents a true alternative stable state requiring amplifying feedbacks, not simple density dependence, remains unknown.

Even within the 'stable' savannas (i.e., savannas that exist as the climax state in lower rainfall regions [Sankaran et al. 2005]) tree cover and biomass can vary widely depending not only on climate, but also other disturbances. In addition to fire, herbivory has been invoked to explain tree cover in savannas (Scholes and Archer 1997, Bucini and Hanan 2007, Staver et al. 2009), but clear evidence is lacking for any consistent effect of herbivory in controlling the distribution of forest, savanna, and grassland at large spatial extents (Murphy and Bowman 2012). Grazing primarily influences tree cover indirectly by reducing fuel loads and fire frequency or intensity (Scholes and Archer 1997). Browsing, especially by large mammals such as elephant or giraffe, can have large direct impacts on tree cover (Asner et al. 2009, Staver et al. 2009), but these effects are location-dependent and tend not to generalize to all savannas.

Even though tropical savannas represent some of the most densely populated biomes by humans most ecological research has focused on 'natural' or 'intact' savannas and forests, either implicitly or explicitly ignoring the role humans play in shaping vegetation structure and biome distributions. Recent work indicates how human manipulation of fire may have aided savanna expansion (Archibald et al. 2012), but most other human impacts have not been explicitly considered in models of savanna and forest vegetation (e.g. Murphy and Bowman 2012, Staver and Levin 2012).

In particular, there is a need to integrate human activities that directly affect tree abundance, biomass, and demography into theoretical models of grassland, savanna, and forest dynamics. Without such theoretical integration, we lack the ability to delineate the stability and dynamics of these states in reference to real world systems inhabited and influenced by humans. To address this shortcoming this paper focuses on the harvesting of trees for fuelwood in Africa by incorporating this process in a population dynamic model of grassland, savanna, and forest systems. Fuelwood is the dominant source of energy in sub-Saharan Africa (SSA) (Bailis et al. 2005, Arnold et al. 2006), so it is important to consider the mechanism by which tree harvest influences vegetation in savannas

and forests, especially since recent advances in savanna ecology make clear the importance of demographic processes (Higgins et al. 2000, Sankaran et al. 2004, Higgins et al. 2007, Hanan et al. 2008). Just as fire has differential effects on savanna and forest trees, we can expect similar dynamics in response to tree harvest.

We examine the effect of tree harvest on the stability of savanna and forest systems. We extend the population dynamic model of Staver and Levin (2012) by incorporating a tree harvest term based on assumptions of the different resprouting abilities of forest and savanna trees following a harvest event. By including tree harvest we can investigate how human activities may interact with other processes (fire, drought) to cause transitions from forest to savanna, and from savanna to grassland. We use the model to address two questions: 1) Does tree harvest change the stable state dynamics at the grassland-savanna ecotone and the savanna-forest ecotone? and 2) Are climax savannas, which are highly populated, vulnerable to large reductions in tree cover under tree harvest? We find that 1) tree harvest can erode stability basins and make transitions to low tree-abundance states via fire and drought more probable, and 2) savannas are resilient to tree harvest due to the resprouting abilities of savanna trees.

5.2 Methods

5.2.1 Modeling Framework

We build upon the modeling framework of Staver and Levin (2012) and add a tree harvest term (ρ; Fig. 5.1A). The model is not spatially explicit but assumes all space is occupied by some proportion of grass (G), savanna saplings (S), savanna trees (T), or forest trees (F) with grass being the default. The full model, following the notation of Staver and Levin (2012), is specified as four

differential equations that sum to 0:

$$\frac{dG}{dt} = \mu S + \nu T + [\phi(\lambda) + \rho]F - \beta GT - \alpha GF, \quad (5.19)$$

$$\frac{dS}{dt} = \beta GT + \rho T - \omega(\lambda)S - \mu S - \alpha SF, \quad (5.20)$$

$$\frac{dT}{dt} = \omega(\lambda)S - (\nu + \rho)T - \alpha TF, \quad (5.21)$$

$$\frac{dF}{dt} = [\alpha(1 - F) - (\phi(\lambda) + \rho)]F. \quad (5.22)$$

All terms are as in Staver and Levin (Table 5.1) with two additions: wood harvest (ρ), and a modified fire frequency term (λ). Grass (G) is the default state: any space occupied by savanna saplings (S), savanna trees (T), or forest trees (F) reverts to grass upon mortality. This is true except for the special case of wood harvest where adult savanna trees revert to the sapling state. An implicit spatial competitive hierarchy is created by only allowing savanna saplings to establish in space occupied by grass, whereas forest trees can establish on areas occupied by grass or savanna saplings and trees. Savanna sapling establishment (β) and forest tree establishment (α) are constant rates relative to the proportion of savanna adult trees and forest trees, respectively. Recruitment of savanna saplings to adult trees is mediated by fire frequency [$\omega(\lambda)$], and thus grass cover (Fig. 5.1B), because fire limits sapling recruitment. Mortality terms of savanna trees (ν) is constant and proportional to occupied area. Mortality of forest trees is conditional upon fire frequency ($\phi(\lambda)$) and proportional to occupied area. Savanna sapling mortality (μ) is constant and proportional to occupied area.

We deviate slightly from Staver and Levin's model by conceiving of fire as a stochastic and annually-discrete event driven by fire frequency (λ) which is a function of proportional grass cover. We assume fire frequency (or, equally, probability of fire in a given year) is a sigmoid function of grass cover with an inflection point at 0.6 proportional grass cover since, as discussed by Staver

and Levin, above 40% tree cover fire tends not to spread whereas below 40% tree cover fire does spread (Fig. 5.1B; also see Archibald et al. 2009; 2012). Fire frequency (λ) varies from 0-1 y^{-1}. We incorporate fire as discrete events, rather than implicitly through alterations in demographic rates, to more closely match reality and to allow for a greater range of system variability than expected using a step-function for fire. Given the value of λ as determined by grass cover (G), fire is a binomial stochastic event with values 1 (fire) or 0 (no fire) and probability λ estimated as

$$\lambda \;=\; \max\left(0, 0.5 + \left(\frac{1.1}{\pi}\right) \times \arctan\left(\pi 4\left(G - 0.6\right)\right)\right). \tag{5.23}$$

Fire affects the demographic rates of forest and savanna trees differently. Adult savanna trees are rarely affected and the main impact of fire in savannas is to reduce sapling recruitment to adult size classes, ω. In the absence of fire, ω approximates the time (t_s, years) it takes for saplings to grow into the adult size class ($\omega_0 = 1/t_s$), while ω approaches zero in the event of fire ($\omega_1 \to 0$) (Higgins et al. 2000, Sankaran et al. 2004, Hanan et al. 2008, Staver et al. 2011a, Staver and Levin 2012). By contrast, both forest saplings and adult trees are typically killed by repeated fires. Forest trees can resprout, but slow accumulation of bark thickness makes them especially prone to fire-induced death, meaning that forest saplings rarely survive under any scenario that includes stochastic fires with return times less than 14 years (Hoffmann et al. 2012). This precludes the need to consider life-stages of forest trees as fire occurrence increases overall forest tree mortality in this general model (Staver and Levin 2012). Thus ϕ in the absence of fire is low, reflecting background mortality rates of adult forest trees ($\phi_0 \to 0$), but ϕ is much higher in fire years ($\phi_1 \to 1$).

We incorporate wood harvest (ρ, the per unit harvest rate) in the model based on assumptions of forest and savanna tree response to being cut at the base. When a savanna tree is harvested, we assume the state does not revert to the grass default but instead reverts to a savanna sapling (Fig. 5.1A). This is based on empirical evidence from wood harvest experiments (Tiedeman and Johnson 1992, Shackleton 2001, Kaschula et al. 2005) and fire experiments (Hoffmann et al. 2003, Hoff-

mann and Solbrig 2003, Hoffmann et al. 2004, Higgins et al. 2007, Hoffmann et al. 2012) that show savanna trees resprout vigorously. Less is known about the response of forest trees to harvest, but limited evidence suggests they can resprout (Mwavu and Witkowski 2008). However, consistent with our assumptions related to forest tree response to fire, we assume that time-averaged resprout success is low for forest trees. Thus, in the model forest trees die following harvest and revert to the grass state (Fig. 5.1A). We assume wood harvest only impacts adult trees, not saplings.

We initially model the harvest rate as a constant proportion of tree cover. This simplification for now ignores that harvest rates likely vary with both density and species composition. Our goal is not to completely model harvest dynamics but rather to discover if, on average and given our current knowledge of savanna systems, fuelwood harvest "matters". After initial analysis of the model, however, we explore a different harvest rate function (see **Modeling Harvest Independent of Tree Abundance**).

5.2.2   Model Simulations

To simulate the model we discretized Eqs. 5.19-5.22 with an annual time step so that $dt = 1$ and for any state X ($X = G, S, T, F$), $X_{t+1} = X_t + \frac{dX}{dt}$. The discrete representation of Eqs. 5.19-5.22 ensures that the demographic effects of stochastic and annually-discrete fire events are realized at appropriate time scales within the model (i.e., demographic rates that vary according to fire/no-fire years). Throughout the rest of the text we provide minimal analytical results and mainly rely on numerical simulations to demonstrate the impact of tree harvest on forest and savanna vegetation state. All model simulations where average states (stochastic equilibriums) are reported ran for 10,000 time steps (years) and average values of grass (G), savanna saplings (S), savanna trees (T), and forest trees (F) were computed after discarding the initial 5,000 time steps. Our focus is on forest-savanna-grassland transitions, so we begin with parameter values that provide stable simulation of those states and then vary tree harvest intensity and selected demographic parameters to explore impacts on vegetation structure. Parameter values for any given simulation are reported in figure legends. For harvest, we simulate a continuum of harvest rates ranging from

0 to 0.1, representing chronic harvest rates between 0 and 10% per year. For most of sub-Saharan Africa we consider this range of values reasonable, even if in some populous regions local demand may lead to increased harvest pressure. In preparatory simulations with $\rho > 0.1$ most systems show precipitous declines to zero tree cover as often observed in reality near urban areas in Africa (Ahrends et al. 2010, Wessels et al. 2013).

We also present some graphical analyses of the model to show how tree harvest can influence the existence and stability of equilibrium points. In these cases we forego our use of stochastic fire and instead follow the step-function approach of Staver and Levin (2012). Using the step-function, ϕ (forest tree death rate) and ω (savanna sapling recruitment rate) are conditional only on grass abundance (G) so that ϕ_0 (low, intrinsic death) occurs when $G < 0.6$ and ϕ_1 (high, fire-related death) occurs when $G > 0.6$. Likewise, ω_0 (high, intrinsic recruitment) occurs when $G < 0.6$ and ω_1 (low, fire-limited recruitment) occurs when $G > 0.6$. Graphical analyses rely on plotting the left- and right-hand sides of stability conditions for equilibrium solutions. Since fire, and in turn relative grass cover, is the hypothesized driver of bifurcations in tree cover (Fig. 5.1B), we differentiate equilibrium solutions with respect to grass cover to obtain stability conditions that can be plotted as a function of grass cover. To visualize equilibria the right- and left-hand side of the equilibrium solutions are each plotted as a function of grass cover and equilibria exist where lines intersect. Stability of equilibria can then be inferred by comparing the slopes of the two functions at intersections. Where we discuss equilibria and their stability mathematically, we note that $\omega(\lambda)$ and $\phi(\lambda)$ are equivalent to $\omega(G)$ and $\phi(G)$, respectively, because we ignore stochasticity when defining equilibria.

5.3 Model Analysis and Results

5.3.1 Savanna Stability and the Savanna to Grassland Transition

If we consider a savanna system where forest trees are absent ($F = 0$) then at non-zero equilibrium (e.g., where $S, T > 0$ and $G < 1$)

$$\omega(\lambda) = \frac{\mu(\nu + \rho)}{\beta G - \nu}. \tag{5.24}$$

Since fire frequency (λ) is a function of grass cover (Fig. 5.1B), both sides of Eq. 5.24 can be plotted as functions of G. Equilibria exist where the plotted functions intersect and these equilibria are stable when the first derivative of the left hand side of Eq. 5.24 with respect to grass cover (G) is greater than the first derivative of the right hand side (Fig. 5.2A), thus

$$\omega'(\lambda) > \frac{-\beta \mu(\nu + \rho)}{(\beta G - \nu)^2}, \tag{5.25}$$

where $\omega'(\lambda)$ denotes the first derivative of $\omega(\lambda)$ with respect to grass cover (G).

As can be seen, depending on harvest rate (ρ), between one and three equilibria exist, with stable points at high and low tree cover (Fig. 5.2A). Under various conditions high tree-cover savannas can be uniquely stable, tree harvest and fire can interact to bifurcate low and high tree-cover savannas, or grassland can be uniquely stable (Fig. 5.2A). The equilibrium states are highly parameter-dependent, but in general high harvest, low sapling recruitment, and high sapling death rate in combination yield a treeless state. Once achieved, the treeless (grassland) state is stable because it is tree-limited. That is, the term βT in Eq. 5.20 goes to zero prohibiting sapling birth, establishment, and subsequent recruitment. However, this model does not take into account meta-population seed-source dynamics that could prevent permanently stable treeless states.

Equation 5.24 indicates that so long as recruitment rate of saplings is equal to sapling and adult-tree death rates (μ and $(\nu + \rho)$, respectively) and there is available space ($G > 0$) the savanna state is stable, whether it be at high or low tree cover, because any level of tree cover, whether adult or sapling, defines savanna at the landscape scale. Since we only allow tree harvest to impact adult savanna trees, low-to-moderate levels of tree harvest have no affect on the stability of savanna (Fig. 5.2B). At high levels of tree harvest the right-hand side of Eq. 5.24 overwhelms the left-hand side to result in high mortality that cannot be compensated for by high sapling recruitment rates (Fig. 5.2B). In that case, only a boundary equilibrium where $G = 1$ is possible (Fig. 5.2A). Thus, the

strength of fire limitation on sapling recruitment rates becomes important (Eq. 5.24): high fire limitation (low ω_1) can result in savanna cover reducing to zero and a shift to the grassland state (Fig. 5.2B, open circles); low fire limitation (high ω_1) results in the maintenance of the savanna state even under high rates of tree harvest, but with reductions in tree cover (Fig. 5.2B, $\times$'s and $\Diamond$'s). Within savanna the effect of tree harvest is likely to vary with precipitation which tends to positively influence recruitment rates.

Though savannas are resilient to tree harvest in general, total tree cover (saplings and adult trees) may belie underlying demographic dynamics. To demonstrate this we plot the ratio of adult trees to savanna saplings at stochastic equilibrium (T:S) using the same simulated data from Fig. 5.2B (Fig. 5.2C). Regardless of fire-year recruitment rate (ω_1) tree harvest drastically reduces the number of adult trees relative to saplings. While not important for the stability of savanna ecosystems as a biome defined broadly by a mix of tree (whether adult or sapling) and grass, savannas dominated by saplings rather than adult trees contain less biomass for human consumption and reduced shade, browse, and other goods and services provided by adult trees.

The stability of savannas as defined by Eqs. 5.24 and 5.25 also depends on sapling death rate (μ) being relatively low since it appears in the numerator. Drought-prone, arid savanna systems under high harvest pressure will be more vulnerable to periodic droughts that impact saplings more heavily than adult trees (increasing μ). Thus, in combination tree harvest and drought could, at least in theory, drive shifts from savanna to grassland (Fig. 5.3A and B). Under drought conditions sapling death rates will be higher and intrinsic recruitment rates lower. Thus, relative to non-drought ('normal') conditions, a transition from stable savanna to grassland can occur at much lower harvest rates (Fig. 5.3A and B). Graphical analysis of the system confirms our simulation results (Fig. 5.3C)

5.3.2 Forest to Savanna Transition

If we consider a forest system where savanna trees (T) and saplings (S) are absent, at non-zero equilibrium (i.e., $F > 0$)

$$\alpha G = [\rho + \phi(\lambda)]. \qquad (5.26)$$

As above, since $\phi(\lambda) = \phi(G)$ if we ignore stochasticity, we can plot both sides of Eq. 5.26 as functions of grass cover (G) to identify equilibria and their stability. This graphical analysis of a forest system without savanna trees or saplings shows how tree harvest easily makes grassland the only possible equilibrium (Fig. 5.4A). At low harvest rate, high and low tree-cover forest equilibria are possible, as found and described by Staver and Levin (2012). At any given harvest rate, assuming low forest tree death, it is forest tree birth rate (α) that will determine whether forest is a stable equilibrium state. For example, if forest tree birth rate is high, then the grey line representing αG in Fig. 5.4A would be more steeply positive, allowing for the possibility of one to two stable forest configurations even at high harvest. Thus, in forests the balance between tree birth rates and harvest rates will be particularly important.

Introducing wood harvest to a stable forest equilibrium sequentially results in a shift from forest coverage to grass coverage (Fig. 5.4B), at which point, given adequate rainfall and seed sources, savanna trees can invade (region ii and iii of Fig. 5.4C). This transition from forest to savanna is co-mediated by wood harvest and fire. The addition of wood harvest short-circuits system stability by removing forest trees and allowing grass establishment (region i and ii of Fig. 5.4C). At a certain level of tree harvest there exists an amplifying feedback wherein fire levels increase dramatically (due to increases in grass cover and the non-linear response of fire frequency to grass cover) and overall forest mortality $[\rho + \phi(\lambda)]$ exceeds births (α). Grass cover continues to increase and with it fire. This amplifying feedback between tree harvest and fire in otherwise stable forest systems can cause dramatic and rapid increases in grass cover (region i and ii of Fig. 5.4C), allowing for invasion by savanna trees with functional traits capable of dealing with both harvest and fire (region

ii and iii of Fig. 5.4C).

Tree harvest in a stable forest can result in complex behavior, such as cycling among states (Fig. 5.4C). In these simulations, cycles occur when initially high forest cover declines under harvesting allowing grass and fire into the system, followed by recruitment of savanna trees and recovery of fire-resistant tree-cover that eventually suppresses grass production and fire (see Fig. 5.2A for savanna equilibria). This re-establishes the conditions under which forest trees can recruit and, over time, supplant the savanna tree functional group. Continued tree harvest, however, stimulates the cycle to begin again. When tree cover surpasses the 40% threshold required to reduce fire frequency forest trees death rates are intrinsic (ϕ_0) rather than elevated by fire (ϕ_1). When this occurs the invasion criteria for forest trees into stable configurations of savanna trees, saplings, and grass ($\alpha > [\phi(\lambda) + \rho]$) is satisfied and forest trees can rebound (region iv of Fig. 5.4C). However, tree harvest does eventually drive forest tree levels down again as forest trees replace savanna trees, and then forest trees are replaced by grass patches which elevates fire frequency, and the cycles continue. Whether these cycles actually occur in nature, and at what time-scales, remains an important question. At higher harvest rates (for example, when $\rho = 0.15$) only a low-tree cover savanna equilibrium is stable, and, since forest tree death rate is higher when grass cover is higher, forest trees cannot invade and the savanna state persists with no cycling.

5.3.3   Modeling Harvest Independent of Tree Abundance

For simplicity we have assumed tree harvest is a constant rate proportional to area occupied by adult trees (T and F). However, this approach may be unrealistic because harvest rates likely depend on local demand for fuelwood which would often be independent of actual tree cover or biomass. To study this possibility, we experimented with an alternative model for tree harvest represented in the model as a constant rate (ρ^*) so Eq. 5.21 becomes

$$\frac{dT}{dt} = \omega(\lambda)S - \nu T - \alpha T F - \rho^* \qquad (5.27)$$

69

and other equations are altered to reflect that change. We set the limitation that ρ^* cannot decrease T to values less than 0. So, where ρ^* would lead to $T < 0$, ρ^* is set equal to the value needed to reduce T to 0. This avoids unrealistic model dynamics. A similar limitation was imposed on the equation for forest trees (F). Also, since in this formulation tree harvest is no longer implicitly scaled by relative abundance, at each time step we split total demand ρ^* into forest tree and savanna tree fractions based on the relative abundance of forest and savanna trees. For example, if $\rho^* = 0.1$, $F = 0.4$, and $T = 0.2$, then $\rho_F^* = 0.1 \left(\frac{0.4}{0.4+0.2} \right) = 0.06667$ and $\rho_T^* = 0.1 - \rho_F^* = 0.03333$.

As expected, including a constant harvest term unrelated to tree relative abundance amplifies the results we report above. Though we cannot compare the two harvest rates (ρ and ρ^*) directly, transitions tend to occur at a fixed harvest rate of $\rho^* = 2.5\%$ (Fig. 5.5), where a density-dependent harvest rate of $\rho = 2.5\%$ has only modest effects (Figs. 5.3 and 5.4). A transition from savanna to grassland occurs at low levels of fixed rate harvest (Fig. 5.5A). Similarly, a transition from forest to grassland occurs at low levels of fixed-rate harvest (Fig. 5.5B). Thus, savannas and forests are less resilient to fixed-rate tree harvest.

The results of this analysis with fixed demand may apply most realistically in wetter, higher tree cover systems at the savanna-forest ecotone. In the more arid and low tree-density savannas there is evidence that people (based on local customs or in response to government mandates) tend to conserve woody populations through harvest of dead wood, rather than live trees (e.g., Shackleton 1998). Crucially, harvest of dead-wood depends on the density and productivity of the woody community, but has no direct demographic feedback. In Mali, West Africa, we have found a relationship between rainfall (and implicitly tree abundance) and the percentage of wood harvested from live trees (Fig. 5.6). In so far as our data from Mali are representative of wood harvest practices elsewhere, they suggest that the dynamics of mesic savannas and forests will be more strongly affected by fuelwood harvest than at intermediate and low rainfall. However, these general patterns can be confounded in highly populous regions where dead wood does not meet human demand. In such cases people may be forced to rely on live wood and rapid tree reductions, consistent with harvest being tree-density independent, can occur (Wessels et al. 2013).

5.4 Discussion

Does tree harvest matter in savannas and forests? In forest systems, we find that tree harvest can act to reverse the dominance of forest trees over savanna trees (implemented in this model by a spatial hierarchy). Since savanna trees are both fire- and harvest-tolerant via resprouting, the savanna state becomes favored under conditions of moderate-to-high tree harvest where forest tree death results in increased grass cover and, in turn, increased fire frequency (Fig. 5.4B, C). Thus, the model successfully reproduces empirical findings of frequent and self-amplifying fire events after forest tree removal (Cochrane et al. 1999, Cochrane and Laurance 2002). This provides a pathway of 'savannization' distinct from the view of tree harvest, and other human impacts, resulting in a 'degraded forest' that structurally resembles savanna but retains forest species (Scholes and Archer 1997, Ratnam et al. 2011). In contrast, since the functional traits of savanna and forest trees differ so greatly in response to fire and tree harvest, our results suggests tree harvest can lead to a shift from forest species to savanna species. The end result being a shift from forest to savanna in both structure (lower tree cover) and function (savanna species) initiated by tree harvest and subsequently driven by fire. Depending on model parameters, post-tree harvest savannas can remain stable, or the system can cycle between savanna, forest, and grassland (Fig. 5.4C).

In arid regions, savanna is the climax state except under very dry conditions below about 150 mm rainfall per year (Sankaran et al. 2005). In these arid savannas seedling establishment is limited by moisture availability and reproductive potential is stored in adult savanna trees with low intrinsic mortality (Higgins et al. 2000, Sankaran et al. 2004). Via this storage effect (Chesson 2000, Miller and Chesson 2009) trees can persist under arid conditions only if adult trees survive between highly variable rainfall events. Harvest of adult trees in arid savannas disrupts the storage potential of the system. This results in an overall reduction in adult individuals and also makes the system more vulnerable to periodic or persistent drought (Fig. 5.2C and Fig. 5.3). This has important implications for the more arid savannas of Africa where climate change is already inducing changes in tree cover (Maranz 2009). Tree harvest has the potential to aggravate the effects of climate change on woody cover in grassland-savanna transition zones. It is important to

note that in many arid regions combinations of cultural and legal norms favor collection of dead wood as opposed to harvesting live wood (Fig. 5.6; Shackleton 1998). In these situations fuelwood harvest would have little effect on woody populations. Rapid and severe reductions in woody cover are likely to occur in arid savannas in populous regions where dead wood supply does not meet human wood demand.

An interesting finding of our analysis is that savannas are generally resilient to low and moderate levels of tree harvest under environmental conditions representative of semi-arid to mesic savannas. The traits that many savanna trees have evolved to cope with frequent fire, resprouting and rapid growth, generally allow savanna trees to cope with tree harvest. Several studies report this result (Chidumayo 1990, Tiedeman and Johnson 1992, Okello et al. 2001, Shackleton 2001, Kaschula et al. 2005), but our analysis is the first to model the demographic consequences of tree harvest on savanna vegetation. While savanna as a biome can sustain tree harvest and maintain its general structure as a mix of woody and herbaceous species, our results suggest the tree component will shift rapidly to smaller size-classes (Fig. 5.2C). This means there will be less available biomass for human appropriation in savannas, even as the savanna biome persists.

Conceptually, our results indicate that tree harvest can erode intrinsic basins of attraction in forests and savannas, and in so doing, make transitions via fire or drought more likely (Fig. 5.7). Where savanna and forest are alternatively stable, we find that tree harvest can erode the intrinsic basin of attraction for forest and make a state transition to savanna or cycles among states via fire more likely (Fig. 5.7A, B). Where savanna is uniquely stable, the savanna state is resilient to all but high levels of tree harvest due to the resprouting abilities of savanna trees, and harvest of live trees mainly alters tree:grass ratios and the relative abundance of savanna saplings compared to savanna trees (Fig. 5.7B). At the arid end of the savanna distribution, tree harvest can overwhelm tree birth and recruitment rates, thus driving down tree populations and making a transition to grassland by drought more likely (Fig. 5.7C). However, tree harvest alone, especially if independent of tree cover, can also cause state shifts without an interaction with drought (Figs. 5.3A, 5.5A). Once in a treeless state the system is tree-limited and the grassland state will remain stable so long as

$\beta T = 0$, or, in ecological terms, so long as a seed source is absent.

In contrast to our theoretical results, many empirical studies report woody encroachment into savannas. In Africa, locally intense grazing can suppress fire frequency and result in woody encroachment into savanna (Archer et al. 1995, Roques et al. 2001, Goetze et al. 2006). There is also some evidence that increasing levels of atmospheric CO_2 concentration may facilitate a competitive advantage of C_3 trees and shrubs over C_4 grasses (Wigley et al. 2010, Bond and Midgley 2012). However, many of these studies have been conducted in areas where fuelwood and timber harvest is disallowed (Goetze et al. 2006) or occurs at low levels (Wigley et al. 2010) (though in these studies tree harvest was not explicitly quantified). Consequently, our results, and those of studies reporting woody encroachment, should be considered context dependent and in some cases the interacting forces of climate change, active fire management, and tree harvest will lead to dynamics not captured by the model presented here. While the importance of increasing CO_2 remains uncertain, it is clear that active fire management will be important in regulating the effects of tree harvest on savanna and forest systems. For example, Holdo et al. (2009) used a simulation model to show how fire and tree removal by elephants, in absence of heavy grazing, reduces woody cover over time via a similar feedback as the harvest–fire dynamic proposed here. In areas with high rates of tree harvest, active fire suppression may be necessary to avoid ecosystem transitions. If we were to include grazing in this theoretical model, the interaction between tree harvest and fire would be dampened because lower grass cover driven by grazing would reduce fire frequency.

The biome transitions predicted by this model are not merely of academic interest. Demand for wood fuels (firewood and charcoal) is very high in most countries of SSA and is projected to increase (Bailis et al. 2005). Additionally, charcoal use and production is predicted to increase across all of SSA (Arnold et al. 2006, Bailis et al. 2005). Charcoal production is an intensive form of land-use that results in the widespread clearing of trees that is consistent with high levels of tree harvest (ρ) in our model. Our analysis suggests that moderate rates of wood harvest – by interacting with fire, or drought – can drive persistent biome transitions from forest to savanna, and from wooded savanna to open grassland. That high rates of wood harvest can reduce tree cover is an intuitive

73

result. More surprising is our result that only moderate rates of tree harvest are required to drive state shifts because harvest interacts with extrinsic disturbances (fire) to amplify demographic consequences. In aggregate, our analysis suggests, as increases in charcoal demand and production are realized across the African continent, sudden transitions could become a widespread phenomenon across the grassland-savanna-forest continuum.

5.4.1 Limitations of Our Approach and Empirical Implications

The model analysis presented here shows tree harvest as a potentially important process in savannas and forests. However, there are several limitations to our approach. First, a simple population dynamic model as presented here can help understand underlying dynamics but can rarely fully represent real systems. The model does indicate the potential importance of tree harvest and provides some insight into the magnitude of harvest required to drive state transitions. However, to estimate the effect of harvest on current biome distribution or to forecast future biome transitions likely requires a more detailed and mechanistic modeling approach.

Second, our results rely on differential demographic responses of savanna trees (they resprout) and forest trees (they do not resprout) to tree harvest. This assumption is well tested in terms of fire response for both tree types (but see Hoffmann et al. 2009 for counter-evidence in South America) and post-harvest resprouting of savanna trees (Shackleton 2001, Wessels et al. 2013), but to our knowledge no data exists on the post-harvest resprout rate of forest trees. However, we note there is strong empirical support for a differential demographic response of forest and savanna trees to fire and for the coppicing ability of savanna trees after harvest.

Third, we assume harvesting of a savanna tree results in reversion to the sapling state. This implies that newly established saplings have the same demographic rates as coppicing saplings from a harvested tree. It may well be the case that coppice regrowth grows faster than saplings growing from seed because they have larger root systems upon which to draw. This would increase sapling-to-adult tree recruitment rates (ω_0 and ω_1) for post-harvest saplings relative to 'regular' saplings. Our qualitative interpretations of the model would not change if we included a separate

74

state for post-harvest saplings, but our quantitative results would, of course, change. If our focus was on forecasting this assumption would be important and require empirical tests.

These limitations, while constraining our inference, highlight opportunities for future empirical and theoretical work. First, our analysis clearly demonstrates the need to include tree harvest in mechanistic models of forest-savanna-grassland vegetation dynamics. Future theoretical work should aim toward explicitly modeling tree and grass biomass since harvest rates in the literature are most often reported in biomass per unit time. Our work here opens the door for more mechanistic and complex modeling approaches that combine vegetation models (e.g., Hanan et al. 2008, Beckage et al. 2009) with fuelwood demand models (e.g., Banks et al. 1996, Wessels et al. 2013) to forecast the impacts of tree harvest into the future. Second, experimental studies in the spirit of Hoffmann et al. (2003) investigating the "harvest ecology" of savanna and forest trees could test our fundamental assumption that savanna and forest trees respond differentially tree harvest. In that same vein, our analysis highlights the need to compare growth rates of "regular" saplings and post-harvest, coppicing saplings, similar to work undertaken by Wakeling et al. (2011).

5.5   Conclusions

In general, savannas are resilient to tree harvest due to the adaptations trees have evolved to cope with frequent fire. Thus, we can conclude that under low-to-moderate levels of tree harvest rates, and in all but the most arid of savannas, harvesting of trees for fuel will act as a modifier of tree:grass ratios (*sensu* Sankaran et al. 2004) in savanna systems. However, at the arid and mesic ends of the grassland-savanna-forest continuum, tree harvest can have a profound and potentially irreversible impact. At the savanna-forest ecotone a runaway feedback between tree harvest and fire frequency can drive a biome transition from forest to savanna that will likely be persistent in the absence of active fire suppression. At the grassland-savanna ecotone tree harvest can make a savanna more vulnerable to periodic droughts which, in the best case, can result in a transition to a grassland or, in the worst case, can induce a pathway of desertification (Reynolds et al. 2007).

Regardless, it is at these ecotones that tree harvest appears to have the greatest influence. As demand for wood fuels, especially charcoal, in sub-Saharan Africa increases in the coming decades we should anticipate the boundaries of the savanna biome relative to forest to shift in response. Tree harvest will likely have small, localized impacts on the stability of the savanna biome, but the demographic shift toward low-biomass saplings predicted by our model analysis could have large impacts on the availability of wood for human appropriation.

5.6 Tables

Table 5.1: Definition of model terms following notation from Staver and Levin (2012), with addition of a wood harvest component.

Model term	Definition
State variables:	
G	grass cover
S	savanna sapling cover
T	adult savanna tree cover
F	forest tree cover
Demographics:	
α	forest tree birth rate
β	savanna sapling birth rate
ω_0	savanna sapling-to-adult recruitment rate; no-fire year
ω_1	savanna sapling-to-adult recruitment rate; fire year
ϕ_0	forest tree death rate; no-fire year
ϕ_1	forest tree death rate; fire year
μ	savanna sapling death rate
ν	adult savanna tree death rate
Disturbances:	
ρ	tree harvest rate
λ	fire frequency

5.7 Figures
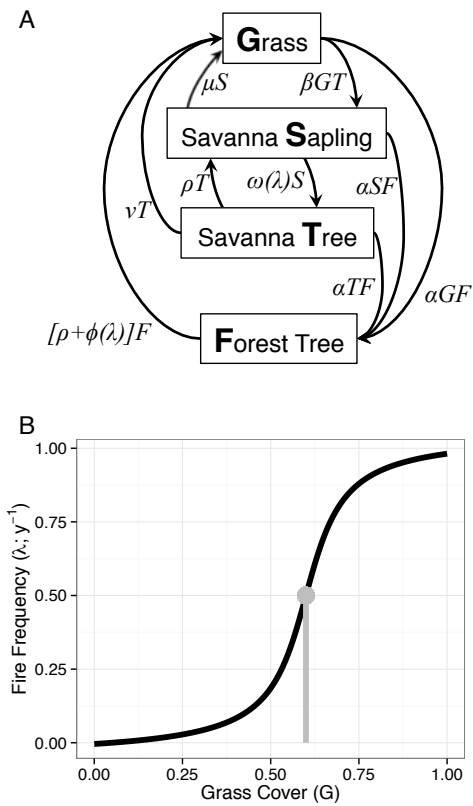
Figure 5.1: Conceptual diagram of the modified model (*A*) and functional form of fire frequency (λ; *B*). λ increases with grass cover (*G*) with a threshold response at 60% grass cover (i.e., 40% tree cover, shown by vertical grey line; see Eq. 5.23).
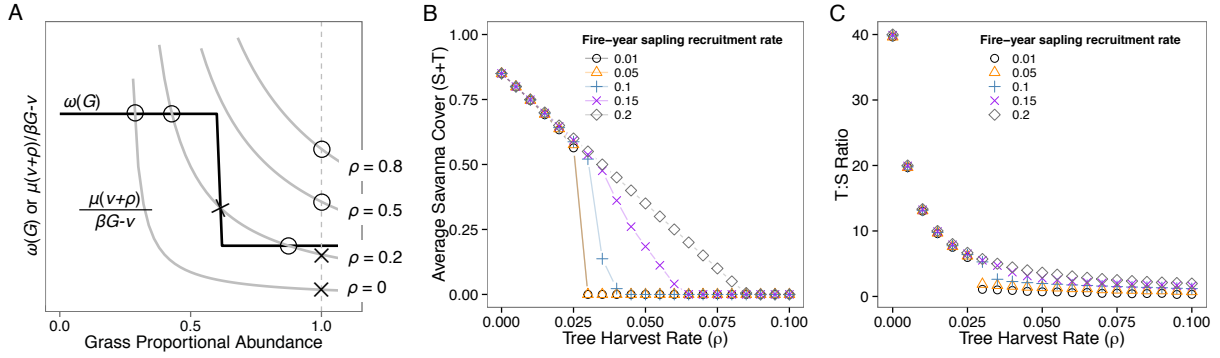
Figure 5.2: Graphical analysis of a system where forest trees are absent ($F = 0$) at different harvest rates (A) and the effect of tree harvest and sapling recruitment rate on total savanna cover (B) and the ratio of savanna trees to savanna saplings (T:S; C). In (A), open circles denote stable equilibria and crosses denote unstable equilibria. In (B) and (C), point values represent the average cover or ratio from a 10,000 year simulation after discarding initial 5,000 time steps. Symbols correspond to different values of sapling-to-tree recruitment during fire years (ω_1) as indicated in legends. Parameter combination represents a stable savanna when wood harvest (ρ) is absent ($\beta = 0.05$, $\mu = 0.1$, $\upsilon = 0.005$, $\omega_0 = 0.2$).
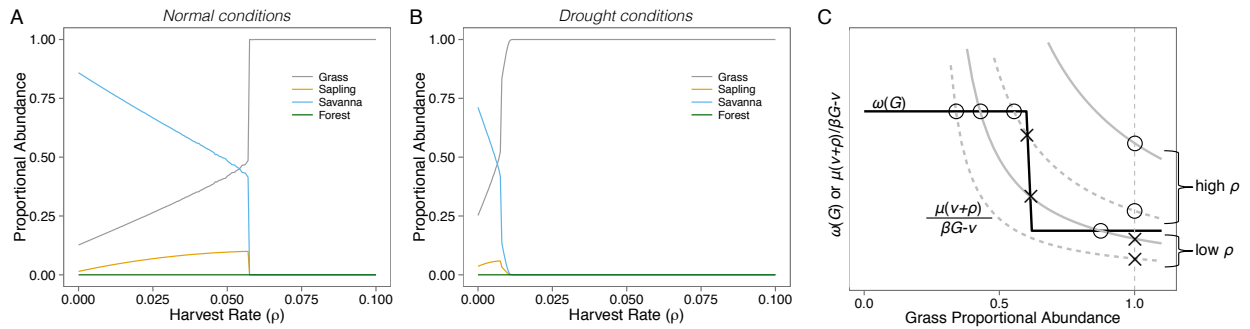
Figure 5.3: The effect of drought and tree harvest on savanna stability through interactions with fire. (A) Relative abundance at stochastic equilibrium of grass, savanna saplings and trees, and forest trees at different harvest rates under 'normal' conditions. (B) Same as in (A) but under drought conditions where, relative to (A), sapling death rate (μ) is higher and sapling intrinsic recruitment (ω_0) is lower. (C) Graphical analysis of a system where forest trees are absent ($F = 0$) at different harvest rates (high, low) and under normal conditions (dashed curves) and drought conditions (solid curves) based on the simulations shown in (A) and (B). Open circles denote stable equilibria, crosses denote unstable equilibria. Parameter combinations: (A) $\beta = 0.05$, $\mu = 0.08$, $\nu = 0.005$, $\omega_0 = 0.3$, $\omega_1 = 0.05$; (B) $\beta = 0.05$, $\mu = 0.15$, $\nu = 0.005$, $\omega_0 = 0.1$, $\omega_1 = 0.05$.
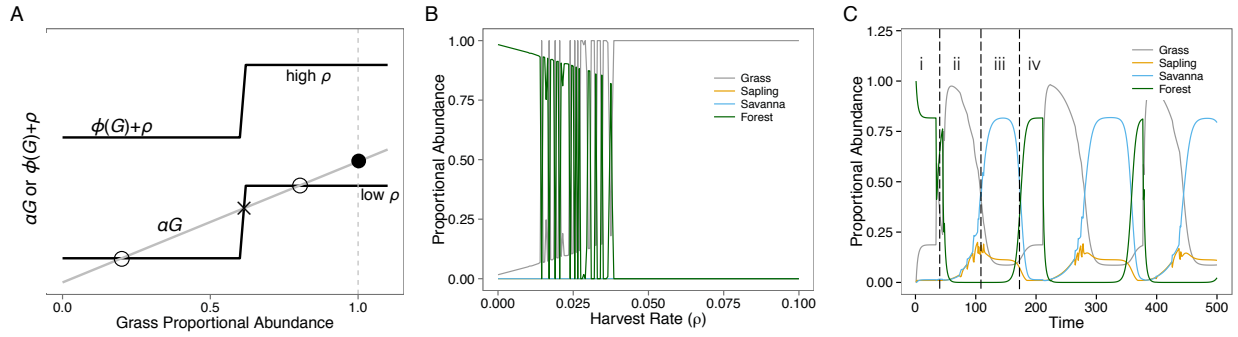
Figure 5.4: Response of a stable forest to tree harvest. (A) Graphical analysis of a system with only forest trees (F) and grass (G). Equilibria exist wherever lines intersect, with conditionally stable equilibria denoted with an open circle and unstable equilibria denoted with a cross. The closed circle represents an unstable boundary equilibrium when tree harvest (ρ) is low, but a stable boundary equilibrium when harvest is high. Tree harvest rapidly results in grassland being the only possible equilibrium when $S + T = 0$. In (B), relative abundance of grass and forest trees at stochastic equilibrium across a range of tree harvest rates. Because we use a stochastic fire term the transition from forest tree to grass dominance is dynamic, but eventually at high harvest rates (greater than about 0.035) forest trees are excluded. (C) When forest trees are excluded by a tree harvest-fire amplifying feedback savanna trees can invade and for many parameter combinations this results in going from an initial forest state (i) to cycles between low (ii) and high (iii) tree cover savannas and periods where all functional types are present (iv). For (C) we allowed low-levels of savanna saplings to be present each year to simulate a seed source in region (i). Parameter combinations: (A) $\alpha = 0.3$, $\phi_0 = 0.005$, $\phi_1 = 0.3$; (B) $\alpha = 0.3$, $\phi_0 = 0.005$, $\phi_1 = 0.5$, $\beta = 0.3$, $\omega_0 = 0.4$, $\omega_1 = 0.1$, $\nu = 0.005$, $\mu = 0.15$, $\rho = 0.05$.
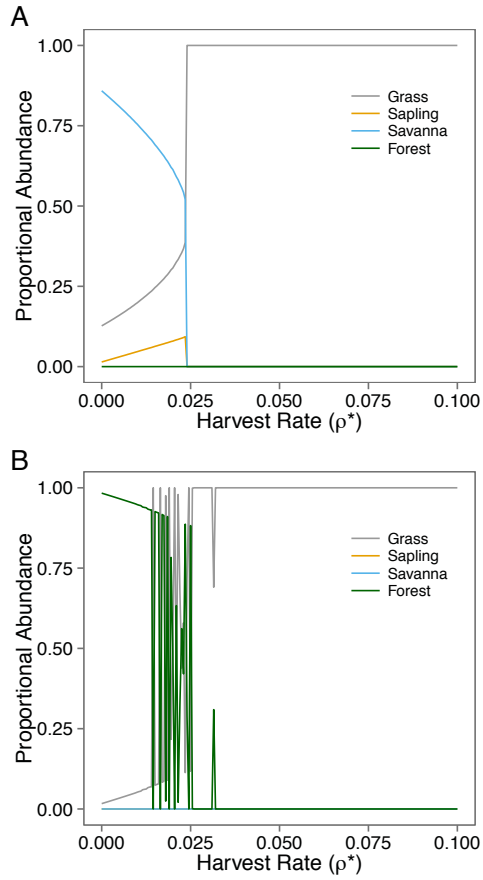
Figure 5.5: Modeling tree harvest independent of tree abundance results in transitions from savanna to grassland in dry systems (*A*) and the forest-grassland-savanna cycles (as in Fig. 5.4B, but here shown as the initial transition to grassland), in mesic systems (*B*) that occur at lower tree harvest rates. With the exception of changing the wood harvest function (ρ replaced with ρ^*), parameter values for (*A*) are as in Fig. 5.3A and for (*B*) are as in Fig. 5.4B.
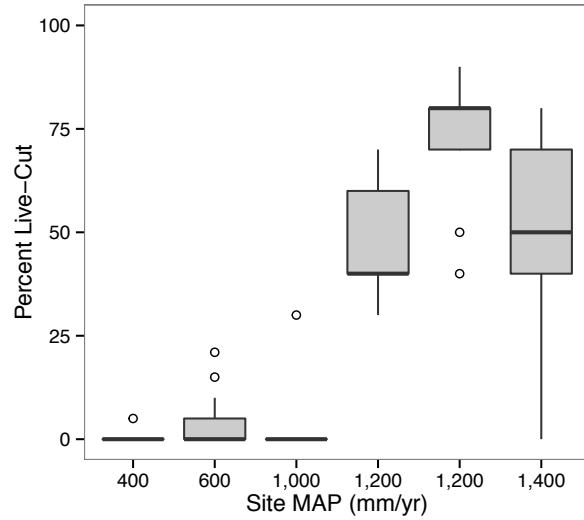
Figure 5.6: Percentage of total wood harvest from live trees across a rainfall gradient in Mali, West Africa. Data for boxplots (solid line = mean, box = upper and lower 75% quantiles, whiskers = upper and lower 95% quantiles, and points are outliers) come from household interviews conducted in 2011. Twenty households were surveyed in each village except for those at 1,200 mm mean annual precipitation where ten households were surveyed. In more arid sites dead wood is preferred.
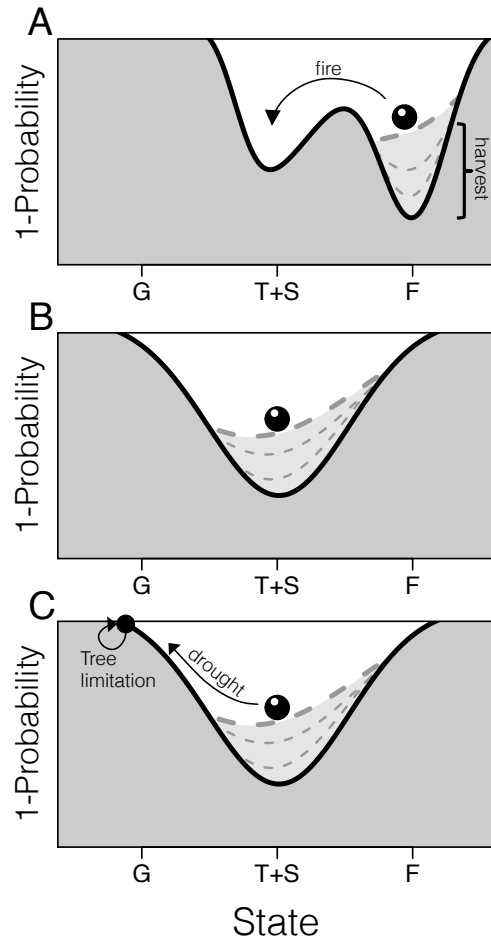
Figure 5.7: Conceptual representation of how tree harvest erodes stability basins and makes state transitions more probable. Black lines represent the 'intrinsic' stability basins of the system and dashed grey lines represent the erosion of basins by tree harvest. (*A*) Forest and savanna are alternate stable states at the mesic end of the savanna distribution (MAP > 800 mm y^{-1} in Africa); harvest erodes the stability basin and makes a transition to savanna via fire more probable. (*B*) Savanna is the climatically deterministic state at intermediate rainfall levels (300 < MAP < 800 mm y^{-1} in Africa), but tree harvest can tip the basin toward lower tree cover. (*C*) Savanna and grassland are continuous states at low rainfall levels (MAP < 300 mm y^{-1} in Africa), but harvest reduces adult tree cover to low levels and drought can more easily cause a transition to the grassland state. In a treeless state, the system is tree-limited and the grassland state is stable (filled black circle in *C*). States on *x*-axes correspond to model states: *F*, forest trees; *T+S*, savanna trees and saplings; *G*, grass. Note that in (*A*) and (*B*) we do not include the trivial equilibrium of G = 1 because we assume dispersal of seed and related recruitment occurs with high probability. MAP ranges for mesic, intermediate, and arid savannas from Sankaran et al. (2005).

Chapter 6

Conclusions

This dissertation seeks to improve our understanding of the patterns, dynamics, and ecological consequences of fuelwood harvesting in sub-Saharan Africa (SSA). I focused on four questions (see Chapter 1) that required diverse approaches at multiple scales of inquiry to answer. Fundamentally, where humans and nature interact our goal as ecologists is to ascertain the impact of essential human activities (such as tree harvest) on ecosystems. To do so requires knowledge of the magnitude and extent of human impacts and how specific human activities interact with other ecological processes. In Chapters 2–4 I focused on applied questions related to estimating the magnitude and extent of tree harvest by humans in SSA. In Chapter 5 I integrated our current knowledge of individual tree response to harvest and our current knowledge of forest and savanna vegetation dynamics. In aggregate, this dissertation represents a major step forward in our understanding of the sustainability of fuelwood harvest in SSA – that is, the ability of forest and savanna systems in SSA to continually provide woody biomass for human consumption.

A first step to quantifying fuelwood supply requires estimating the current standing stock of woody biomass in a given area. While seemingly trivial, these estimates provide the basis for any work aimed at assessing the sustainability of fuelwood harvest or the impact of harvest on an ecosystem. In Chapter 2 I found that a theoretical model of allometric scaling based on optimizing assumptions, and underpinned by evolutionary theory, provides accurate predictions for the relationship between stem diameter and stem biomass. Where locally derived allometric equations are unavailable, my works shows that Metabolic Scaling Theory can be used to estimate biomass from easily measured variables like stem diameter. Beyond these applied implications, I also found that savanna trees in Mali, West Africa tended to be taller relative to stem diameter than expected under Metabolic Scaling Theory. In line with observations from other savannas, I hypothesize these deviations reflect an evolutionary response to frequent fire in savanna systems. Thus, I propose

that Metabolic Scaling Theory provides useful baselines for allometric scaling, but that we may be able to predict deviations based on the life histories of species.

Quantifying fuelwood supply at spatial extents relevant to management requires mapping woody biomass across landscapes. In Chapter 3 I used the most widely available remote sensing data from the Landsat Thematic Mapper 5 satellite to estimate total available woody biomass in Mali, West Africa. Using simple statistical methods I developed a statistical model relating Landsat TM 5 reflectances and indices and a MODIS soil albedo index to a database of 147 field measurements of woody biomass. The estimates are associated with high uncertainty, but my regionally based estimates are greater than estimated by globally trained remote sensing models. In savannas, where the mixture of woody and herbaceous biomass is a challenge for remote sensors, it is likely that local and regional models should be used to estimate woody biomass. Not only does this provide more accurate information for the management of important resources, but careful tracking of woody biomass may allow countries with vast savannas to take part in global conservation efforts like UN-REDD+. I anticipate that including radar data in the analysis presented in Chapter 3 will reduce the uncertainty associated with my estimates.

Chapter 4 presented a novel framework for bringing together multiple sources of data to estimate, with explicit quantification of uncertainty, annual fuelwood supply and demand at large spatial extents. It is the key step of using remote sensing data to estimate parameters in a simple growth model of tree communities, and the hierarchical dependence of parameters on effective rainfall (MAP:PET), at the landscape scale that can provide a basis for monitoring fuelwood dynamics through time. Based on the best-available data I found that current annual fuelwood demand in SSA is 17-35% of annual wood production. In most parts of the continent annual fuelwood supply far outpaces demand. However, this does not preclude locally intense fuelwood shortages in many areas. Thus, I analyzed the data at multiple spatial resolutions to show how local-level demand can be met by non-local wood production. At a spatial resolution relevant to walking distances (10 km), I found that only 40% of people live in a positive fuelwood balance, and at 1,000 km still 20% of people live in negative balance. This implies that horizontal flows

of fuelwood via markets, and when necessary perhaps government programs, are vital to avoid fuelwood shortages.

Notably, many of the local fuelwood shortages exist in large cities where fuelwood markets currently exist. More troublesome are shortages in moderately populated regions that are more isolated from fuelwood markets. Future analyses focused on fuelwood distribution can build on my work here. One significant limitation of my work is that the growth model used implicitly assumes annual supply in forested regions near bioclimatic maximum biomass is near zero. However, in these resource rich environments trees would likely regrow quickly after harvest, assuming fire is controlled (see Chapter 5). So, the negative fuelwood balance I report in Chapter 4 for regions like the Congo Basin would change if I was to model fuelwood supply and demand dynamically. This is an important avenue for future research.

Lastly, in Chapter 5 I used a population dynamic model to explore the impact of tree harvest on the stable state dynamics of savanna and forest. My modeling results hinge on the assumption that savanna trees resprout successfully after harvest while forest trees, on average, do not. Under this assumption, I found that tree harvest in otherwise stable forest can result in a rapid transition to savanna because of tree harvest-fire feedback: tree harvest allows for grass growth which, in turn, increases fire frequency. Alternatively, in savannas tree harvest did not affect the stability of savanna as a biome, except under high harvest rates in parameter space representative of arid savannas. The same adaptations savanna trees have evolved to respond to frequent fire (see Chapter 2 also) make them resilient to all but the highest rates of tree harvest. This implies that tree harvest is a sustainable livelihood in savannas under at least some conditions. However, my theoretical results also suggest that tree harvest can cause a demographic shift toward low biomass trees (saplings) on the landscape. While the savanna biome may be resilient to tree harvest, the ability for savannas to provide critical ecosystem services may be undermined by chronic harvest that traps savanna saplings in the flame zone of fires.

Synthetically, the results from Chapters 4 and 5 suggest tree harvest can be a sustainable livelihood strategy, if certain caveats are considered. In Chapter 4 I found that fuelwood demand is

highest in the populated savanna regions of SSA (see Figure 4.1a and b). It is those very same regions, the savannas, that are predicted to have highest annual biomass increment increases at the landscape scale (Figure 4.1c-e) since tree biomass is often below climatic maximum (e.g., Sankaran et al. 2005). Thus, the savannas provide the most annually renewable wood biomass for harvest. Much like a savings account, tree harvest for fuelwood in moderately populated savannas takes away from interest rather than the principle. This is also consistent with my modeling results from Chapter 5.

As seen in Chapters 4 (semi-empirically) and 5 (theoretically), even in the savannas fuelwood demand can outpace supply, resulting in a loss of tree biomass and potentially a transition to a tree-less (grassland) state. This is most likely in arid savannas with relatively high populations where dead wood does not meet annual demand (Chapter 5). For example, in Chapter 4 I found the annual appropriation of annual biomass growth to fuelwood demand is very high (sometimes exceeding 100%) in the northern Sahel, Ethiopia, and Sudan (Figure 4.2b). In these arid regions drought may limit tree regrowth after harvest, resulting in low tree biomass (Chapter 5). Populated arid regions should be monitored closely. It is in these areas where researchers should focus on empirically based, mechanistic modeling of savanna vegetation (e.g., Hanan et al. 2008) and fuelwood demand (e.g., Wessels et al. 2013) to forecast fuelwood availability and ecosystem transitions. Where fuelwood harvest is deemed unsustainable, as in Wessels et al. (2013), my work in Chapter 4 can provide guidance on where best to seek wood biomass that can be transported to alleviate local shortages.

A remaining challenge is to develop linked vegetation-demand models as discussed above to forecast location-specific fuelwood dynamics. Such an approach allows for explicit consideration of annual demand based on population size, the percentage of annual demand met from live tree harvest, and tree growth with and without harvest informed by empirical data. Incorporating grass growth would result in more realistic fire dynamics in arid regions where grass biomass can limit fires (Higgins et al. 2000). This grass biomass limitation on fire is absent from my analysis in Chapter 5. Understanding the feedback between tree harvest and fire under different precipitation

regimes will be critical for effective forecasting. My work suggests broadly where and under what conditions tree harvest is likely to be sustainable, now the challenge is to confront these predictions with empirical observations.

Literature Cited

Adler, P. B., H. J. Dalgleish, and S. P. Ellner. 2012. Forecasting plant community impacts of climate variability and change: when do competitive interactions matter? Journal of Ecology **100**:478–487.

African Economic Outlook, 2010. African Economic Outlook Data and Statistics.

Ahrends, A., N. D. Burgess, S. A. H. Milledge, M. T. Bulling, B. Fisher, J. C. R. Smart, G. P. Clarke, B. E. Mhoro, and S. L. Lewis. 2010. Predictable waves of sequential forest degradation and biodiversity loss spreading from an African city. Proceedings of the National Academy of Sciences **107**:14556–14561.

Amezaga, J. M., J. Harrison, G. von Maltitz, T. Tennigkeit, S. Tiwari, and K. Windhorst, 2009. RE-Impact: Forest Based Bioenergy for Sustainable Development in Developing Countires. Technical report, European Aid Co-operation Office.

Anyamba, A., and C. J. Tucker. 2005. Analysis of Sahelian vegetation dynamics using NOAA-AVHRR NDVI data from 1981-2003. Journal of Arid Environments **63**:596–614.

Archer, S., D. Schimel, and E. Holland. 1995. Mechanisms of shrubland expansion: land use, climate or CO2? Climatic Change **29**:91–99.

Archibald, S., and W. J. Bond. 2003. Growing tall vs growing wide: tree architecture and allometry of Acacia karroo in forest, savanna, and arid environments. Oikos **102**:3–14.

Archibald, S., D. P. Roy, B. W. Van Wilgen, and J. Scholes, Robert. 2009. What limits fire? An examination of drivers of burnt area in Southern Africa. Global Change Biology **15**:613–630.

Archibald, S., A. C. Staver, and S. A. Levin. 2012. Evolution of human-driven fire regimes in Africa. Proceedings of the National Academy of Sciences **109**:847–952.

Arnold, J. E. M., G. Köhlin, and R. Persson. 2006. Woodfuels, livelihoods, and policy interventions: Changing Perspectives. World Development **34**:596–611.

Arnold, M., G. Kohlin, R. Persson, and G. Shepherd, 2003. Fuelwood Revisited: What Has Changed in the Last Decade? CIFOR Occasional Paper No. 3. Technical report, Center for International Forestry Research.

Asner, G. P., S. R. Levick, T. Kennedy-Bowdoin, D. E. Knapp, R. Emerson, J. Jacobson, M. S. Colgan, and R. E. Martin. 2009. Large-scale impacts of herbivores on the structural diversity of African savannas. Proceedings of the National Academy of Sciences **106**:4947–4952.

Babanyara, Y. Y., and U. F. Saleh. 2010. Urbanisation and the Choice of Fuel Wood as a Source of Energy in Nigeria. Journal of Human Ecology **31**:19–26.

Baccini, A., N. Laporte, S. J. Goetz, M. Sun, and H. Dong. 2008. A first map of tropical Africa's above-ground biomass derived from satellite imagery. Environmental Research Letters **3**:045011.

Bailis, R., M. Ezzati, and D. M. Kammen. 2005. Mortality and Greenhouse Gas Impacts of Biomass and Petroleum Energy Futures in Africa. Science **308**:98–103.

Banks, D. I., N. J. Griffin, C. M. Shackleton, S. E. Shackleton, and J. M. Mavrandonis. 1996. Wood supply and demand around two rural settlements in a semi-arid Savanna, South Africa. Biomass & Bioenergy **11**:319–331.

Barker, S., G. Cumming, and K. Horsfield. 1973. Quantitative morphometry of the branching structure of trees. Journal of Theoretical Biology **40**:33 – 43.

Barnes, D. F., K. Krutilla, and W. F. Hyde. 2005. The Urban Household Energy Transition. Resources for the Future, Washington, D. C.

Beckage, B., W. J. Platt, and L. J. Gross. 2009. Vegetation, Fire, and Feedbacks: A Disturbance Mediated Model of Savannas. The American Naturalist **174**:805–818.

Benjaminsen, T. 1997. Is there a fuelwood crisis in rural Mali? **43**:163–174–.

Bentley, L. P., J. C. Stegen, V. M. Savage, D. D. Smith, E. I. von Allmen, J. S. Sperry, P. B. Reich, and B. J. Enquist. 2013. An empirical assessment of tree branching networks and implications for plant allometric scaling models. Ecology Letters **16**:1069–1078.

Bertram, J. 1989. Size-dependent differential scaling in branches: the mechanical design of trees revisited **3**:241–253.

Biran, A., J. Abbot, and R. Mace. 2004. Families and Firewood: A Comparative Analysis of the Costs and Benefits of Children in Firewood Collection and Use in Two Rural Communities in Sub-Saharan Africa. Human Ecology **32**:1–25.

Bond, W. J. 2008. What Limits Trees in C4 Grasslands and Savannas? Annual Review of Ecology, Evolution, and Systematics **39**:641–659.

Bond, W. J., and J. E. Keeley. 2005. Fire as a global 'herbivore': the ecology and evolution of flammable ecosystems. Trends in Ecology & Evolution **20**:387–394.

Bond, W. J., and G. F. Midgley. 2012. Carbon dioxide and the uneasy interactions of trees and savannah grasses. Philosophical transactions of the Royal Society of London. Series B, Biological sciences **367**:601–12.

Bond, W. J., F. I. Woodward, and G. F. Midgley. 2005. The global distribution of ecosystems in a world without fire. New Phytologist **165**:525–538.

Brocard, D., J. Lacaux, G. Kouadio, and V. Yoboue, 1996. Emissions from the combustion of biofuels in western Africa. Chapter emissions from the combustion of biofuels in western africa, pages 350–360 *in* J. Levine, editor. Biomass Burning and Global Change. MIT Press.

Brouwer, R. 2004. Wood fuel consumption in Maputo, Mozambique. Biomass and Bioenergy **27**:233–245.

Brown, J. H., G. B. West, and B. J. Enquist. 2005. Yes, West, Brown and Enquist's model of allometric scaling is both mathematically correct and biologically relevant. Functional Ecology **19**:735–738.

Bucini, G., 2010. Woody Cover in African Savannas: Mapping Strategies and Ecological Insights at Regional and Continental Scales. Ph.D. thesis, Colorado State University.

Bucini, G., and N. P. Hanan. 2007. A continental-scale analysis of tree cover in African savannas. Global Ecology and Biogeography **16**:593–605.

Bucini, G., N. P. Hanan, R. B. Boone, I. P. J. Smit, S. S. Saatchi, M. A. Lefsky, and G. P. Asner, 2010. Woody fractional cover in Kruger National Park, South Africa: remote-sensing-based maps and ecological insights. *in* M. J. Hill and N. P. Hanan, editors. Ecosystem Function in Savannas: Measurement and Modeling at Landscape and Global Scales. CRC/Taylor and Francis, New York.

Cardinale, B. J. 2013. Towards a general theory of biodiversity for the Anthropocene. Elementa **1**:000014.

Cardinale, B. J., J. E. Duffy, A. Gonzalez, D. U. Hooper, C. Perrings, P. Venail, A. Narwani, G. M. Mace, D. Tilman, D. A. Wardle, A. P. Kinzig, G. C. Daily, M. Loreau, J. B. Grace, A. Larigauderie, D. S. Srivastava, and S. Naeem. 2012. Biodiversity loss and its impact on humanity. Nature **486**:59–67.

Carreiras, J., M. J. Vasconcelos, and R. M. Lucas. 2012. Understanding the relationship between aboveground biomass and ALOS PALSAR data in the forests of Guinea-Bissau (West Africa). Remote Sensing of Environment **121**:426 – 442.

Center for International Earth Science Information Network, 2005. Gridded Population of the World (GPW).

Chapin III, F. S., S. R. Carpenter, G. P. Kofinas, C. Folke, N. Abel, W. C. Clark, P. Olsson, D. M. S. Smith, B. Walker, O. R. Young, F. Berkes, R. Biggs, J. M. Grove, R. L. Naylor, E. Pinkerton, W. Steffen, and F. J. Swanson. 2010. Ecosystem stewardship: sustainability strategies for a rapidly changing planet. Trends in Ecology & Evolution **25**:241–249.

Chapin III, F. S., and E. Fernandez. 2013. Proactive ecology for the Anthropocene. Elementa **1**:000013.

Chesson, P. 2000. Mechanisms of Maintenance of Species Diversity. Annual Review of Ecology and Systematics **31**:343–366.

Chesson, P., R. L. E. Gebauer, S. Schwinning, N. Huntly, K. Wiegand, M. S. K. Ernest, A. Sher, A. Novoplansky, and J. F. Weltzin. 2004. Resource Pulses, Species Interactions, and Diversity Maintenance in Arid and Semi-Arid Environments. Oecologia **141**:236–253.

Chidumayo, E. N. 1990. Above-ground woody biomass structure and productivity in a Zambezian woodland. Forest Ecology and Management **36**:33–46.

Chidumayo, E. N., year unknown. Project Report: Inventory of Wood Used in Charcoal Production in Zambia.

Chidumayo, E. N., I. Masialeti, H. Ntalasha, and O. S. Kalumiana, 2002. Charcoal Potential in Southern Africa (CHAPOSA): Final Report for Zambia. Technical report, University of Zambia.

Clément, J. 1982. Estimation des volumes et de la productivité des formations mixtes forestières et graminéennes trtropical. Revue Bois et Forêts des Tropiques **198**:35–58.

Cline-Cole, R. A., H. A. C. Main, and J. E. Nichol. 1990. On fuelwood consumption, population dynamics and deforestation in Africa. World Development **18**:513–527.

Cochrane, M. A., A. Alencar, M. D. Schulze, C. M. Souza, D. C. Nepstad, P. Lefebvre, and E. A. Davidson. 1999. Positive Feedbacks in the Fire Dynamic of Closed Canopy Tropical Forests. Science **284**:1832–1835.

Cochrane, M. A., and W. F. Laurance. 2002. Fire as a large-scale edge effect in Amazonian forests. Journal of Tropical Ecology **18**:311–325.

Coomes, D. A. 2006. Challenges to the generality of WBE theory. Trends in Ecology & Evolution **21**:593–596.

Coomes, D. A., and R. B. Allen. 2009. Testing the Metabolic Scaling Theory of tree growth. Journal of Ecology **97**:1369–1373.

Costes, E., and Y. Guédon. 2012. Deciphering the ontogeny of a sympodial tree. Trees **26**:865–879.

Crutzen, P. J. 2002. Geology of mankind. Nature **415**:23–23.

Dahle, G., and J. Grabosky. 2010. Allometric patterns in Acer platanoides (Aceraceae) branches **24**:321–326.

Day, J. S., and K. S. Gould. 1997. Vegetative Architecture of Elaeocarpus hookerianus. Periodic Growth Patterns in Divaricating Juveniles. Annals of Botany **79**:607–616.

Dellaportas, P., and D. A. Stephens. 1995. Bayesian Analysis of Errors-in-Variables Regression Models. Biometrics **51**:1085–1095.

Desert Research Foundation of Namibia, year unknown. Biomass Energy FACT Sheet.

Dietze, M. C., M. S. Wolosin, and J. S. Clark. 2008. Capturing diversity and interspecific variability in allometries: A hierarchical approach. Forest Ecology and Management **256**:1939–1948.

Dodonov, P., I. C. Lucena, M. B. Leite, and D. M. Silva Matos. 2011. Allometry of some woody plant species in a Brazilian savanna after two years of a dry season fire. Brazilian Journal of Biology **71**:527–535.

Dovie, D., E. Witkowski, and C. Shackleton. 2004. The Fuelwood Crisis in Southern Africa: Relating Fuelwood Use to Livelihoods in a Rural Village **60**:123–133.

Ellis, J. E., and D. M. Swift. 1988. Stability of African Pastoral Ecosystems: Alternate Paradigms and Implications for Development. Journal of Range Management **41**:450–459.

Enquist, B. J. 2002. Universal scaling in tree and vascular plant allometry: toward a general quantitative theory linking plant form and function from cells to ecosystems. Tree Physiology **22**:1045–1064.

Enquist, B. J., and L. P. Bentley, 2012. Land Plants: New Theoretical Directions and Empirical Prospects, Chapter 14, pages 164 – 187 . Wiley-Blackwell, Hoboken, NJ.

Enquist, B. J., and K. J. Niklas. 2002. Global Allocation Rules for Patterns of Biomass Partitioning in Seed Plants. Science **295**:1517–1520.

Foley, J. A., R. DeFries, G. P. Asner, C. Barford, G. Bonan, S. R. Carpenter, F. S. Chapin, M. T. Coe, G. C. Daily, H. K. Gibbs, J. H. Helkowski, T. Holloway, E. A. Howard, C. J. Kucharik, C. Monfreda, J. A. Patz, I. C. Prentice, N. Ramankutty, and P. K. Snyder. 2005. Global Consequences of Land Use. Science **309**:570–574.

Food and Agriculture Organization of the United Nations, 2010. FAOSTAT 2010 Database.

Galvin, K. A. 2009. Transitions: Pastoralists Living with Change. Annual Review of Anthropology **38**:185–198.

Galvin, K. A., and R. S. Reid, 2011. People in Savanna Ecosystems. Pages 481–495 *in* M. J. Hill and N. P. Hanan, editors. Ecosystem Function in Savannas: Measurement and Modeling at Landscape to Global Scales. CRC Press, Boca Raton.

Gandar, M., 1994. Status report on biomass resources, fuelwood demand and supply strategies in South Africa. A report for Biomass Inititative. Technical report, Department of Mineral and Energy Affiars, Pretoria.

Gelman, A. 2006. Prior distributions for variance parameters in hierarchical models. Bayesian Analysis **1**:515 – 533.

Gelman, A., J. B. Carlin, H. S. Stern, and D. B. Rubin. 2004. Bayesian data analysis. Chapman and Hall / CRC, London.

Gelman, A., and J. Hill. 2009. Data analysis using regression and multilevel/hierarchical modeling. Cambridge University Press, Cambridge, UK.

Gignoux, J., J. Clobert, and J.-C. Menaut. 1997. Alternative fire resistance strategies in savanna trees. Oecologia **110**:576–583.

Goetze, D., B. Hörsch, and S. Porembski. 2006. Dynamics of forest-savanna mosaics in north-eastern Ivory Coast from 1954 to 2002. Journal of Biogeography **33**:653–664.

Good, S. P., and K. K. Caylor. 2011. Climatological determinants of woody cover in Africa. Proceedings of the National Academy of Sciences **108**:4902–4907.

Goren-Inbar, N., N. Alperson, M. E. Kislev, O. Simchoni, Y. Melamed, A. Ben-Nun, and E. Werker. 2004. Evidence of Hominin Control of Fire at Gesher Benot Ya'aqov, Israel. Science **304**:725–727.

Gowlett, J. A. J., J. W. K. Harris, D. Walton, and B. A. Wood. 1981. Early archaeological sites, hominid remains and traces of fire from Chesowanja, Kenya. Nature **294**:125–129.

Grassi, G., S. Monni, S. Federici, F. Achard, and M. D. 2008. Applying the conservativeness principle to REDD to deal with uncertainties of estimates. Environmental Research Letters **3**:3.

Hanan, N. P., W. B. Sea, G. Dangelmayr, and N. Govender. 2008. Do fires in savannas consume woody biomass? A comment on approaches to modeling savanna dynamics. American Naturalist **171**:851–856.

Hanan, N. P., A. T. Tredennick, L. Prihodko, G. Bucini, and J. Dohn. 2013. Analysis of stable states in global savannas: is the CART pulling the horse? Global Ecology and Biogeography **23**:259–263.

Hansen, M. C., R. S. DeFries, J. R. G. Townshend, M. Carroll, C. Dimiceli, and R. A. Sohlberg. 2003. Global Percent Tree Cover at a Spatial Resolution of 500 Meters: First Results of the MODIS Vegetation Continuous Fields Algorithm. Earth Interactions **7**.

Hansen, M. C., P. V. Potapov, R. Moore, M. Hancher, S. A. Turubanova, A. Tyukavina, D. Thau, S. V. Stehman, S. J. Goetz, T. R. Loveland, A. Kommareddy, A. Egorov, L. Chini, C. O. Justice, and J. R. G. Townshend. 2013. High-Resolution Global Maps of 21st-Century Forest Cover Change. Science **342**:850–853.

Hao, W. M., and M.-H. Liu. 1994. Spatial and temporal distribution of tropical biomass burning. Global Biogeochem. Cycles **8**:495–503.

Heidelberger, P., and P. D. Welch. 1983. Simulation run length control in the presence of an initial transient. Operations Research **31**:1109–1144.

Held, I. M., T. L. Delworth, J. Lu, K. L. Findell, and T. R. Knutson. 2005. Simulation of Sahel drought in the 20th and 21st centuries. Proceedings of the National Academy of Sciences of the United States of America **102**:17891–17896.

Higgins, S. I., W. J. Bond, E. C. February, A. Bronn, D. I. W. Euston-Brown, B. Enslin, N. Govender, L. Rademan, S. O'Regan, A. L. F. Potgieter, S. Scheiter, R. Sowry, L. Trollope, and W. S. W. Trollope. 2007. Effects of four decades of fire manipulation on woody vegetation structure in savanna. Ecology **88**:1119–1125.

Higgins, S. I., W. J. Bond, and W. S. W. Trollope. 2000. Fire, resprouting and variability: a recipe for grass-tree coexistence in savannas. Journal of Ecology **88**:213–229.

Higgins, S. I., S. Scheiter, and M. Sankaran. 2010. The stability of African savannas: insights from the indirect estimation of the parameters of a dynamic model. Ecology **91**:1682–1692.

Hill, M. J., and N. P. Hanan, editors. 2011. Ecosystem Function in Savannas: Measurement and Modeling at Landscape to Global Scales. CRC Press.

Hirota, M., M. Holmgren, E. H. Van Nes, and M. Scheffer. 2011. Global Resilience of Tropical Forest and Savanna to Critical Transitions. Science **334**:232–235.

Hobbs, N. T., H. Andrén, J. Persson, M. Aronsson, and G. Chapron. 2012. Native predators reduce harvest of reindeer by Sámi pastoralists. Ecological Applications **22**:1640–1654.

Hoffmann, W. A., R. Adasme, M. Haridasan, M. T. de Carvalho, E. L. Geiger, M. A. B. Pereira, S. G. Gotsch, and A. C. Franco. 2009. Tree topkill, not mortality, governs the dynamics of savanna-forest boundaries under frequent fire in central Brazil. Ecology **90**:1326–1337.

Hoffmann, W. A., E. L. Geiger, S. G. Gotsch, D. R. Rossatto, L. C. R. Silva, O. L. Lau, M. Haridasan, and A. C. Franco. 2012. Ecological thresholds at the savanna-forest boundary: how plant traits, resources and fire govern the distribution of tropical biomes. Ecology Letters **15**:759–768.

Hoffmann, W. A., B. Orthen, and A. C. Franco. 2004. Constraints to seedling success of savanna and forest trees across the savanna-forest boundary. Oecologia **140**:252–260.

Hoffmann, W. A., B. Orthen, and P. K. V. D. Nascimento. 2003. Comparative Fire Ecology of Tropical Savanna and Forest Trees. Functional Ecology **17**:720–726.

Hoffmann, W. A., and O. T. Solbrig. 2003. The role of topkill in the differential response of savanna woody species to fire. Forest Ecology and Management **180**:273–286.

Holdo, R. M., R. D. Holt, and J. M. Fryxell. 2009. Grazers, browsers, and fire influence the extent and spatial pattern of tree cover in the Serengeti. Ecological Applications **19**:95–109.

Horn, H., 2000. Scaling in Biology, Chapter twigs, trees, and the dynamics of carbon in the landscape . Oxford University Press.

Huete, A. 1988. A soil-adjusted vegetation index (SAVI). Remote Sensing of Environment **25**:295–309.

Huete, A., K. Didan, T. Miura, E. Rodriguez, X. Gao, and L. Ferreira. 2002. Overview of the radiometric and biophysical performance of the MODIS vegetation indices. Remote Sensing of Environment **83**:195–213.

Institute, W. R., 2007. EarthTrends: Environmental Information.

International Energy Agency, 2000. World Energy Outlook, 2000.

Kaptué, A. T., N. P. Hanan, and L. Prihodko. 2013. Characterization of the spatial and temporal variability of surface water in the Soudan-Sahel region of Africa. Journal of Geophysical Research: Biogeosciences **118**:1472–1483.

Kaptué, A. T., J.-L. Roujean, and S. Faroux. 2010. ECOCLIMAP-II: An ecosystem classification and land surface parameters database of Western Africa at 1-km resolution for the African Monsoon Multidisciplinary Analysis (AMMA) project. Remote Sensing of Environment **114**:961–976.

Kaschula, S. A., W. C. Twine, and M. C. Scholes. 2005. The effect of catena position and stump characteristics on the coppice response of three savannah fuelwood species. Environmental Conservation **32**:76–84.

Kebede, E., J. Kagochi, and C. M. Jolly. 2010. Energy consumption and economic development in Sub-Sahara Africa. Energy Economics **32**:532–537.

Keller, M., D. S. Schimel, W. W. Hargrove, and F. M. Hoffman. 2008. A continental strategy for the National Ecological Observatory Network. Frontiers in Ecology and the Environment **6**:282–284.

Kerkhoff, A. J., and B. J. Enquist. 2009. Multiplicative by nature: Why logarithmic transformation is necessary in allometry. Journal of Theoretical Biology **257**:519–521.

Kgathi, D. L., and P. Zhou. 1995. Biofuel use assessments in Africa: Implications for greenhouse gas emissions and mitigation strategies. Environmental Monitoring and Assessment **38**:253–269.

Kityo, P., 2004. Productivity and Utilisation of natural fuel wood resources: An evaluation of the current situation in some parts of Gaza Province, Mozambique. Msc. thesis.

Knopfle, M., 2004. A Study on Charcoal Supply in Kampala: Final Report.

Kozĺowski, J., and M. Konarzewski. 2004. Is West, Brown and Enquist's model of allometric scaling mathematically correct and biologically relevant? Functional Ecology **18**:283–289.

Krämer, P., 2003. Wood Fuel Scarcity in the Sahel and the Potential of Solar Cookers. *in* Solar Energy for Afrika Conference, Düsseldorf.

Lawes, M. J., H. Adie, J. Russell-Smith, B. Murphy, and J. J. Midgley. 2011. How do small savanna trees avoid stem mortality by fire? The roles of stem diameter, height and bark thickness. Ecosphere **2**:art42.

Leach, G., and M. M. Gowen. 1987. Household energy handbook: An interim guide and reference manual. World Bank, Washington D.C.

Lehmann, C. E. R., S. A. Archibald, W. A. Hoffmann, and W. J. Bond. 2011. Deciphering the distribution of the savanna biome. New Phytologist **191**:197–209.

Leopold, L. B. 1971. Trees and streams: The efficiency of branching patterns. Journal of Theoretical Biology **31**:339 – 354.

Levine, J. M., and C. M. D'Antonio. 2003. Forecasting Biological Invasions with Increasing International Trade. Conservation Biology **17**:322–326.

Lucas, R. M., A. C. Lee, J. Armston, J. M. B. Carreiras, K. M. Viergever, P. Bunting, D. Clewley, M. Moghaddam, P. Siqueira, and I. Woodhouse, 2011. Quantifying Carbon in Savannas: The Role of Active Sensors in Measurements of Tree Structure and Biomass, Chapter 8, pages 155–174 . CRC Press.

Madubansi, M., and C. M. Shackleton. 2007. Changes in fuelwood use and selection following electrification in the Bushbuckridge lowveld, South Africa. Journal of Environmental Management **83**:416–426.

Maranz, S. 2009. Tree mortality in the African Sahel indicates an anthropogenic ecosystem displaced by climate change. Journal of Biogeography **36**:1181–1193.

Masek, J., E. Vermote, N. Saleous, R. Wolfe, F. Hall, K. Huemmrich, F. Gao, J. Kutler, and T.-K. Lim. 2006. A Landsat surface reflectance dataset for North America, 1990-2000. Geoscience and Remote Sensing Letters, IEEE **3**:68 – 72.

McConnaughay, K. D. M., and J. S. Coleman. 1999. Biomass allocation in plants: ontogeny or optimality? A test along three resource gradients. Ecology **80**:2581–2593.

McMahon, T. 1973. Size and Shape in Biology. Science **179**:1201–1204.

McMahon, T. A., and R. E. Kronauer. 1976. Tree structures: Deducing the principle of mechanical design. Journal of Theoretical Biology **59**:443–466.

Mekonnen, A., and G. Köhlin, 2009. Determinants of household fuel choice in major cities in Ethiopia. Working Papers in Economics 399, Department of Economics, School of Business, Economics, and Law at University of Gothenburg.

Miller, A., and P. Chesson. 2009. Coexistence in Disturbance-Prone Communities: How a Resistance-Resilience Trade-Off Generates Coexistence via the Storage Effect. The American Naturalist **173**:E30–E43.

Mitchard, E. T. A., S. S. Saatchi, I. H. Woodhouse, G. Nangendo, N. S. Ribeiro, M. Williams, C. M. Ryan, S. L. Lewis, T. R. Feldpausch, and P. Meir. 2009. Using satellite radar backscatter to predict above-ground woody biomass: A consistent relationship across four different African landscapes. Geophysical Research Letters **36**:L23401.

Mitchell, T. D., and P. D. Jones. 2005. An improved method of constructing a database of monthly climate observations and associated high-resolution grids. International Journal of Climatology **25**:693–712.

Moncrieff, G. R., S. Chamaillié-Jammes, S. I. Higgins, R. B. O'Hara, and W. J. Bond. 2011. Tree allometries reflect a lifetime of herbivory in an African savanna. Ecology **92**:2310–2315.

Morton, J. A. 2007. Fuelwood Consumption and Woody Biomass accumulation in Mali, West Africa. Ethnobotany Research and Applications **5**:037–044.

Muller-Landau, H. C., R. S. Condit, J. Chave, S. C. Thomas, S. A. Bohlman, S. Bunyavejchewin, S. Davies, R. Foster, S. Gunatilleke, N. Gunatilleke, K. E. Harms, T. Hart, S. P. Hubbell, A. Itoh, A. R. Kassim, J. V. LaFrankie, H. S. Lee, E. Losos, J.-R. Makana, T. Ohkubo, R. Sukumar, I. F. Sun, M. N. Nur Supardi, S. Tan, J. Thompson, R. Valencia, G. V. Munoz, C. Wills, T. Yamakura, G. Chuyong, H. S. Dattaraja, S. Esufali, P. Hall, C. Hernandez, D. Kenfack, S. Kiratiprayoon, H. S. Suresh, D. Thomas, M. I. Vallejo, and P. Ashton. 2006. Testing metabolic ecology theory for allometric scaling of tree size, growth and mortality in tropical forests. Ecology Letters **9**:575–588.

Murphy, B. P., and D. M. Bowman. 2012. What controls the distribution of tropical forest and savanna? Ecology Letters **15**:748–758.

Mwampamba, T. H. 2007. Has the woodfuel crisis returned? Urban charcoal consumption in Tanzania and its implications to present and future forest availability. Energy Policy **35**:4221–4234.

Mwavu, E. N., and E. T. Witkowski. 2008. Sprouting of woody species following cutting and tree-fall in a lowland semi-deciduous tropical rainforest, North-Western Uganda. Forest Ecology and Management **255**:982 – 992.

Myneni, R. B., W. Yang, R. R. Nemani, A. R. Huete, R. E. Dickinson, Y. Knyazikhin, K. Didan, R. Fu, R. I. Negrón Juárez, S. S. Saatchi, H. Hashimoto, K. Ichii, N. V. Shabanov, B. Tan, P. Ratana, J. L. Privette, J. T. Morisette, E. F. Vermote, D. P. Roy, R. E. Wolfe, M. A. Friedl, S. W. Running, P. Votava, N. El-Saleous, S. Devadiga, Y. Su, and V. V. Salomonson. 2007. Large seasonal swings in leaf area of Amazon rainforests. Proceedings of the National Academy of Sciences **104**:4820–4823.

Niklas, K. J. 1994. Plant allometry the scaling of form and process. University of Chicago Press, Chicago.

Niklas, K. J., and H.-C. Spatz. 2004. Growth and hydraulic (not mechanical) constraints govern the scaling of tree height and mass. Proceedings of the National Academy of Sciences of the United States of America **101**:15661–15663.

Okello, B. D., T. G. O'Connor, and T. P. Young. 2001. Growth, biomass estimates, and charcoal production of Acacia drepanolobium in Laikipia, Kenya. Forest Ecology and Management **142**:143–153.

Oki, J. A., 1985. Domestic Energy Use in Two Villages: Addendum to Botswana Village Energy Survey. Technical report, Associates in Rural Development, Inc.

Olthof, I., D. Pouliot, R. Fernandes, and R. Latifovic. 2005. Landsat-7 ETM+ radiometric normalization comparison for northern mapping applications. Remote Sensing of Environment **95**:388–398.

Osada, N., H. Takeda, A. Furukawa, and M. Awang. 2001. Leaf dynamics and maintenance of tree crowns in a Malaysian rain forest stand. Journal of Ecology **89**:774–782.

Ouedraogo, B. 2006. Household energy preferences for cooking in urban Ouagadougou, Burkina Faso. Energy Policy **34**:3787–3795.

Parton, W. J., D. S. Schimel, D. S. Ojima, and C. V. Cole, 1994. A gereral model for soil organic matter dynamics: Sensitivity to litter chemistry, texture and management., volume SSSA Spec. Publ. 39, Pages 137–167 . ASA, CSSA, and SSA, Madison, WI.

Parton, W. J., R. J. Scholes, K. Day, J. O. Carter, and R. Kelly, 2010. CENTURY-SAVANNA Model for Tree-Grass systems. *in* M. J. Hill and N. P. Hanan, editors. Ecosystem Function in Savannas: Measurement and Modeling at Landscape to Global Scales. CRC Press, Taylor and Francis Group, Boca Raton, Florida.

Plummer, M., 2003. JAGS: a program for analysis of Bayesian graphical models using Gibbs sampling.

Plummer, M., N. Best, K. Cowles, and K. Vines, 2010. coda: Output analysis and diagnostics for MCMC. R package version 0.14-4.

Price, C. A., and B. J. Enquist. 2007. Scaling mass and morphology in leaves: an extension of the WBE model. Ecology **88**:1132–1141.

Price, C. A., B. J. Enquist, and V. M. Savage. 2007. A general model for allometric covariation in botanical form and function. Proceedings of the National Academy of Sciences **104**:13204–13209.

Price, C. A., J. F. Gilooly, A. P. Allen, J. S. Weitz, and K. J. Niklas. 2010. The metabolic theory of ecology: prospects and challenges for plant biology. New Phytologist **188**:696–710.

Price, C. A., K. Ogle, E. P. White, and J. S. Weitz. 2009. Evaluating scaling models in biology using hierarchical Bayesian approaches. Ecology Letters **12**:641–651.

Price, C. A., and J. S. Weitz. 2012. Allometric covariation: a hallmark behavior of plants and leaves. New Phytologist **193**:882–889.

Price, C. A., J. S. Weitz, V. M. Savage, J. Stegen, A. Clarke, D. A. Coomes, P. S. Dodds, R. S. Etienne, A. J. Kerkhoff, K. McCulloh, K. J. Niklas, H. Olff, and N. G. Swenson. 2012. Testing the metabolic theory of ecology. Ecology Letters **15**:1465–1474.

R Development Core Team, 2010. R: a language environment for statistical computing. R Foundation for Statistical Computing, Vienna, Austria.

R Development Core Team, 2012. R: a language environment for statistical computing.

Ratnam, J., W. J. Bond, R. J. Fensham, W. A. Hoffmann, S. Archibald, C. E. R. Lehmann, M. T. Anderson, S. I. Higgins, and M. Sankaran. 2011. When is a forest a savanna, and why does it matter? Global Ecology and Biogeography **20**:653–660.

Reid, R. S. 2012. Savannas of Our Birth: People, Wildlife, and Change in East Africa. University of California Press.

Renton, M., Y. Guédon, C. Godin, and E. Costes. 2006. Similarities and gradients in growth unit branching patterns during ontogeny in 'Fuji' apple trees: a stochastic approach. Journal of Experimental Botany **57**:3131–3143.

Reynolds, J. F., D. M. S. Smith, E. F. Lambin, B. L. Turner, M. Mortimore, S. P. J. Batterbury, T. E. Downing, H. Dowlatabadi, R. J. Fernández, J. E. Herrick, E. Huber-Sannwald, H. Jiang, R. Leemans, T. Lynam, F. T. Maestre, M. Ayarza, and B. Walker. 2007. Global Desertification: Building a Science for Dryland Development. Science **316**:847–851.

Roques, K., T. O'Connor, and A. Watkinson. 2001. Dynamics of shrub encroachment in an African savanna: relative influences of fire, herbivory, rainfall and density dependence. Journal of Applied Ecology **38**:268–280.

Rüger, N., and R. Condit. 2012. Testing metabolic theory with models of tree growth that include light competition. Functional Ecology **26**:759–765.

Russo, S. E., S. K. Wiser, and D. A. Coomes. 2007. Growth-size scaling relationships of woody plant species differ from predictions of the Metabolic Ecology Model. Ecology Letters **10**:889–901.

Saatchi, S. S., N. L. Harris, S. Brown, M. Lefsky, E. T. A. Mitchard, W. Salas, B. R. Zutta, W. Buermann, S. L. Lewis, S. Hagen, S. Petrova, L. White, M. Silman, and A. Morel. 2011. Benchmark map of forest carbon stocks in tropical regions across three continents. Proceedings of the National Academy of Sciences **108**:9899–9904.

Sander, K., S. W. Haider, and B. Hyseni. 2011. Wood-Based Biomass Energy Development for Sub-Saharan Africa: Issues and Approaches. The International Bank for Reconstruction and Development/The World Bank Group.

Sankaran, M., N. P. Hanan, R. J. Scholes, J. Ratnam, D. J. Augustine, B. S. Cade, J. Gignoux, S. I. Higgins, X. Le Roux, F. Ludwig, J. Ardo, F. Banyikwa, A. Bronn, G. Bucini, K. K. Caylor, M. B. Coughenour, A. Diouf, W. Ekaya, C. J. Feral, E. C. February, P. G. H. Frost, P. Hiernaux, H. Hrabar, K. L. Metzger, H. H. T. Prins, S. Ringrose, W. Sea, J. Tews, J. Worden, and N. Zambatis. 2005. Determinants of woody cover in African savannas. Nature **438**:846–849.

Sankaran, M., J. Ratnam, and N. P. Hanan. 2004. Tree-grass coexistence in savannas revisited: insights from an examination of assumptions and mechanisms invoked in existing models. Ecology Letters **7**:480–490.

Scholes, R. J., and S. R. Archer. 1997. Tree-Grass Interactions in Savannas. Annual Review of Ecology and Systematics **28**:517–544.

Shackleton, C. 1993. Fuelwood harvesting and sustainable utilisation in a communal grazing land and protected area of the eastern transvaal lowveld. Biological Conservation **63**:247 – 254.

Shackleton, C. M. 1998. Annual production of harvestable deadwood in semi-arid savannas, South Africa. Forest Ecology and Management **112**:139–144.

Shackleton, C. M. 2001. Managing regrowth of an indigenous savanna tree species (Terminalia sericea) for fuelwood: the influence of stump dimensions and post-harvest coppice pruning. Biomass and Bioenergy **20**:261–270.

Sharpe, G. 1976. Introduction to Forestry. 4th edition. MacGraw-Hill Book Company, New York.

Shinozaki, K., K. Yoda, K. Hozumi, and T. Kira. 1964. A quantitative analysis of plant form; the pipe model theory, I. Japanese Journal of Ecology **14**:97–105.

Smeets, E., F. X. Johnson, and G. Ballard-Tremeer. 2012. Keynote Introduction: Traditional and Improved Use of Biomass for Energy in Africa Bioenergy for Sustainable Development in Africa pages 3–12.

Sone, K., K. Noguchi, and I. Terashima. 2005. Dependency of branch diameter growth in young Acer trees on light availability and shoot elongation. Tree Physiology **25**:39–48.

Sperry, J. S., D. D. Smith, V. M. Savage, B. J. Enquist, K. A. McCulloh, P. B. Reich, L. P. Bentley, and E. I. von Allmen. 2012. A species-level model for metabolic scaling in trees I. Exploring boundaries to scaling space within and across species. Functional Ecology pages n/a–n/a.

Stark, S. C., L. P. Bentley, and B. J. Enquist. 2011. Response to Coomes & Allen (2009): 'Testing the metabolic scaling theory of tree growth'. Journal of Ecology **99**:741–747.

Staver, A. C., S. Archibald, and S. Levin. 2011*a*. Tree cover in sub-Saharan Africa: Rainfall and fire constrain forest and savanna as alternative stable states. Ecology **92**:1063–1072.

Staver, A. C., S. Archibald, and S. A. Levin. 2011*b*. The global extent and determinants of savanna and forest as alternative biome states. Science **334**:230–232.

Staver, A. C., W. J. Bond, M. D. Cramer, and J. L. Wakeling. 2012. Top-down determinants of niche structure and adaptation among African Acacias. Ecology Letters **15**:673–679.

Staver, A. C., W. J. Bond, W. D. Stock, S. J. van Rensburg, and M. S. Waldram. 2009. Browsing and fire interact to suppress tree density in an African savanna. Ecological Applications **19**:1909–1919.

Staver, A. C., and S. A. Levin. 2012. Integrating Theoretical Climate and Fire Effects on Savanna and Forest Systems. The American Naturalist **180**:211–224.

Sultan, S. E. 2000. Phenotypic plasticity for plant development, function and life history. Trends in Plant Science **5**:537–542.

Tiedeman, J., and D. Johnson. 1992. *Acacia cyanophylla* for forage and fuelwood in North Africa. Agroforestry Systems **17**:169–180.

Tilman, D., J. HilleRisLambers, S. Harpole, R. Dybzinski, J. Fargione, C. Clark, and C. Lehman. 2004. Does metabolic theory apply to community ecology? It's a matter of scale. Ecology **85**:1797–1799.

Trabucco, A., and R. Zomer. 2009. Global Aridity Index (Global-Aridity) and Global Potential Evapo-Transpiration (Global-PET) Geospatial Database. CGIAR Consortium for Spatial Information .

Tsoularis, A. 2001. Analysis of Logistic Growth Models. Research Letters of Informatics and Math Sciences pages 23–46.

Tucker, C. J. 1979. Red and Photographic Infrared Linear Combinations for Monitoring Vegetation. Remote Sensing of Environment **8**:127–150.

United Nations, D. o. E., and P. D. Social Affairs. 2011. World Population Prospects: 2010 Revision. United Nations, New York.

von Allmen, E. I., J. S. Sperry, D. D. Smith, V. M. Savage, B. J. Enquist, P. B. Reich, and L. P. Bentley. 2012. A species-level model for metabolic scaling of trees II. Testing in a ring- and diffuse-porous species. Functional Ecology **26**:1066–1076.

Wakeling, J. L., A. C. Staver, and W. J. Bond. 2011. Simply the best: the transition of savanna saplings to trees. Oikos **120**:1448–1451.

Wessels, K. J., M. S. Colgan, B. F. N. Erasmus, G. P. Asner, W. C. Twine, R. Mathieu, J. A. N. van Aardt, J. T. Fisher, and I. P. J. Smit. 2013. Unsustainable fuelwood extraction from South African savannas. Environmental Research Letters **8**:014007.

West, G. B., J. H. Brown, and B. J. Enquist. 1999. A general model for the structure and allometry of plant vascular systems. Nature **400**:664–667.

White, T. D., B. Asfaw, D. DeGusta, H. Gilbert, G. D. Richards, G. Suwa, and F. Clark Howell. 2003. Pleistocene Homo sapiens from Middle Awash, Ethiopia. Nature **423**:742–747.

Wigley, B. J., W. J. Bond, and M. T. Hoffman. 2010. Thicket expansion in a South African savanna under divergent land use: local vs. global drivers? Global Change Biology **16**:964–976.

Woldeamlak, B. 2005. Biofuel Consumption, Household Level Tree Planting and Its Implications for Environmental Management in the Northwestern Highlands of Ethiopia. Eastern Africa Social Science Research Review **21**:19–38.

World Resources Institute, 2007. EarthTrends: Environmental Information.

Xiao, X., E. P. White, M. B. Hooten, and S. L. Durham. 2011. On the use of log-transformation vs. nonlinear regression for analyzing biological power laws. Ecology **92**:1887–1894.

Zanne, A. E., G. Lopez-Gonzalez, D. A. Coomes, J. Illic, S. Jansen, S. L. Lewis, R. B. Miller, N. G. Swenson, M. C. Wiemann, and J. Chave, 2009. Global wood density database.

Appendix

Appendix for Chapter 4

A.8   Supplementary Methods

A.8.1   Continental fuelwood demand

A.8.1.1   National-level per capita fuelwood demand

The United Nations Food and Agricultural Organization (FAO) maintains an extensive database on international forest products (http://faostat.fao.org). As part of this database, the FAO reports national annual "production" for fuelwood (including wood combusted directly and as charcoal) based on government reported statistics or FAO estimates. The database contains estimates for 41 sub-Sarahan African countries and thus represents the most complete picture of continental fuelwood demand and use. We acknowledge that FAO estimates are likely low due to under-reporting of rural activities in developing nations and we address this shortcoming by using FAO estimates as "low" estimates and develop a simple model based on published fuelwood consumption estimates to derive "high" estimates (see §A.8.1.2).

FAO data for 2008 is reported in cubic meters (m^3) per country, and woody biomass consumed as charcoal has already been converted to cubic meters of "raw" wood. We first converted this estimate to m^3 person^{-1} based on national population in 2010 from a 2.5' gridded database (same as used for estimating continental patterns of wood use; Center for International Earth Science Information Network (2005)). For comparison of wood demand to wood production and standing stocks we converted cubic meters to kilograms based on an average density (mean = 605 kg m^{-3}, s.d. = 161 kg m^{-3}, n = 2833 species) of tropical and extratropical tree species in Africa from the Global Wood Density Database (Zanne et al. 2009). The FAO data for 2008, including original estimates from FAO and our conversions, are shown in Table S1.

A.8.1.2 Low and high estimates of wood consumption

In developing nations it is likely that wood consumption and demand in rural regions is under-reported by governments. Indeed, this is substantiated by an extensive literature and alternative database search (Table S2). However, fuelwood demand estimates published in the literature are lacking in two considerable ways: 1) reports are limited to regional or household data that must be scaled up to the national level, and 2) only a small subset of African nations are represented (38 accurate estimates for the entire continent). To overcome the limitations of both datasets and to address the inherent uncertainty in our analysis, we treat the FAO estimates as a "low" estimate of fuelwood demand, and explored the relationship(s) between published estimates and various economic indicators.

First, fuelwood demand was estimated from a variety of variables reported in the literature. In the simplest case, daily, monthly, or yearly wood consumption was reported in kg person^{-1}. This resulted in a very limited dataset so we designed a set of equations that allowed us to gather any number of available variables associated with wood consumption/demand and derive an estimate of total annual per capita wood demand. We began by assuming that total wood biomass energy ($\bar{E}$) is comprised of wood and charcoal such that:

$$\bar{E} = a_i e_{wood} + b_i e_{charcoal} \tag{A.28}$$

where $\bar{E}$ is total wood biomass energy use (kJ) per unit of time per person for ith country, a_i is the amount of wood (kg) used per unit time per person for country i, b_i is the amount of charcoal (kg) used per unit time per person for country i, and e_{wood} and $e_{charcoal}$ are the conversion factors (kJ kg^{-1}) for wood and charcoal, equal to 16,000 kJ kg^{-1} (Barnes et al. 2005) and 29,000 kJ kg^{-1} (Leach and Gowen 1987) , respectively. This equation allowed us to utilize the WRI Earthtrends database that reports total wood biomass energy used by African countries (World Resources Institute 2007).

To include woody biomass attributed to charcoal use we use the equation:

$$B_i = a_i + b_i \varepsilon_{w \to c} \qquad (A.29)$$

where B_i is the total woody biomass (kg) used per unit time per person for country i, a and b are as in equation 1, and $\varepsilon_{w \to c}$ is the conversion factor for kg of wood to kg of charcoal. The conversion factor of wood to charcoal is an average of estimates from published studies from five sites across Africa (mean = 0.182, s.d. = 0.059; Table A6).

Lastly, some studies simply reported the relative amounts of wood and charcoal that make up household or per capita energy use. We use these reported values as fractions of total energy derived from wood (or charcoal) such that:

$$b_i = \frac{\bar{E}_i (1 - R_w)}{e_{charcoal}} \qquad (A.30)$$

where R_w is the fraction of total energy derived from wood (or charcoal, R_c). Using this set of three equations (Eqs. A.28–A.30) we were able to use a variety of variables to estimate wood consumption by a population and in many cases derive multiple estimates (either from the above equations or multiple literature sources).

The majority of our estimates of total fuelwood demand per year are derived via Eq. A.29 since many studies reported a or b (Tables A3 and A4). We first averaged a_i and b_i for each country including those values derived from Eqs. A.28 and A.30. For countries with estimates of a and b we calculated B_i using average values as in Eq. A.29. In some cases, there were direct estimates of B_i, and in those cases all estimates of B_i (direct estimates and those calculated using a and b) were averaged for that country. This resulted in a database of fuelwood estimates for 38 African countries (Table A2; see Tables A3 and A4 for complete database and data sources).

We used this database to explore relationships between the average published estimate and FAO data and myriad economic indicators from the African Economic Outlook Database (African Economic Outlook 2010) we postulated would have an effect on the amount fuelwood in demand, including: 'Human Development Index', 'access to electricity', 'per capita gross domestic prod-

uct', 'international aid flows', 'inactivity rate', 'percent in poverty', and 'participation in economy rate'. We developed candidate statistical models where the average published estimate was the response variable and the FAO estimate or one of the economic indicators was the independent variable. All models were assessed using ordinary least squares regression as implemented in the statistical package R (R Development Core Team 2010). We inter-compared the R^2 and P values of each candidate model to choose the "best" model (i.e. the one with highest R^2 and lowest P) . The best linear model had the percent of country living below the poverty line as the explanatory variable and explained ~50% of the variation in the data (R^2 = 0.48, n = 33, $F_{1,31}$ = 30.11, P = 0.000004815; Table A5 and Figure A1). Of the 38 countries for which we obtained fuelwood demand estimates from the literature and database sources, 33 were represented in the African Economic Outlook Database (African Economic Outlook 2010) (see Table A2). We used this model to calculate "high" estimates of fuelwood demand based on each country's percentage of people living below the international poverty line (African Economic Outlook 2010). When summed for SSA, our model estimates total annual fuelwood demand to be 529.51 Tg year^{-1}. These results are shown in comparison to FAO estimates in Table A2.

We chose to only test candidate models with one explanatory variable because our goal was to extrapolate beyond the data in-hand. Had our primary goal been to simply describe the variation in the data, we would have used a step-wise multiple linear regression. However, while multiple linear regressions are useful to discover what variables influence certain patterns seen in the data, there always remains a possibility to over-fit the model, thus compromising prediction from the model. Likewise, multiple linear regressions would lead to models that may not make logical sense because of interactions among correlated variables. For these reasons, we constrained our candidate models to those with only one explanatory variable.

Though we have data for the entire continent, estimates of biomass limited the scope of the analysis to sub-Saharan Africa only, with the additional exclusion of Madagascar. Thus, we only present maps for the area of our analysis (e.g., Figure 4.1) but data for the entirety of Africa is presented in Table A1. Data used in Figure 4.1b can be re-created using the linear regression

discussed above (Table A5) and data in Table A1. Data for percent in poverty can be found in African Economic Outlook (2010).

A.8.2 Continental wood production

The first two steps in estimating annual wood production available for fuelwood supply were (1) to convert remotely-sensed estimates of woody cover in Africa to units of biomass per area and (2) to estimate climatic-potential biomass per area. For (1) we converted a 1 km resolution woody cover map of Africa produced by Bucini (2010) to biomass units using an empirical relationship between biomass divided by percent cover $\left(\frac{B}{C}\right)$ and the ratio of mean annual precipitation:potential evapotranspiration (PPT:PET). Data for $\frac{B}{C}$ came from databases compiled by Sankaran et al. (2005) and Bucini (2010), and data for mean annual precipitation and PET came from global databases (Mitchell and Jones 2005 and Trabucco and Zomer 2009, respectively). We used a linear model with intercept equal to zero assuming that at PPT:PET = 0 biomass will be zero as well. The linear fit is significant ($P \ll 0.001$) and has an $R^2 = 0.85$ (Figure A2). Thus, we used a continental scale map of PPT:PET at 1 km resolution to estimate $\frac{B}{C}$ via the linear model and then converted those estimates to biomass units using the SSA woody cover map of Bucini (2010). We placed an upper limit on the linear regression at $\frac{B}{C} = 60$ since even though some local forest patches may have biomass greater than 600 tonnes per hectare, most previous global and continental scale biomass maps do not report values exceeding 600 tonnes per hectare at spatial resolutions ~1 km (Baccini et al. 2008, Saatchi et al. 2011).

To estimate climatic-potential biomass we used the approach of Sankaran et al. (2005) with an extended database of percent woody cover. Following Sankaran et al. (2005), we used a bent-cable piecewise 99th percentile regression to approximate the upper bound of the relationship between woody cover and PPT:PET (Figure A3). The bent-cable approach allows for a smooth transition at an estimated breakpoint between two linear pieces of the model. We used the 'quantreg' library in 'R' to fit the 99th percentile piecewise regression and made sure that the proportion of model residuals less than or equal to the desired quantile (0.99) was close to that value as measure of

when the 'quantreg' procedure had converged on an adequate solution. The 'quantreg' procedure is very sensitive to starting values and tolerances, so we used a range of starting values before using the final model shown in Figure A3, where the proportion of residuals less than or equal to 0.99 is approximately 0.97. The model estimates a breakpoint at PPT:PET = 0.38441 ($\pm$0.14537), and the equation for the upper bound on woody cover as related to PPT:PET is Woody Cover (%) = 324.39(PPT:PET) - 24.99. Above the breakpoint woody cover is equal to 100%. We used this model and the continental database of PPT:PET, made by combining the datasets of Mitchell and Jones 2005 (PPT) and Trabucco and Zomer 2009 (PET), to make a map of climatic-potential woody cover at 1 km resolution. Lastly, we combined the potential woody cover map with our $\frac{B}{C}$ linear model described above to convert potential woody cover units to potential biomass per hectare. Armed with these maps, we were then able to apply the logistic growth model described next.

Given estimates of actual and potential biomass for Africa based on remote sensing, we estimated annual per unit biomass wood production using the Hyper-Gompertz logistic growth model:

$$\frac{dB}{dt} = rB_0 \left[\ln \left(\frac{K}{B_0} \right) \right]^\gamma \tag{A.31}$$

dB/dt is the stand-level biomass growth rate at any given time (kg yr^{-1}), *r* is the intrinsic growth rate (yr^{-1}), B_0 is the biomass at some time *t*-1 (kg), *K* is the stand-level carrying capacity (or potential biomass; kg), and γ is a fitted model parameter that influences the inflection point Tsoularis (2001). We chose the Hyper-Gompertz logistic equation because its functional form best fit the simulated *dB/dt* data (see below for description of simulated data) and the logistic equation has a firm theoretical basis, including biologically meaningful parameters for which we can substitute data.

To estimate wood production for the continent, we first had to derive *r*. To do so we provided data for the other terms in Eq. A.31 and used a hierarchical Bayesian approach to estimate *r* and its dependence on mean annual precipitation (MAP) (see below for full description of model). Empirical data for *dB/dt* (and B_0) were primarily only available for undisturbed 'natural' tropical

forests where growth rates are extremely low, making it difficult to derive Eq. A.31 based on published data. Therefore, in the absence of adequate field data we simulated tree growth over time for 15 sites spanning the African precipitation gradient (Figure A5).

To simulate tree growth we used the biogeochemical model CENTURY (Parton et al. 1994) as parameterized for African systems (Parton et al. 2010). CENTURY has been used across the globe for systems ranging from grasslands, to savannas, to forests. We simulated tree growth along a virtual transect of 15 sites in Africa spanning the rainfall gradient that decreases from its maximum in central Africa and the western coasts (maximum MAP = 3,000mm) to the dry edge of the Sahara desert (minimum MAP = 200mm). We used 100-year monthly weather for each site from the CRU 3.0 dataset (Mitchell and Jones 2005; http://badc.nerc.ac.uk/) to drive the model. At each site, the model was run to equilibrium, and we then simulated a clear-cut where all woody vegetation is removed. We then allowed the trees to grow back without disturbance until woody biomass again reached equilibrium (i.e. the growth curve asymptotes), repeating the 100-yr monthly weather as necessary. This resulted in a simulated yield table of 940 years of wood growth at 15 sites across Africa.

CENTURY has yet to be used in humid tropical forests where mean annual precipitation is greater than 1200mm, so we tuned the model to operate outside its parameterization space using our potential biomass estimates. Specifically, we calibrated the turn-over rate of woody biomass such that asymptotic woody biomass was attained via CENTURY that closely matched our potential biomass estimates.

To estimate r we constructed a Bayesian hierarchical model that portrayed r as a 3rd order polynomial function of mean annual precipitation (MAP):

$$r = 0 + b_1 M + b_2 M^2 + b_3 M^3 \tag{A.32}$$

where M is MAP and b_i is the coefficient. We set the intercept to 0 following the biological assumption that at 0mm MAP the intrinsic rate of growth will be 0. In turn, specific values for r at given MAP (i.e., the 'observations' for Eq. A.32) came from Eq. A.31 and the data described

above. The full model is specified as:

$$
\begin{aligned}
\Pr(\mathbf{b}, \mathbf{r^{obs}}, \boldsymbol{\gamma}, \sigma_{\mathbf{b}}, \sigma_{obs}, \sigma_{pred}, \sigma_{\mathbf{B}}|\mathbf{M}, \mathbf{X}) \quad \propto \quad & \prod_{i=1}^{940}\prod_{j=1}^{4}\prod_{k=1}^{15}\mathrm{normal}(r_{j,k}^{obs}|\mathbf{X}, \sigma_{obs}) \times \\
& \mathrm{normal}(\gamma_{j,k}|\mathbf{X}, \sigma_{obs})\mathrm{normal}(\mathbf{b}|\mathbf{B}, \sigma_{\mathbf{b}}) \times \\
& \mathrm{normal}(\mathbf{B}|0, 10^{-5})\mathrm{gamma}(\sigma_{\mathbf{b}}^{-2}|.001, .001) \times \\
& \mathrm{gamma}(\sigma_{\mathbf{B}}^{-2}|.001, .001)\mathrm{gamma}(\sigma_{pred}^{-2}|.001, .001) \times \\
& \mathrm{gamma}(\sigma_{obs}^{-2}|.001, .001) \qquad\qquad\qquad\qquad (A.33)
\end{aligned}
$$

where $\mathbf{b}$ is a 3×4 matrix of polynomial coefficients for Eq. A.32 for each soil type j, $\mathbf{M}$ is the 3,500 element vector of MAP values associated with site simulations from CENTURY, $\mathbf{X}$ is the $15\times4\times940$ array of potential biomass (K), actual biomass (B_0), and annual biomass change (dB/dt) for observation i at site k (relates to MAP) on soil type-tree parameterization j (sand-luqm, loam-acacia, loam-luqm, clay-acacia) from CENTURY simulations. r^{obs} is r in Eq. A.31 and γ is as in Eq. A.31. Coefficients $\mathbf{b}$ for each soil type-tree parameterization j were drawn hierarchically from a vector of 'global' coefficient distributions, $\mathbf{B}$. Error terms for each parameter are indicated with σ along with appropriate subscript. Priors for error terms followed an uninformative gamma distribution. Posterior distributions of model parameters were estimated using Markov Chain Monte Carlo as implemented in 'JAGS' (Plummer 2003). We recovered parameter distributions from three MCMC chains after assuring each chain had achieved convergence using the Gelman diagnostic in the 'coda' package Plummer et al. (2010) of 'R'. For an example of the fitted model compared to CENTURY data see Figure A6.

The estimated r values for each soil type, their relationship with MAP (from Eq. A.32), and the average prediction line is shown in Fig. A7. There was no significant difference among soil type-tree parameters in Equation A.32, so we use the average prediction line (r^{pred}) of the four polynomials calculated for each soil type-tree parameterization:

$$r^{pred} = \frac{\sum\limits_{j=1}^{4} P_j}{4} \qquad\qquad (A.34)$$

where P_j is the polynomial (Eq. A.32) for soil type-tree parameterization j. Averaging of polynomial coefficients, or drawing them hierarchically from the 'global' parameter population, results in awkward non-linear behavior. So we chose to use Eq. A.34 to calculate the average prediction for r^{pred} based on MAP as shown in Fig. SA7. Note that under the Bayesian hierarchical framework we explicitly estimate uncertainty around both estimated r values and the average prediction line. There was no statistical variation in γ so we used its average value.

To make estimates of r^{pred} spatially-explicit we applied the mean, 2.5% quantile, and 97.5% quantile estimates of r^{pred} to a gridded 96-year average precipitation database at 1km resolution (Mitchell and Jones 2005). Thus, we derived three maps for the mean, upper 95% CI, and lower 95% CI estimates of r to be input to Eq. A.31. Likewise, from remote-sensing estimates (Bucini 2010) we have the parameters B_0 (actual biomass) and K (potential biomass). Using those estimates, and average γ, we derived three maps of *dB/dt* (Figures 4.1c-d) based on Eq. A.31: (1) median *dB/dt*, (2) high *dB/dt* (using upper 95% CI for r), and (3) low *dB/dt* (using lower 95% CI for r).

A.9 Supplementary Tables

Table A1: FAO estimates of wood production for sub-Saharan Africa. Production in kg converted from production in cubic meters using average African wood density (see text for details).

Country	Population (2008)	FAO Production ($m^3 \ yr^{-1}$)	FAO Production ($m^3 \ cap^{-1} \ yr^{-1}$)	FAO Production ($kg \ cap^{-1} \ yr^{-1}$)
Algeria	31,663,454	7,968,439	0.252	152.255
Angola	16,004,456	3,827,738	0.239	144.696
Benin	8,524,364	6,184,200	0.725	438.911
Botswana	1,636,163	673,900	0.412	249.186
Burkina Faso	15,760,981	12,418,300	0.788	476.688
Burundi	8,722,442	8,965,300	1.028	621.845
Cameroon	17,775,682	9,732,500	0.548	331.248
Cape Verde	214,532	1,845	0.009	5.203
Central African Republic	4,475,223	6,016,500	1.344	813.363
Chad	10,806,258	6,830,300	0.632	382.402
Comoros	212,000	na	na	na
Democratic Rep. of Congo	71,015,763	74,315,257	1.046	633.109
Rep. of Congo	4,270,402	1,295,100	0.303	183.481

Cote d'Ivoire	19,079,777	8,834,900	0.463	280.146
Djibouti	402,054	na	na	na
Egypt	72,840,590	17,283,000	0.237	143.549
Equatorial Guinea	461,002	188,800	0.410	247.773
Eritrea	5,016,988	2,564,800	0.511	309.290
Ethiopia	79,959,980	98,489,400	1.232	745.199
Gabon	1,198,031	534,100	0.446	269.718
Gambia	537,756	674,900	1.255	759.293
Ghana	24,044,705	35,363,400	1.471	889.795
Guinea	9,655,578	11,845,500	1.227	742.216
Guinea-Bissau	1,241,876	422,000	0.340	205.584
Kenya	36,409,407	21,140,900	0.581	351.290
Lesotho	1,964,387	2,076,100	1.057	639.406
Liberia	4,306,577	6,502,500	1.510	913.489
Libyan Arab Jamahiriya	5,568,774	926,200	0.166	100.624
Madagascar	19,803,646	33,761,900	1.705	1031.424
Malawi	13,617,831	5,293,000	0.389	235.152
Mali	15,264,907	5,202,900	0.341	206.209
Mauritania	3,314,549	1,747,100	0.527	318.896

Mauritius	286,000	6,600	0.023	13.962
Morocco	27,662,398	425,000	0.015	9.295
Mozambique	21,239,265	16,724,000	0.787	476.383
Namibia	1,813,987	na	na	na
Niger	16,030,462	9,431,900	0.588	355.966
Nigeria	142,626,076	62,388,600	0.437	264.644
Rwanda	9,278,697	9,591,200	1.034	625.376
Sao Tome and Principe	73,847	na	na	na
Senegal	8,473,364	5,365,800	0.633	383.119
Sierra Leone	5,899,572	5,508,800	0.934	564.926
Somalia	12,362,925	11,806,600	0.955	577.775
South Africa	42,826,611	19,560,400	0.457	276.324
Sudan	38,492,651	18,325,600	0.476	288.029
Swaziland	999,626	1,028,400	1.029	622.415
United Rep. of Tanzania	42,280,003	22,351,700	0.529	319.839
Togo	4,764,718	5,927,000	1.244	752.581
Tunisia	9,426,203	2,170,000	0.230	139.277
Uganda	32,221,420	38,467,800	1.194	722.284
Zambia	13,106,420	8,839,900	0.674	408.055
Zimbabwe	14,906,500	8,543,100	0.573	346.733

AFRICA TOTAL	950,540,882	637,543,179	NA	NA

Table A2: Fuelwood demand estimates from published studies and from FAO estimates. On average, FAO underestimates fuelwood demand compared to reported statistics in the literature.

Country	Average Published Estimate (kg cap^{-1} yr^{-1})	FAO Estimate (kg cap^{-1} yr^{-1})	Percent of Country Living in Poverty (<1 USD day^{-1})*
Algeria	6.280841182	152.255	0.9
Angola	1042.483115	144.696	54.31
Benin	515.9111857	438.9114639	47.3
Botswana	582.425296	249.1863743	31.2
Burkina Faso	769.8741904	476.6880662	56.5
Cameroon	685.4470383	331.248197	32.8
Congo	413.6159448	183.4805126	54.1
Democratic Republic of Congo	578.173575	633.1091671	59.22
Cote d'Ivoire	662.2667714	280.1455392	23.3
Egypt	51.40772144	143.5492907	1.99
Eritrea	260.7889373	309.2899491	na
Ethiopia	641.7194558	745.1988711	39.04
Gabon**	2208.232204	269.7179163	4.84
Gambia	727.187156	759.2926194	34.3
Ghana	640.0471725	889.794963	30
Guinea	1017.923387	742.2163111	70.1

Guinea-Bissau	761.0752294	205.5841873	48.8
Kenya	745.2843077	351.2895544	19.72
Liberia	877.3012392	913.4893663	83.7
Libyan Arab Jamahiriya	72.36410772	100.6237605	na
Malawi	690.7306588	235.1523595	73.86
Mali	488.1809801	206.2085624	51.4
Mauritania	366.2389908	318.8957232	21.2
Morocco	42.56816372	9.295108731	2.5
Mozambique	795.1187802	476.3827681	74.7
Namibia	268.3126723	na	32.8
Niger	336.8486464	355.9660141	65.9
Nigeria	960.8128506	264.6437736	64.4
Senegal	495.6308455	383.119246	33.5
Sierra Leone	852.2582569	564.9263978	53.4
South Africa	680.0640693	276.3244998	26.2
Sudan	907.3355223	288.0286908	na
Tanzania	1007.526515	319.8386388	88.52
Togo	897.3460506	752.5807119	38.7
Tunisia	311.1937028	139.2766533	2.55
Uganda	978.495517	722.2840779	51.5
Zambia	1148.286756	408.0549432	64.29

Zimbabwe	1057.30301	346.7329986	61.9
AVERAGE	**672.212128**	**388.8507642**	**NA**

*From African Economic Outlook Database (http://www.africaneconomicoutlook.org/po/)

**Excluded from analysis as an outlier

Table A3: Published estimates of energy demand in African countries. Variables correspond to those outlined in Appendix A, **Low and high estimates of wood consumption**. Detailed data for South Africa is in Table A4.

Country	Source	Variable	Estimate
Algeria	WRI 2007	*B*	6.28
Algeria	WRI 2007	*b*	18.23
Angola	WRI 2007	*B*	1042.48
Angola	WRI 2007	*b*	54.28
Benin	WRI 2007	*B*	513.26
Benin	Brocard et al. (1996)	*a*	456.25
Benin	WRI 2007	*b*	19.72
Benin	Brocard et al. (1996)	*b*	2.92
Botswana	Oki (1985)	*a*	359.52
Botswana	WRI 2007	*b*	38.82
Burkina Faso	Brocard et al. (1996)	*a*	613.20
Burkina Faso	WRI 2007	*b*	28.46
Cameroon	WRI 2007	*B*	807.59
Cameroon	Cline-Cole et al. (1990)	*a*	514.91
Cameroon	WRI 2007	*b*	8.79
Cape Verde	WRI 2007	*b*	4.66
Central African Rep.	WRI 2007	*b*	8.69
Chad	WRI 2007	*b*	31.62
Congo	WRI 2007	*B*	413.62
Congo, Dem. Rep.	WRI 2007	*B*	578.17
Congo, Dem. Rep.	WRI 2007	*b*	20.39
Cote d'Ivoire	WRI 2007	*B*	626.90
Cote d'Ivoire	Brocard et al. (1996)	*a*	408.80

Cote d'Ivoire	WRI 2007	*b*	46.54
Cote d'Ivoire	Brocard et al. (1996)	*b*	58.40
Egypt	WRI 2007	*B*	51.41
Egypt	WRI 2007	*b*	16.87
Eritrea	WRI 2007	*B*	260.79
Eritrea	WRI 2007	*b*	18.96
Ethiopia	WRI 2007	*B*	641.72
Ethiopia	Mekonnen and Köhlin (2009)	*a*	405.30
Ethiopia	Woldeamlak (2005)	*a*	353.90
Gabon	WRI 2007	*B*	2208.23
Gambia	Brocard et al. (1996)	*a*	379.60
Gambia	Brocard et al. (1996)	*b*	63.15
Ghana	WRI 2007	*B*	641.76
Ghana	Brocard et al. (1996)	*a*	401.50
Ghana	WRI 2007	*b*	29.11
Ghana	Brocard et al. (1996)	*b*	56.94
Guinea	Brocard et al. (1996)	*a*	897.90
Guinea	Brocard et al. (1996)	*b*	13.51
Guinea	WRI 2007	*b*	30.10
Guinea-Bissau	Brocard et al. (1996)	*a*	481.80
Guinea-Bissau	Brocard et al. (1996)	*b*	50.73
Kenya	WRI 2007	*B*	924.68
Kenya	Cline-Cole et al. (1990)	*a*	496.69
Kenya	WRI 2007	*b*	12.57
Liberia	Brocard et al. (1996)	*a*	653.35
Liberia	WRI 2007	*b*	45.23
Liberia	Brocard et al. (1996)	*b*	36.13

Libya	WRI 2007	*B*	72.36
Madagascar	WRI 2007	*b*	35.34
Malawi	Biran et al. (2004)	*a*	525.20
Malawi	WRI 2007	*b*	30.07
Mali	Benjaminsen (1997)	*a*	368.75
Mali	Morton (2007)	*a*	379.97
Mali	Brocard et al. (1996)	*a*	609.55
Mali	WRI 2007	*b*	6.67
Mali	Brocard et al. (1996)	*b*	6.21
Mauritania	Brocard et al. (1996)	*a*	193.45
Mauritania	Brocard et al. (1996)	*b*	31.39
Mauritius	WRI 2007	*b*	2.79
Morocco	WRI 2007	*B*	42.57
Mozambique	WRI 2007	*B*	867.97
Mozambique	Kityo (2004)	*a*	607.81
Mozambique	Brouwer (2004)	*a*	423.40
Mozambique	WRI 2007	*b*	16.69
Mozambique	Brouwer (2004)	*b*	58.40
Namibia	WRI 2007	*B*	268.31
Niger	Cline-Cole et al. (1990)	*a*	379.12
Niger	Brocard et al. (1996)	*a*	266.45
Niger	Cline-Cole et al. (1990)	*b*	2.56
Niger	Brocard et al. (1996)	*b*	2.56
Nigeria	WRI 2007	*B*	1498.04
Nigeria	Cline-Cole et al. (1990)	*a*	280.82
Nigeria	Brocard et al. (1996)	*a*	481.80
Nigeria	WRI 2007	*b*	6.23

Nigeria	Brocard et al. (1996)	*b*	9.12
Reunion	WRI 2007	*b*	1.22
Rwanda	WRI 2007	*b*	14.30
Senegal	WRI 2007	*B*	368.11
Senegal	Brocard et al. (1996)	*a*	379.96
Senegal	Brocard et al. (1996)	*b*	63.15
Senegal	WRI 2007	*b*	25.21
Sierra-Leone	Brocard et al. (1996)	*a*	653.35
Sierra-Leone	Brocard et al. (1996)	*b*	36.13
South Africa	WRI 2007	*B*	838.12
South Africa	average from Table A4	*a*	510.18
South Africa	WRI 2007	*b*	2.15
Sudan	WRI 2007	*B*	907.34
Sudan	WRI 2007	*b*	20.64
Tanzania	WRI 2007	*B*	1077.34
Tanzania	Biran et al. (2004)	*a*	473.20
Tanzania	Mwampamba et al. (2007)	*b*	138.60
Tanzania	WRI 2007	*b*	30.17
Togo	WRI 2007	*B*	1095.09
Togo	Brocard et al. (1996)	*a*	332.15
Togo	WRI 2007	*b*	78.03
Togo	Brocard et al. (1996)	*b*	55.48
Tunisia	WRI 2007	*B*	311.19
Tunisia	WRI 2007	*b*	20.75
Uganda	Amezaga et al. (2009)	*E*	11777440.00
Uganda	Amezaga et al. (2009)	*a*	680.00
Uganda	Amezaga et al. (2009)	*a*	240.00

Uganda	WRI 2007	b	23.24
Uganda	Amezaga et al. (2009)	b	4.00
Uganda	Amezaga et al. (2009)	b	120.00
Uganda	Knöpfle (2004)	r_w	0.92
Uganda	Knöpfle (2004)	r_w	0.25
Uganda	Knöpfle (2004)	r_c	0.08
Uganda	Knöpfle (2004)	r_c	0.75
Zambia	WRI 2007	B	1119.06
Zambia	Kgathi and Zhou (1995)	a	1200.00
Zambia	Kgathi and Zhou (1995)	a	150.00
Zambia	WRI 2007	b	55.16
Zambia	Chidomayo et al. (2002)	b	120.00
Zambia	Kgathi and Zhou (1995)	b	20.00
Zambia	Kgathi and Zhou (1995)	b	170.00
Zambia	Chidomayo et al. (2002)	r_w	0.24
Zambia	Chidomayo et al. (2002)	r_c	0.76
Zimbabwe	WRI 2007	B	1057.30
Zimbabwe	WRI 2007	b	0.66

Notes: Not all values reported here were used in final country-level estimates. We used *B* whenever possible, and calculated *B* for countries where we had estiamtes of *a* and *b*. We report the full database here becase the World Resource Institute Earthtrends database is no longer operational and these data may prove useful for others in the future. In table, WRI = World Resource Institute Earthtrends Database. All data source can be found in the **Literature Cited section.**

Table A4: Published annual wood demand (kg per capita per year; *a*) estimates for South Africa.

a	Source
505.20	Banks et al. (1996)
352.80	Banks et al. (1996)
692.00	Dovie et al. (2004)
237.00	Gandar (1994)
270.00	Gandar (1994)
297.00	Gandar (1994)
302.00	Gandar (1994)
371.00	Gandar (1994)
375.00	Gandar (1994)
394.00	Gandar (1994)
409.00	Gandar (1994)
484.00	Gandar (1994)
485.00	Gandar (1994)
498.00	Gandar (1994)
500.00	Gandar (1994)
505.00	Gandar (1994)
540.00	Gandar (1994)
560.00	Gandar (1994)
572.00	Gandar (1994)
620.00	Gandar (1994)
610.00	Gandar (1994)
640.00	Gandar (1994)
650.00	Gandar (1994)
655.00	Gandar (1994)

740.00	Gandar (1994)
760.00	Gandar (1994)
766.00	Gandar (1994)
772.00	Gandar (1994)
806.00	Gandar (1994)
1120.00	Gandar (1994)
26.00	Gandar (1994)
40.00	Gandar (1994)
134.00	Gandar (1994)
213.00	Gandar (1994)
376.00	Gandar (1994)
450.00	Gandar (1994)
648.00	Gandar (1994)
742.00	Gandar (1994)
780.00	Madubansi and Shackleton (2006)

Table A5: Details of linear model used to estimate upper bound of fuelwood demand**.** Analysis is based on values presented in Supplementary Table A2 with Gabon excluded as an outlier. Model: Lit-Base ~ Perc_Pov, $R^2 = 0.48$, n = 33, $F_{1,31} = 30.11$, $P = 0.000004815$

Coefficient	Estimate	SE	*P*
Intercept	260.062	80.335	0.00281
Percent in Poverty (Slope)	8.867	1.616	0.00000482

Notes: "Lit-Base" refers to fuelwood demand estimates derived from country-level averages of published studies and Earthtrends estimates (World Resources Institute 2007). "Perc_Pov" refers to the percent of people in a country living below the international poverty line, defined as living on less than 1 USD day^{-1}. Literature-based estimates are shown in Table A2. Percent in poverty values were obtained from the African Economic Outlook (2010).

Table A6: Wood to charcoal conversion factors ($\varepsilon_{w \to c}$; kg charcoal per kg wood).

Country	$\varepsilon_{w \to c}$ (kg charcoal/kg wood)	Source
Zambia	0.230	Chidumayo (year unknown)
Zambia	0.265	Chidumayo et al. (2002)
Mozambique	0.14	Brouwer (2004)
Namibia	0.2	Desert Research Foundation of Namibia
Uganda	0.125	Knopfle (2004)
Chad	0.13	Krämer (2003)
AVERAGE	**0.182**	
Std. Dev.	**0.059**	

A.10 Supplementary Figures
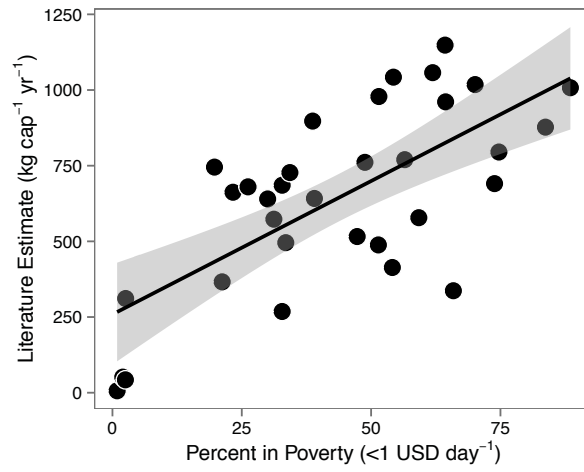
Figure A1: Linear model to estimate upper bound of fuelwood demand. Filled circles show data based on averaged fuelwood demand as derived from literature search and Earthtrends estimates (Gabon excluded as outlier) and the percent of the country living below the international poverty line (<1 USD per day). Solid line shows linear model (R^2 = 0.48, n=33, $F_{1,32}$ = 30.11, P = 0.000004815) and dashed lines show the 95% confidence intervals. See Table A5 for model details. The model is inherently bounded by 0 and 100 on the x-axis thus allowing for robust extrapolation to other countries based on the percent in poverty.
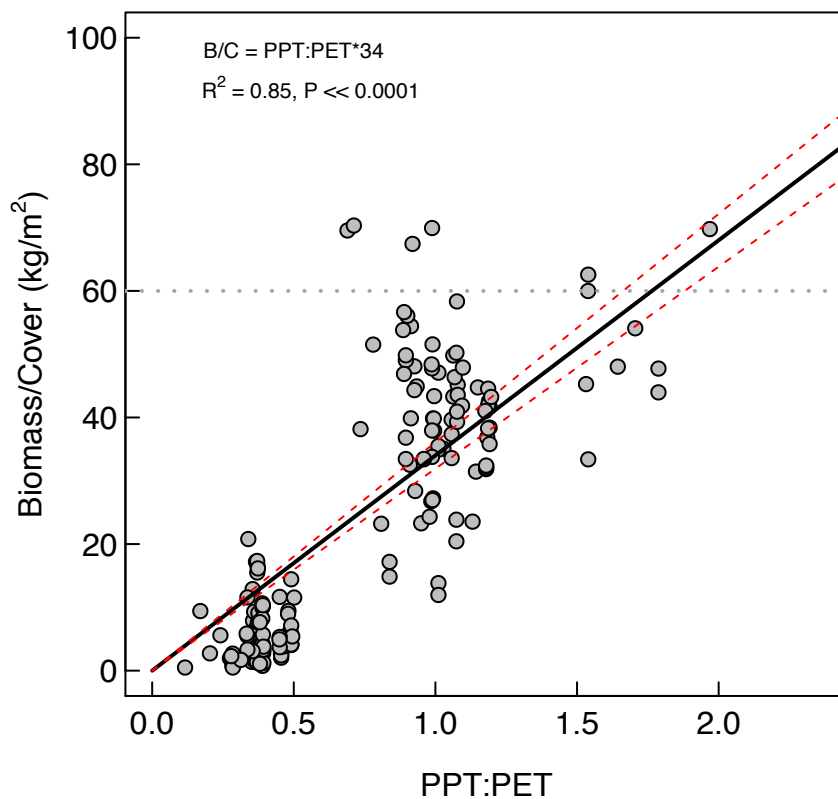
Figure A2: Empirical relationship between $\frac{B}{C}$ and PPT:PET used to convert woody cover units (%) to biomass (kg ha^{-1}). We set the intercept = 0 under the assumption that at PPT:PET = 0, biomass will also equal 0. Black line is the mean estimate and red lines are the upper and lower 95% confidence intervals. The dashed grey line shows the upper limit we used when actually extrapolating the linear model based on continental databases of PPT and PET. Data points come from a combined database from Sankaran et al. (2005) and Bucini (2010) (n = 205) See text for details.
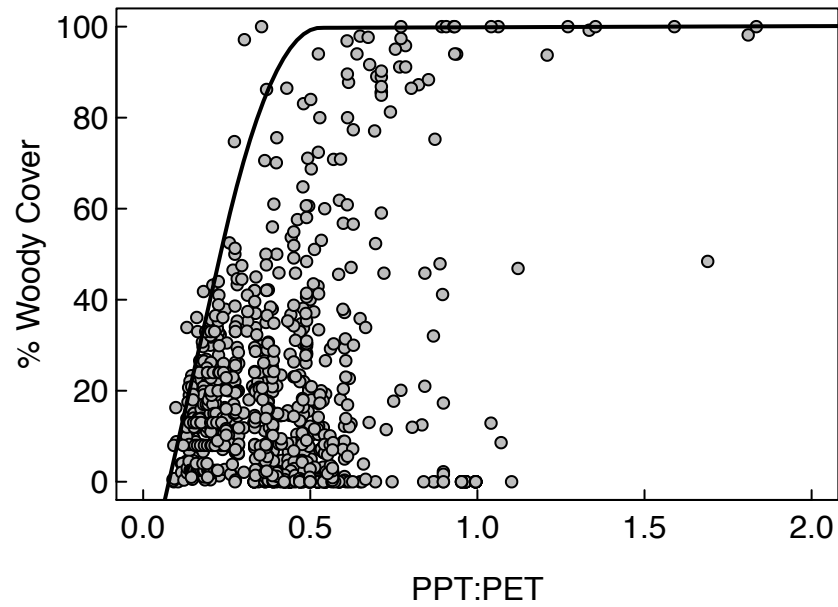
Figure A3: Bent-cable piece-wise 99th percentile regression representing climatic-potential woody cover. Data points come from a combined database from Sankaran et al. (2005) and Bucini (2010) (n = 842). See text for details.
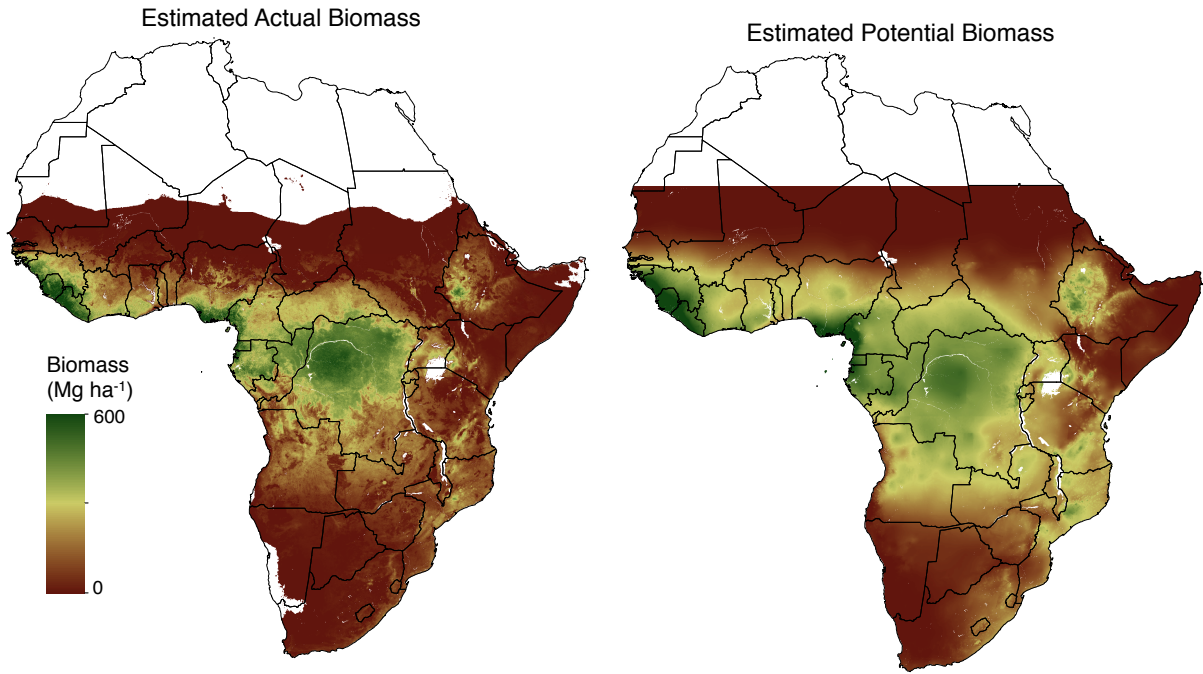
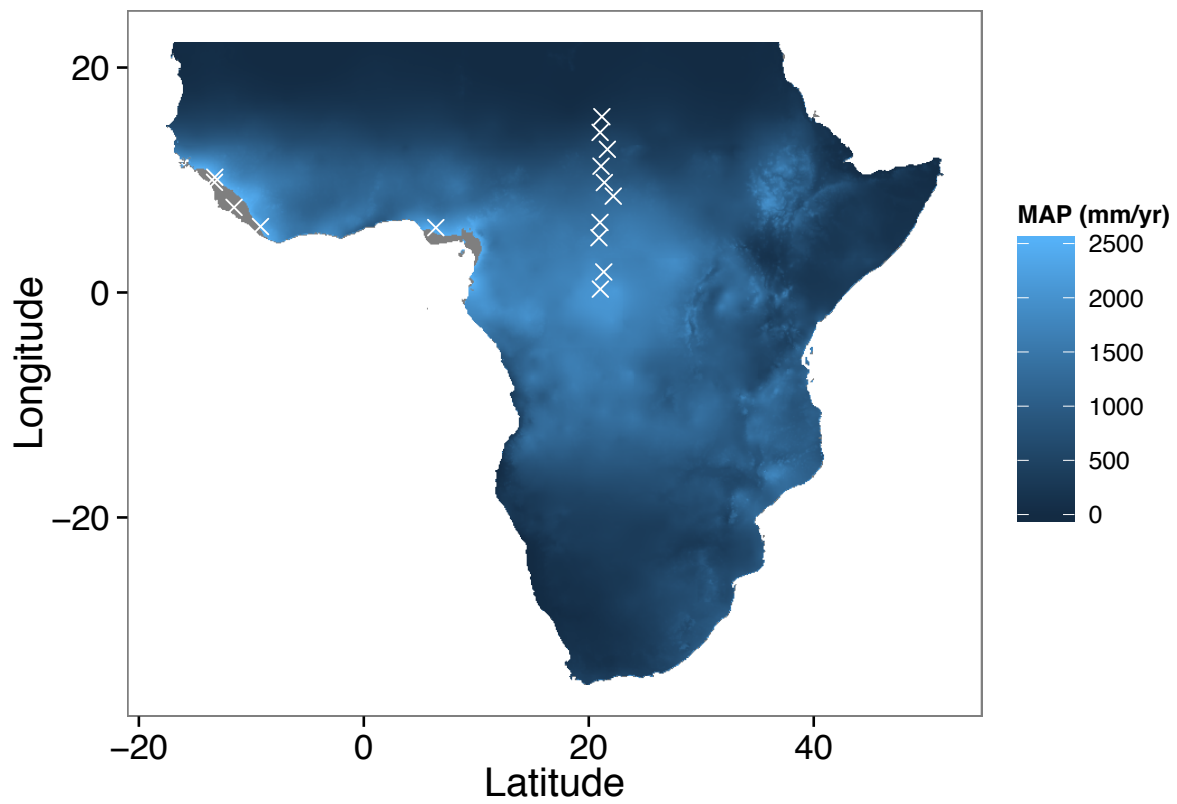*Figure A4:* Actual and potential biomass for SSA.

Figure A5: Map of SSA showing point locations of CENTURY simulations. Grey areas are those above 2,500 mm precipitation per year. Most of Africa receives less than or equal to 2,500 mm precipitation.
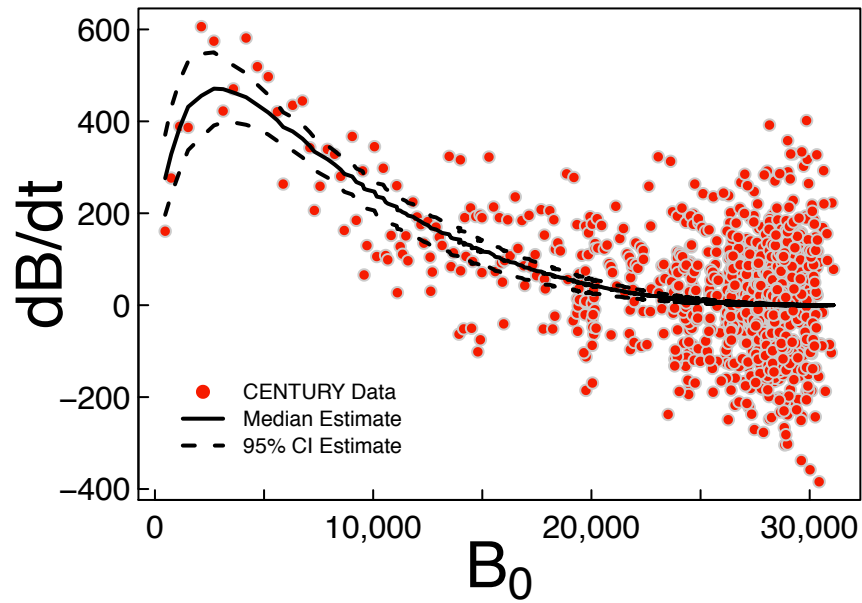
Figure A6: Example of the Hyper-Gompertz logistic model fit to CENTURY data. B_0 on the *x*-axis refers to the standing stock of biomass and dB/dt on the *y*-axis refers to the annual incremental biomass change associated with each B_0. The terms displayed in this figure are described in the Appendix text and refer to Equation A.31.
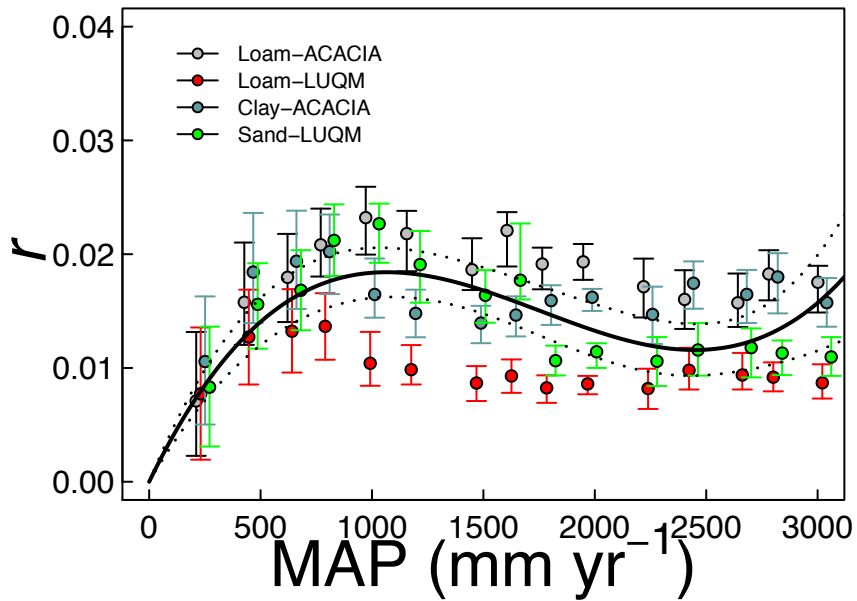
Figure A7: Relationship between mean annual precipitation and *r*. Points represent model estimates of *r* on individual soils (loam run under two different parameterizations) at individual rain-levels with whiskers representing their 95% credible intervals. The solid line is the mean polynomial across all four soil types with dashed lines showing the 95% credible intervals. The curve follows an expected near 'hump-shape' where *r* is highest at intermediate MAP and lower at low MAP due to water limitations and also lower at high MAP due to leaching of nutrients. Points at each rainfall level are staggered for visualization purposes.
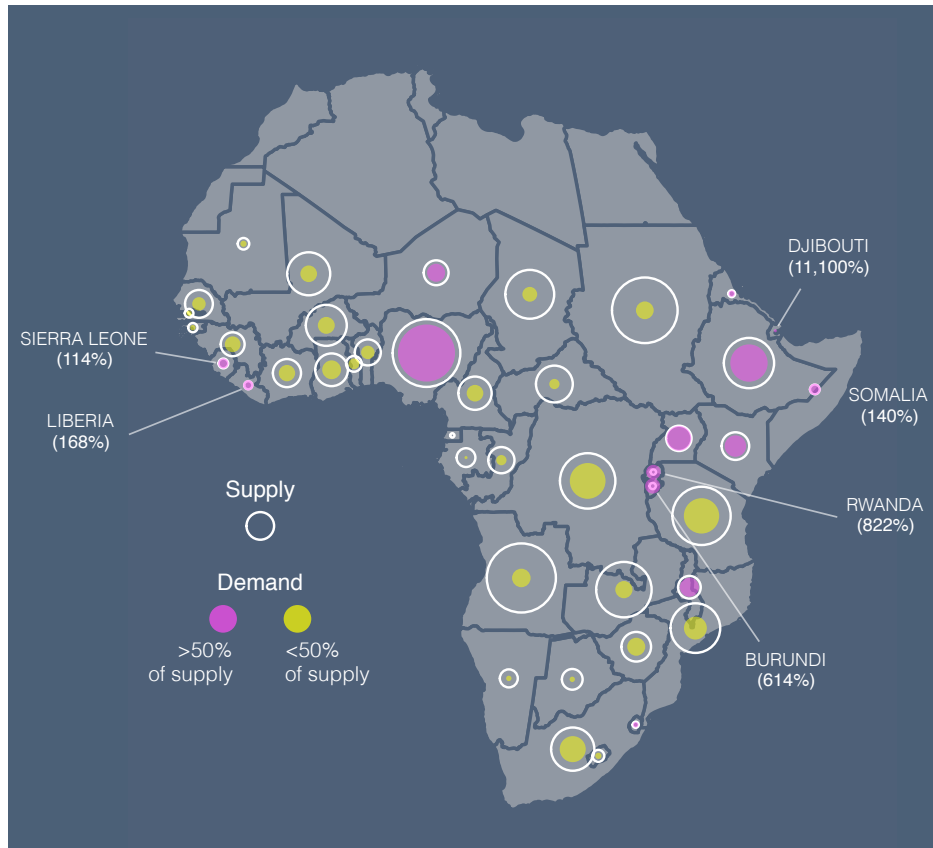
Figure A8: National-level fuelwood supply and demand for Sub-Saharan Africa using high estimates of fuelwood demand. Circles represent supply (open, white circles; from median estimates) and demand (closed, colored circles; from high estimates) summed for each country. The area of the circles is scaled by supply and demand so that larger circles represent larger supply or demand. Color of demand circles corresponds to the percentage of annual supply (wood production) appropriated to annual demand as indicated in the figure. Labeled countries are those where annual demand is greater than 100% of annual supply, with percentage shown in parentheses. A similar figure, using the low demand estimates, is found in the main text as Figure 4.3.
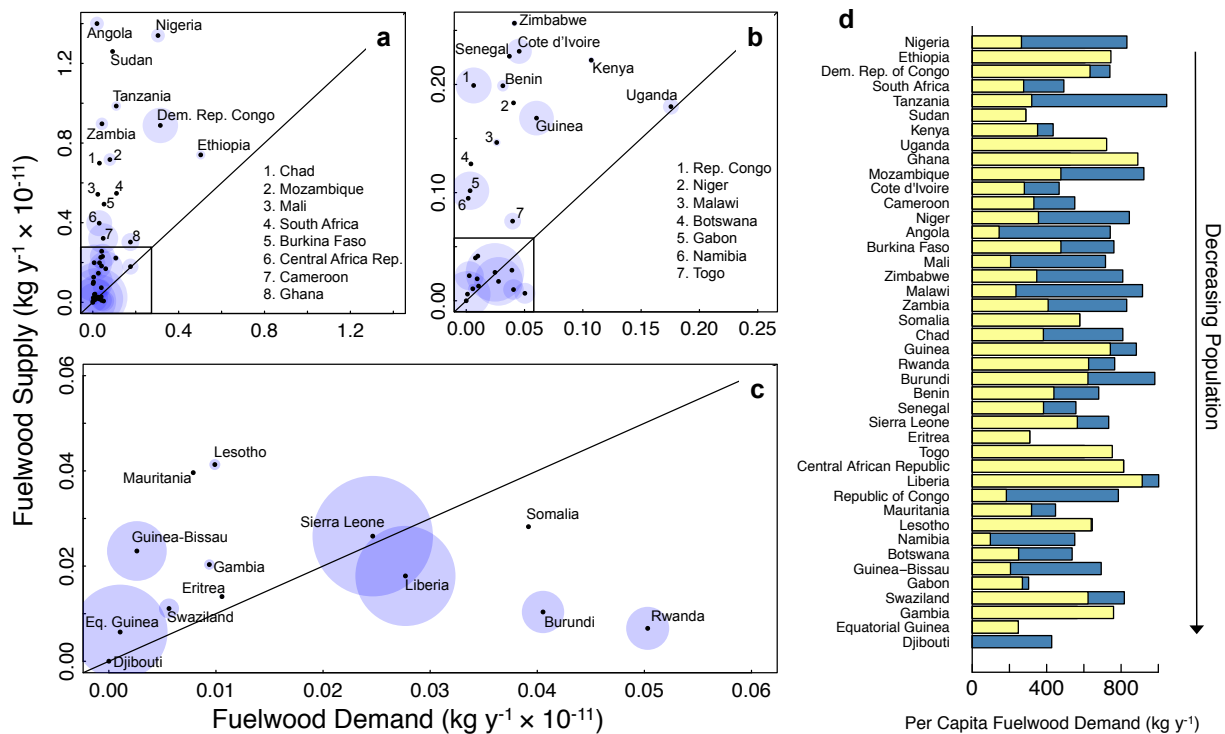
135

Figure A9: National level fuelwood supply and demand for Sub-Saharan Africa shown in supply-demand space. a, all countries in SSA. b, subset of panel a indicated by box in lower left corner of a. c, subset of panel b indicated by box in lower left corner of b. Circles are scaled by total available biomass per area for each country. Demand values are low estimates and supply values are the mean estimates. The 1:1 line, indicating supply = demand, is shown. Countries falling below the line are in negative fuelwood balance. d, per capita fuelwood demand for each country included in this analysis, ranked by population (greatest to least). Yellow bars show the low estimate and blue bars show the high estimate. Where blue bars are not visible our linear model predicted per capita demand lower than FAO values; in those cases we used the FAO values as the high and low estimate.

136